Effect of Season of Year on Pavement Response

ROY F. BIBBENS, CHRIS A. BELL, and R. GARY HICKS

ABSTRACT

The effect of season of year on pavement response in terms of changes in subgrade resilient modulus should be known for effective pavement design and management. To measure changes in modulus, deflection, subgrade moisture content, and subgrade soil suction were monitored at two locations in the Oregon Cascade Range. Changes in deflection were measured with a Dynaflect, Benkelman beam, and falling weight deflectometer. Changes in suction and moisture content were measured with resistivity cells installed in the subgrade. Frost tubes were also installed to record any frost penetration into the subgrade. Each site was monitored at least six times during 1981, mostly during the spring (the season of lowest subgrade strength). The collected data were used to develop a method for predicting subgrade modulus from suction and moisture content and for estimating subgrade modulus from surface deflection. The results indicate that measuring suction, moisture content, and deflection can result in reasonable estimates of subgrade modulus, with deflection measurements from the falling weight deflectometer being the quickest and most reliable.

In many areas of the Pacific Northwest seasonal variations in soil moisture cause a reduction in pavement system strength. This contributes to increased maintenance costs, inconvenience, and economic losses to organizations and people that use or depend on the transportation facility. (Note that this assessment was made by David B. Trask, Director of Engineering, Pacific Northwest Region, Forest Service, U.S. Department of Agriculture, during a seminar at the Transportation Research Institute, Oregon State University, February 22, 1978.)

In Region 6 of the Forest Service, transportation managers are concerned with seasonal variation in the strength of their service roads, particularly the impact of heavy truck loads during spring thaw periods, a time when pavement strength is greatly reduced. Currently, the thickness design used incorporates regional factors developed from experience, in an attempt to account for seasonal factors that result in lowered pavement strength. However, regional factors are not applicable to the evaluation of relative pavement damage during spring periods, and the utility of seasonal versus all-year haul alternatives.

The purpose of this investigation was to (a) measure changes in pavement strength, in the form of deflection, with changes in season, and (b) develop a method of predicting seasonal changes in modulus from easy-to-measure field data (i.e., deflection, soil moisture, and soil suction). With this development it should then be possible to assess pavement damage during spring periods and from various timber haul activities.

STUDY APPROACH

The experimental program used in this study for the evaluation of changes in pavement strength included identification of two test sites and the measurement of

1. Surface deflection,
2. Subgrade moisture,
3. Subgrade suction,
4. Frost penetration, and
5. Resilient modulus determination.

The field data collection consisted of a minimum of six visits during 1981, spread to touch all four seasons, with the majority of the site visits being in the spring in an attempt to measure reduced pavement strengths as observed by other studies (1-3). The results of the deflection measurements were used to back-calculate the subgrade moduli, which were then compared with laboratory-determined values corresponding to the in situ moisture contents measured at the same time as the deflections.

In addition to measurements of deflection, moisture, suction, and frost penetration, each site visit required measurements of air, pavement, and subgrade temperatures for use in deflection corrections and monitoring of freezing conditions. Details regarding the measurement of all parameters may be obtained by referring to Bibbens (4).

Site Descriptions

To select appropriate test sites for the study, three basic criteria for site selection were considered: (a) accessibility; (b) that they be representative of forest road subgrades, climate, and topography in the area; and (c) availability of weather data. On the basis of these criteria, two sites were identified, one in the Deschutes National Forest and the second in the Willamette National Forest (Figure 1).

The site in the Deschutes National Forest (USFS Road 2301) was approximately 4,420 ft (1350 m) above sea level, with an average annual rainfall of 25 in. (64 cm). The Willamette National Forest location (USFS Road 2233) was about 2,000 ft (610 m) above sea level, with an average annual rainfall of 70 in. (180 cm). Figure 2 shows the respective typical section and subgrade soils of each site. Location of the test sites on opposite sides of the Cascade Range results in sampling two of the more common climates and topographies in the Oregon Cascades and two of the more common subgrade materials in the region.

Deflection Instrumentation

Deflection of pavement sections was recorded on all site visits by a Dynaflect, a Benkelman beam on several occasions, and once by a falling weight deflectometer (FWD). Established points were used for all devices because deflection values vary with position because of pavement variables.

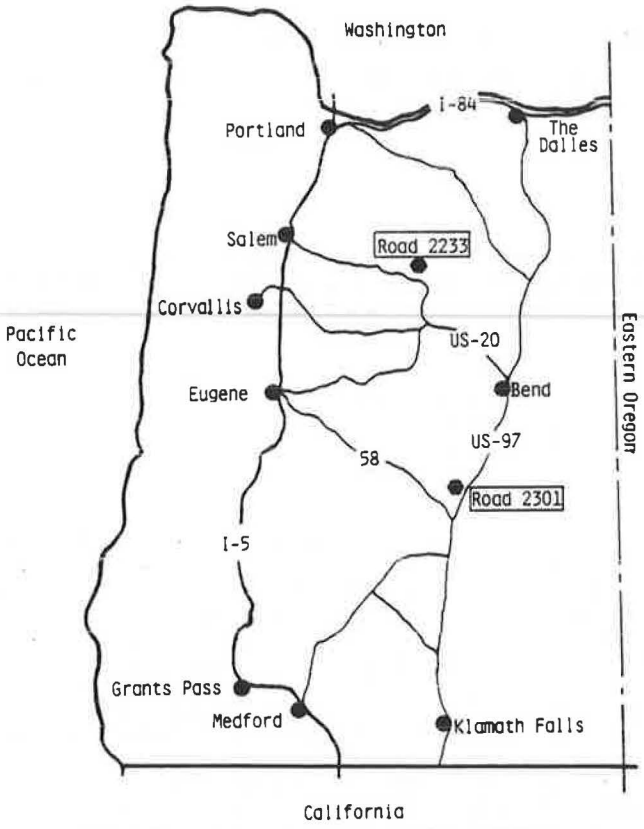

FIGURE 1 Partial map of Oregon showing location of test sites.

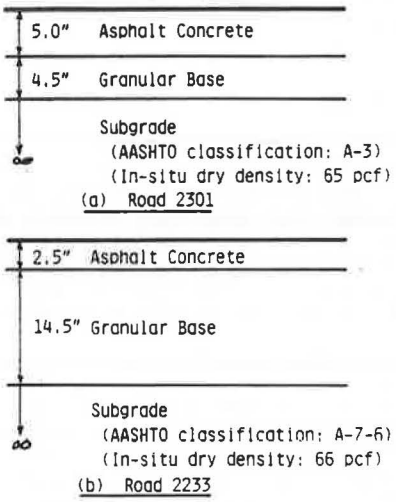

FIGURE 2 Typical cross sections for each test site.

Soil Suction and Moisture Measurement

Soil cells were used to measure soil moisture and soil suction in the field. Total soil suction has components of osmotic soil suction and matrix soil suction. If a soil is extremely low in dissolved salts or the amount of salts is a constant, then osmotic soil suction is zero and hence total soil suction equals matrix soil suction (5). The techniques used in this study only measured matrix soil suction because the amount of salts was so small that osmotic soil suction was nearly zero.

Soil cells have been successfully used to measure suction in the field by various researchers (6-8). Soil cells measure electrical resistivity of the soil as a function of moisture content. Those used (shown in Figure 3) were a modified version of a gypsum block and were chosen because of simplicity of operation, relative durability, resistance to damage during handling, fairly wide range of operation (approximately 2 to 5 pF), and low cost (6). Soil cells have the disadvantage in that salts in pore water affect resistivity and cause hysteresis effects between wetting and drying cycles, but they are well suited for in situ measurements under existing roadways.

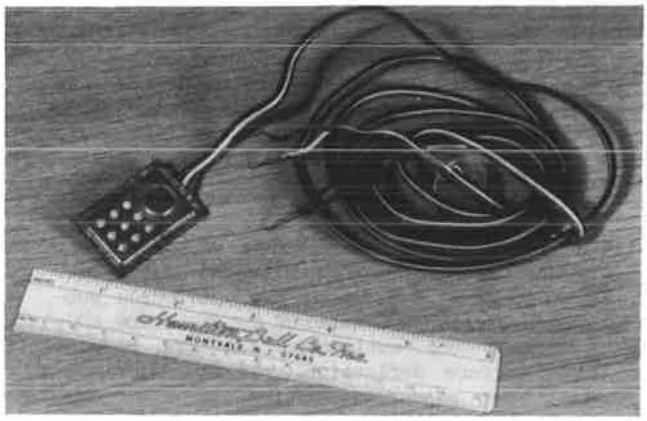

FIGURE 3 MC-310A standard soil moisture-temperature cell.

To obtain suction and moisture content values from soil cell readings, the cells were calibrated in the laboratory by using recompacted samples of subgrade soil at in situ unit weight (4). At both test locations four cells were installed, three beneath the pavement surface in the top 18 in. (0.46 m) of subgrade, and the fourth approximately 12 in. (0.30 m) below original ground, on the shoulder, in soil identical to the subgrade soil. This was done as a check on the soil cells and calibration curves. At each site visit tensiometer readings were taken near the fourth cell and at the approximate depth to check the suction values of the soil cell. Soil samples were also taken near the cell, to be used for moisture content determination by gravimetric technique. This was done to measure the accuracy of the soil cell for indicating moisture content.

Frost Penetration Instrumentation

The importance of establishing changes in subgrade modulus with easy-to-measure field data is for observing the effects of decreased subgrade support during changes in season. Measuring change in modulus is especially critical in areas that experience seasonal frost action. In these areas the spring thaw period is the period of least subgrade strength (9). Reduction in subgrade strength during thaw--termed thaw weakening--is a result of high subgrade moisture contents with poor drainage conditions.

To indicate the presence of frost penetration and to establish the thaw period, frost tubes were installed in each test section. Frost tubes change color on freezing. The tubes were made by placing an indicator solution of methylene blue, a fluorescent dye (0.1 percent solution), with Ottawa sand in

a polyethylene tube, which was then placed beneath the pavement in a permanently installed outer tube.

Determination of Resilient Modulus

Pavement cores, base soils, and subgrade soils taken from the sites were tested in the laboratory to determine their resilient moduli (M_R) for possible input into layered elastic programs and for providing data to predict subgrade modulus from easy-to-measure field data. To this end resilient moduli of the bases and subgrades were determined at several different water contents and unit weights (10) to establish the relative effect water has on M_R, such that the moisture content determined in the field could be used in the prediction of M_R. Standard indicator tests were also performed to classify the soils.

RESULTS

In this section the data collected are summarized and discussed. The following section presents the predictions of resilient modulus for the subgrade soils, which were based on these data. The data are presented in a series of figures, and the data from site visits are summarized in Tables 1 and 2.

Temperature

Figures 4 and 5 show a plot of air, pavement, and subgrade temperatures versus time from each site visit for USFS Roads 2233 and 2301, respectively. The figures also show a plot of the average daily temperature versus time for 6-day intervals, which indicate that the subgrade did not freeze during the test program because there were insufficient periods when air temperatures were below the freezing point. Because there were no frozen subgrades, it was not possible to observe the seasonal strength variations caused by subgrade freezing and the associated reductions in spring thaw strength. Therefore, any effect temperature had on deflection was taken into account by correcting the recorded Benkelman beam deflections to a standard temperature of 70°F (21°C), as presented in a subsequent section.

Subgrade Moisture and Suction

In addition to temperatures, the resistivity of the soil was recorded during each site visit and converted to moisture contents and soil suction values by using calibration charts developed by Bibbens (4). Figures 6 and 7 show plots of average daily precipitation over 6-day increments versus time and moisture content versus time for Roads 2233 and 2301, respectively. From the data in these figures it appears that subgrade moisture content reflected trends in precipitation and changes in season, as suggested by other researchers (11,12).

The resistivity-determined moisture content for the subgrade revealed good correlation with the measured deflection in the test section for Road 2233, using a least-squares fit. As shown in Figure 8, deflection clearly increases with increased moisture content for Road 2233, but for Road 2301 the relationship between deflection and moisture content was not as expected: deflection decreases with increased moisture content. However, laboratory determination of resilient modulus of Road 2301 subgrade clearly indicated that increasing moisture content decreased the modulus (10). This discrepancy was probably

TABLE 1 Summary of Site Visit Data for Road 2233

		Temp.		Soil Cell Readings						Soil		Tensiometer			Frost Tube	
Date	Weather	Pave. (°F)	Air (°F)	Cell #	Temp. (°F)	Resis. (ohms)	Corr. Resis. (ohms)	w/c (%)	Suction (pF)	Sample #	w/c (%)	Rdg. #	Suction (pF)	D. (in.)	Tube #	D. (in.)
01/27/81	Rain	38	38	1	38.3	2.3x1k	1.7×10^3	69	1.87	1	67.5	1	2.01	12	1	None
				2	37.4	3.0x1k	2.1×10^3	65	1.95	2	54.0	2	2.01	12	2	None
				3	39.2	1.3x10k	9.0×10^3	57	2.11	Ave	60.8	3	1.96	12		
				4	37.4	6.0x10k	3.8×10^4	45	2.31			Ave	1.99	12.0		
03/25/81	Cloudy	51	47	1	42.8	6.0x1k	4.5×10^3	62	2.01	1	69.3	1	1.91	10	1	None
				2	41.0	1.4x10k	1.0×10^4	56	2.12	2	58.2	2	1.85	10	2	None
				3	41.0	1.4x10k	1.0×10^4	56	2.12	Ave	63.8	3	1.85	13		
				4	42.8	6.0x10k	4.4×10^4	44.5	2.33			Ave	1.87	11.0		
04/20/81	Cloudy	46	51	1	44.0	1.9x10k	1.4×10^4	53	2.16	1	58.7	1	2.01	11	1	None
				2	43.0	2.4x10k	1.8×10^4	50	2.20	2	59.4	2	1.71	11	2	None
				3	42.0	1.8x10k	1.3×10^4	54	2.16	Ave	59.0	3	2.05	12		
				4	44.0	8.5x10k	6.2×10^4	43	2.38			Ave	1.92	11.3		
05/19/81	Rain	51	50	1	52.0	0.9x10k	7.8×10^3	58	2.08	1	65.3	1	1.85	15	1	None
				2	52.0	1.5x10k	1.3×10^3	73	1.83	2	58.5	2	1.85	10	2	None
				3	51.0	1.2x10k	1.0×10^4	56	2.12	Ave	61.9	3	1.91	9		
				4	52.0	5.5x10k	4.8×10^4	44	2.35			Ave	1.87	11.3		
07/16/81	Sunny	66.6	59.4	1	65.0	1.1x10k	1.2×10^4	54	2.14	1	47.8	1	2.39	14	1	Removed
				2	63.0	1.9x10k	2.0×10^4	49	2.22	2	40.1	2	2.42	14	2	Removed
				3	61.0	1.5x10k	1.5×10^4	52	2.17	Ave	43.9	3				
				4	61.0	1.3x10k	1.3×10^5	38	2.51			Ave	2.41	14.0		
11/19/81	Rain	45	44	1	41.0	1.4x10k	1.0×10^4	56	2.12	1	59.7	1	1.79	10	1	None
				2	42.0	2.2x10k	1.6×10^4	51	2.18	2	59.3	2	1.79	12	2	None
				3	43.0	1.5x10k	1.1×10^4	55	2.13	Ave	59.5	3	1.91	12		
				4	39.0	1.0x10k	6.6×10^4	42	2.40			Ave	1.83	11.3		

TABLE 2 Summary of Site Visit Data for Road 2301

		Temp.		Soil Cell Readings						Soil		Tensiometer			Frost Tube	
Date	Weather	Pave. (°F)	Air (°F)	Cell #	Temp. (°F)	Resis. (ohms)	Corr. Resis. (ohms)	w/c (%)	Suction (pF)	Sample #	w/c (%)	Rdg. #	Suction (pF)	D. (in.)	Tube #	D. (in.)
01/28/81	Snowing	37	38	1	34.7	1.4x10k	$8.8x10^3$	49	2.56	1	63.1	1	1.79	11	1	None
				2	35.6	3.6x10k	$2.2x10^4$	35	2.87	2	60.7	2	1.66	12	2	None
				3	36.5	2.7x10k	$1.7x10^4$	44	2.79	3	66.3	3	1.71	13		
				4	37.4	1.5x10k	$9.8x10^3$	48	2.61	Ave	63.4	Ave	1.72	12		
03/24/81	Partly Cloudy	70	54	1	39.2	18.0x1k	$1.2x10^4$	47	2.67	1	76.1	1	1.91	11	1	None
				2	41.0	6.0x10k	$4.1x10^4$	26	3.04	2	77.6	2	1.79	10	2	None
				3	41.0	4.9x10k	$3.4x10^4$	28	2.99	Ave	76.8	3	1.71	14		
				4	39.2	3.0x10k	$2.1x10^4$	39	2.85			Ave	1.80	11.7		
04/21/81	Partly Cloudy	69	56	1	52.0	1.9x10k	$1.6x10^4$	44	2.77	1	66.7	1	1.71	12	1	None
				2	51.0	5.0x10k	$4.1x10^4$	26	3.04	2	67.4	2	1.61	12	2	None
				3	50.0	4.9x10k	$4.0x10^4$	27	3.04	Ave	67.1	3	1.71	12		
				4	46.0	4.0x10k	$3.0x10^4$	29	2.98			Ave	1.68	12		
05/18/81	Rain	51	49	1	54.0	1.8x10k	$1.7x10^4$	44	2.79	1	58.0	1	2.01	12	1	None
				2	54.0	4.5x10k	$4.2x10^4$	26	3.05	2	59.2	2	1.79	16	2	None
				3	54.0	4.5x10k	$4.2x10^4$	26	3.05	Ave	58.6	3	1.61	12		
				4	49.0	4.6x10k	$3.7x10^4$	27	3.02			Ave	1.80	13.3		
07/16/81	Sunny, Warm	102	79	1	72.0	1.6x10k	$2.0x10^4$	41	2.83	1	49.5	1	2.05	15	1	Removed
				2	71.0	3.6x10k	$4.5x10^4$	25	3.07	2	53.3	2	2.01	14	2	Removed
				3	69.0	4.1x10k	$5.0x10^4$	24	3.09	Ave	51.4	3				
				4	58.0	5.5x10k	$5.5x10^4$	23	3.12			Ave	2.03	14.5		
11/18/81	Clear	38	31	1	37.0	2.5x10k	$1.6x10^4$	44	2.76	1	67.8	1	1.49	11	1	None
				2	39.0	4.9x10k	$3.4x10^4$	28	2.99	2	61.6	2	1.71	16	2	9"
				3	41.0	4.8x10k	$3.5x10^4$	28	3.00	Ave	64.7	3	1.61	16		
				4	40.0	4.1x10k	$2.8x10^4$	30	2.96			Ave	1.60	14.3		

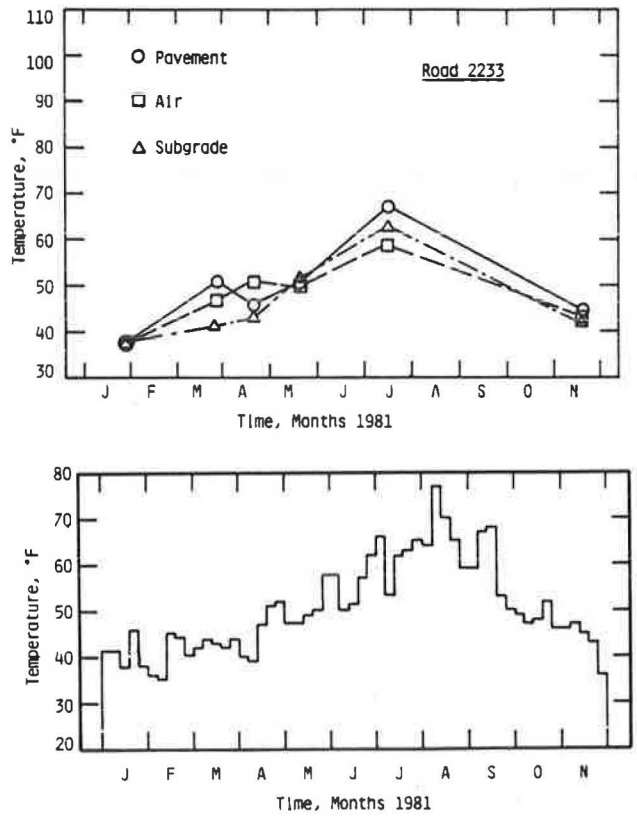

FIGURE 4 Temperatures versus time for Road 2233.

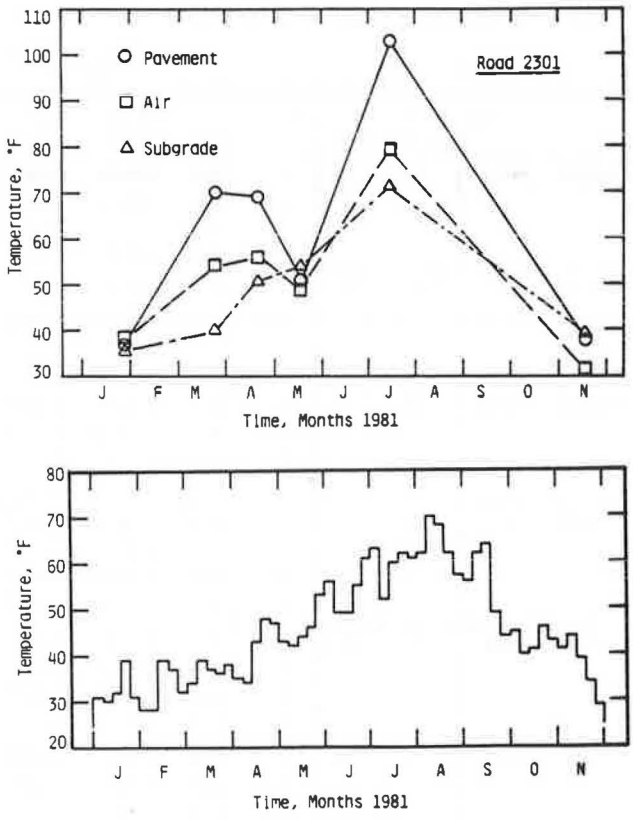

FIGURE 5 Temperatures versus time for Road 2301.

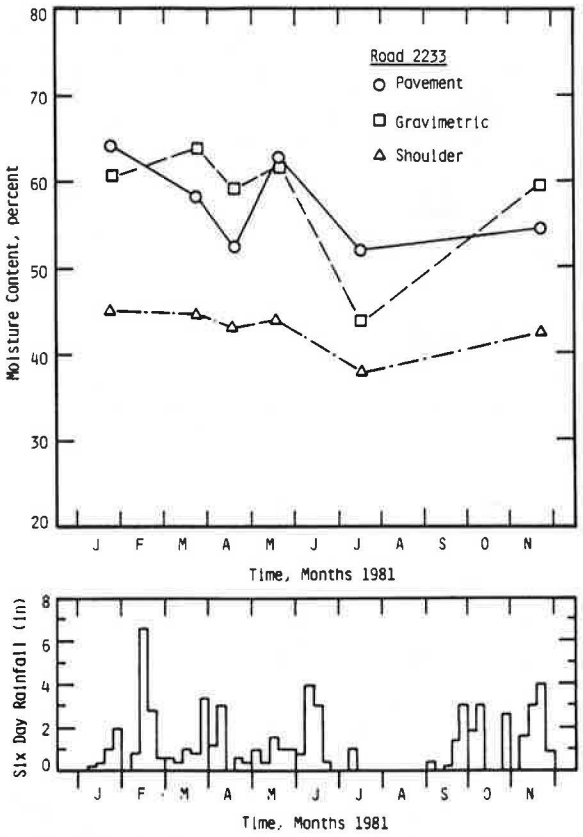

FIGURE 6 Moisture content versus time for Road 2233.

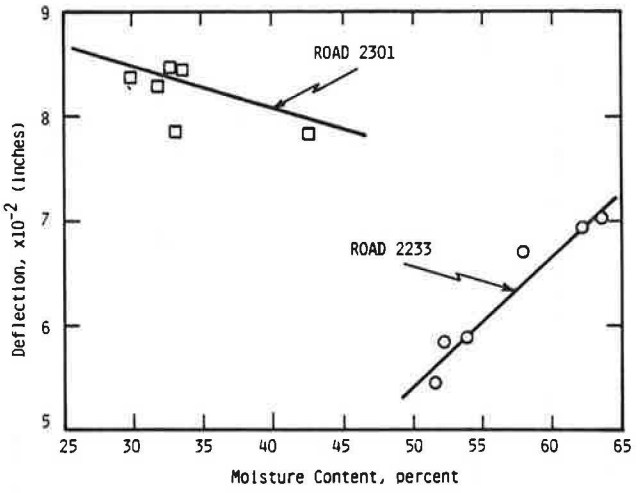

FIGURE 8 Deflection versus moisture content.

caused by inaccuracies in the measurement of moisture content using soil cells at Road 2301.

The soil cell and tensiometer measurements of suction for Road 2233 are shown in Figure 9, which shows average 6-day precipitation versus time and suction versus time, and also reflect the effect of rainfall on measured suction values. It was also found (Figure 10) that pavement deflection decreased with increased suction for Road 2233. This indicates that the road gained strength corresponding to increases in soil suction, as would be expected,

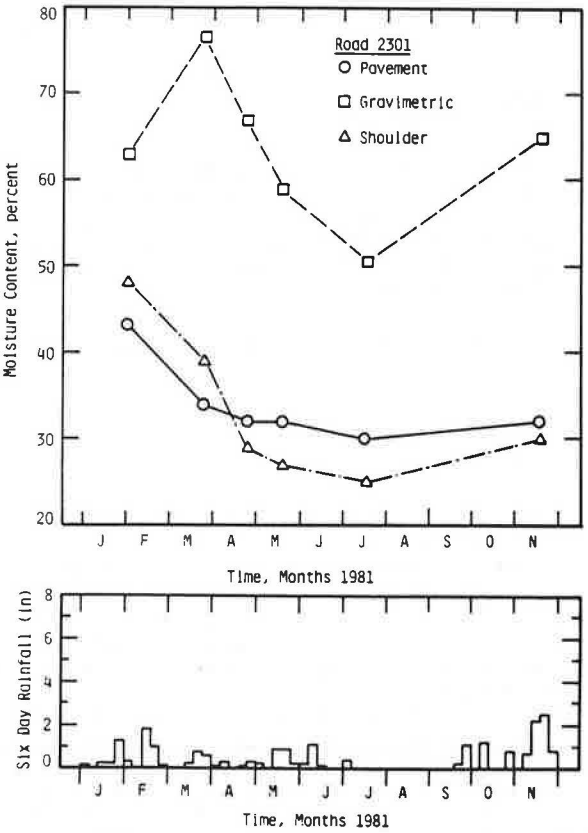

FIGURE 7 Moisture content versus time for Road 2301.

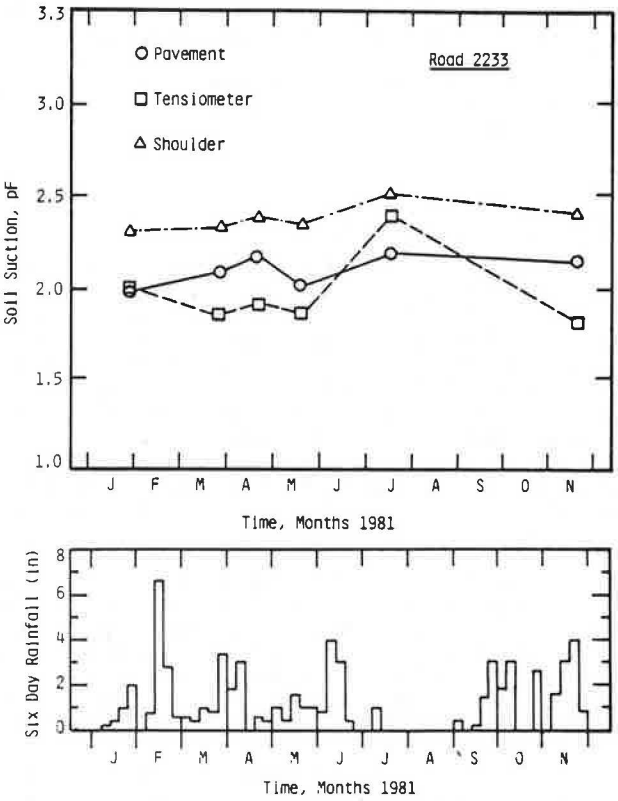

FIGURE 9 Soil suction versus time for Road 2233.

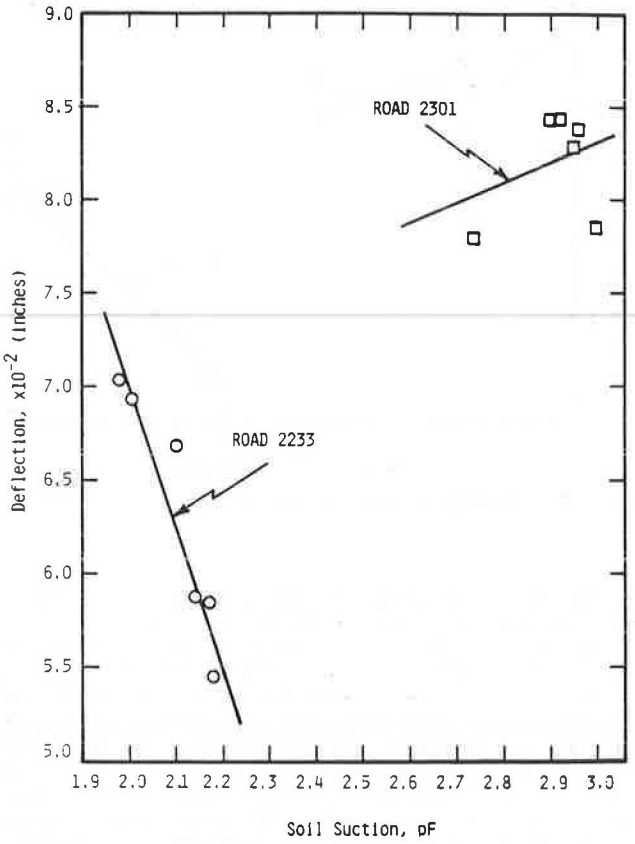

FIGURE 10 Deflection versus soil suction.

because increasing suction is associated with decreasing moisture content.

The data for Road 2301 revealed the opposite effect (i.e., decreasing deflection with increasing suction when a linear-regression fit was applied to the data), again leading to the conclusion that there was some error in the measurement of suction for this site.

Problems with Moisture Data Collection

Unfortunately, the results from the fourth soil cell, installed in the shoulder at Road 2301, could not be used to explain the anomalies found between measured deflection and moisture contents and suctions determined from the three cells installed below the pavement. Because of an oversight, soil cell calibration curves were only determined for below pavement subgrade densities (4) and not for the shoulder material. The densities of materials from the two locations were different, and therefore the calibration curves, which are sensitive to density (13), were inappropriate for the fourth soil cell.

There are three possible sources of error in the use of resistivity gauges such as the soil cells used in this study, which may explain the strange results obtained for Road 2301. First, hysteresis effects cause different responses in wetting and drying cycles and may cause an erroneous estimate if the condition below the pavement was different from that for the calibration. Cells were calibrated for a drying cycle, and if the subgrade soil was in a wetting cycle, estimates would be inaccurate. Second, soluble salts in the pore water can cause inaccuracies (6,14). However, the measured concentrations, less than 96 parts per million (ppm), were judged to be too low to cause problems. Third, a good contact between the gauge and the surrounding soil is necessary for accurate measurements. The subgrade soil at Road 2301 was a pumice, and it was difficult to achieve a good contact. This problem is the most tangible reason for poor measurements at Road 2301. For Road 2233, a good contact was achieved between the silty soil and the cells, and this probably accounts for the much better results obtained.

Pavement Deflection

Maximum deflection is a key parameter in various methods of determining moduli of pavement material. Figure 11 shows the plot of maximum deflection ver-

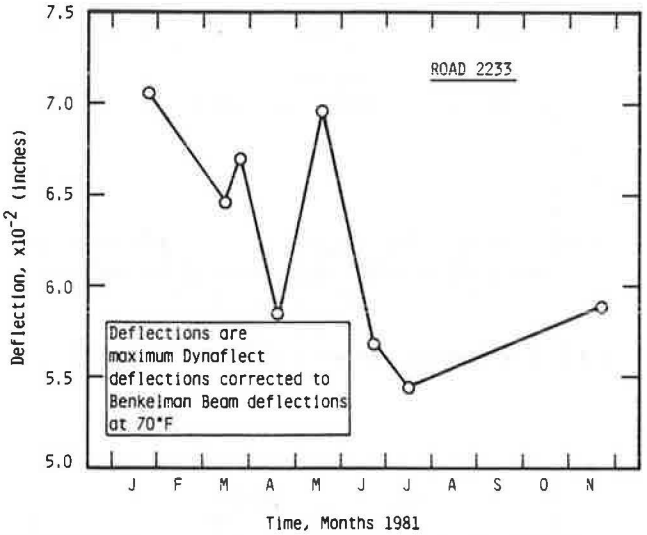

FIGURE 11 Maximum deflection versus time for Road 2233.

sus time for Road 2233. The deflections plotted in the figure were the average deflections over the test section, at the time of measurement, of the maximum Dynaflect deflections converted to Benkelman beam (2) and corrected for temperature (1) by using the following equations:

$$\text{Equivalent Benkelman beam deflection} = 20.09 \times (\text{maximum Dynaflect deflection}) \quad (1)$$

and

$$X_{70} = X_{(T)} + [(70 - T)/5{,}000] \quad (2)$$

where T is the pavement temperature, and X_{70} is the temperature-corrected deflection.

Although the maximum deflection is an important parameter for overlay design and for use in determining modulus of pavement materials, deflection basins are also important inputs into most of the published techniques for the prediction of modulus from deflection.

The range of measured deflection basins for all Dynaflect site visits are shown in Figure 12 for Roads 2233 and 2301. The plotted deflection basins were determined for each site visit at a test section by averaging sensor deflections individually. The plotted basins, for the most part, were similar in shape for each road, no matter when the measurements were taken. Not only were the shapes fairly

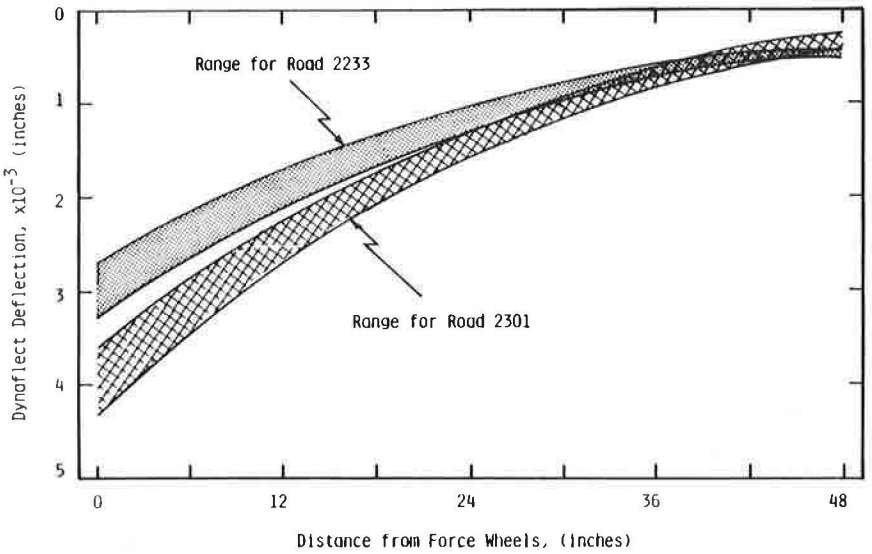

FIGURE 12 Dynaflect deflection basins for Roads 2233 and 2301.

similar from site visit to site visit, but the range in deflections at each sensor was not great. This implies that changes in the subgrade resilient modulus were small during the period studied, unlike those expected during a thaw weakening period. When comparing the general shape of the deflection basins for each road, it was observed that the deflections at the first and second sensors were greater for Road 2301 than for Road 2233. This implies that the asphalt concrete pavement moduli for Road 2233 were greater than that for Road 2301. In fact this was borne out in the laboratory by the determination of resilient moduli of the two surfaces by using the diametral test. Diametral testing yielded a resilient modulus for Road 2233 that was 3.5 times higher than that for Road 2301. Further, the shapes of the basins for Road 2233 were generally convex indicating weaker base layers and a strong surface, whereas for Road 2301 the basin shapes were concave near the force wheels indicating a weak surface and convex at the outer sensors indicating weak base layers.

Frost Penetration

Frost tubes were installed to observe any frost penetration into the subgrade. They indicated that no frost penetrated the upper levels of the structural section during the test period. The thermistors on the soil cells also indicated no freezing temperatures, as shown in Figures 4 and 5.

Testing of Subgrade Resilient Modulus

The data needed from resilient modulus testing were relationships of M_R versus moisture content for each subgrade soil at or near in situ dry unit weight, over the range of moisture contents monitored in the field during the study period, and under approximate stress conditions associated with an 18-kip (80-kN) single-axle dual-tire load. Selection of the appropriate stress condition for an 18-kip load was based on a layered elastic analysis. It was found that for Road 2233 the stress condition of σ_3 = 2 psi (13.8 kN/m^2) and σ_d = 2 psi was most appropriate, whereas for Road 2301 the stress condition of σ_3 = 2 psi and σ_d = 4 psi (27.6 kN/m^2) was the best choice.

The average dry unit weights for two locations at each test site were γ_d = 57 lb/ft^3 (9.0 kN/m^3) and γ_d = 65 lb/ft^3 (10.2 kN/m^3) for Roads 2233 and 2301, respectively. However, difficulties in sample preparation of the subgrade soil for Road 2233 required use of γ_d = 66 lb/ft^3 (10.4 kN/m^3).

Finally, modulus testing needed to be performed over the range of measured field moisture contents (see Figures 6 and 7 for Roads 2233 and 2301, respectively). This proved to be possible for Road 2301. The range needed (Figure 7) was from 30 to 42.7 percent, whereas testing was performed over the range of 29 to 42.5 percent. However, for Road 2233, the highest moisture content (at γ_d = 66 lb/ft^3) that could be run was 50 percent. From Figure 6 it can be seen that the range of moisture contents was 51.7 to 63.7 percent; thus the M_R versus moisture content curve for Road 2233 would need to be extended to obtain a value of M_R representative of measured field conditions. The results of the laboratory testing are shown in Figure 13.

To avoid problems of performing modulus testing on recompacted samples at in situ unit weight and moisture contents, it is suggested that undisturbed samples (if possible) of the subgrade be taken for M_R testing, and moisture content determination be made during each site visit. This would serve two purposes: (a) it would result in more accurate M_R results, and (b) it would serve as a more accurate check of the resistivity-determined moisture contents than a soil cell placed in the shoulder.

PREDICTION OF SUBGRADE MODULUS

M_R predictions were made for three seasons of the year in 1981: winter, spring, and summer. Examples are presented using data collected on Road 2233 on January 27, 1981 (see Table 1); note that all predictions are summarized in Table 3.

Prediction from Moisture and Suction Measurements

To predict M_R from moisture content requires plots of M_R versus moisture content and resistivity versus moisture content determined from laboratory testing, and field values of resistivity determined

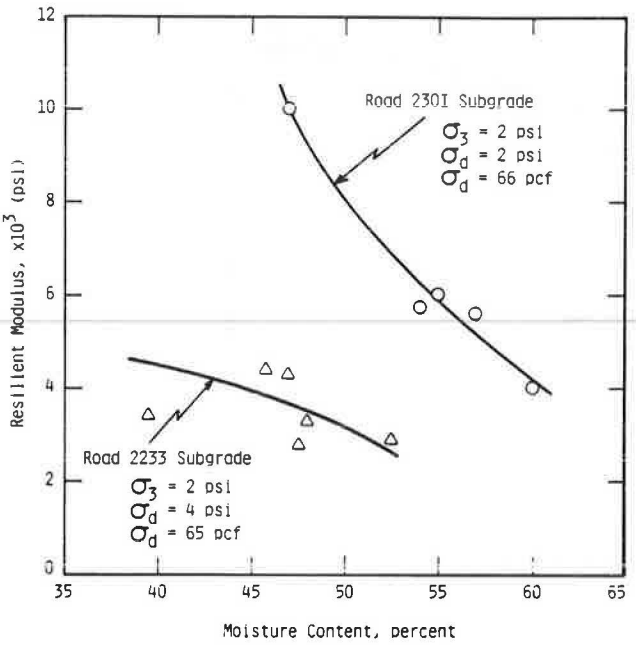

FIGURE 13 Laboratory-determined resilient modulus versus moisture content for both test sites.

from soil cells. The procedure for predicting M_R, using Road 2233 as an example, is as follows:

1. From Table 1, the resistivity measurements beneath the pavement on 1/27/81 were 1.7×10^3, 2.1×10^3, and 9.0×10^3 ohms;
2. From calibration curves the preceding resistances correspond to moisture contents of 69, 65, and 57 percent, of which the average was 63.7 percent; and
3. Using ω = 63.7 percent, enter Figure 13 and determine M_R = 900 psi (6.2 MN/m^2).

To predict the M_R values given in Table 3 for Road 2301, the same general procedure was used, except it was necessary to substitute the data from Table 2 and the appropriate calibration curve.

The method used to predict M_R from suction was similar to that for prediction of M_R from moisture content. The procedure, using Road 2233 as an example, was as follows:

1. From Table 1, the resistances on 1/27/81 were 1.7×10^3, 2.1×10^3, and 9.0×10^3 ohms, and from calibration curves the corresponding suctions were 1.87, 1.95, and 2.11 pF;
2. The average suction = 1.98 pF;
3. Using suction = 1.98 pF and calibration curves, it was determined that moisture content = 61.1 percent; and
4. With moisture content = 61.1 percent and using Figure 13, it was determined that M_R = 1,500 psi (10.3 MN/m^2).

To predict the M_R values given in Table 3 for Road 2301, the same procedure was used, except it was necessary to substitute the data from Table 2 and the appropriate calibration curves.

Predictions from Deflection Measurements

To predict resilient modulus (M_R) from deflection, various techniques were used (15-17). The techniques fell into two classes: one was the use of several published nomographs and the other was estimating subgrade modulus from deflection basin values by using a computer. The nomograph techniques used were by Treybig et al. (15) and Vaswani (16), both using Dynaflect deflections. The results are given in Table 3. Two computer programs were used, the first, ISSEM4, "utilizes a quasi-finite element approach in order to back calculate, through iteration, elastic or resilient modulus values ('E-values') for a layered (nonlinear) elastic system from surface deflections resulting from a wheel load simulating force pattern as initiated by an FWD test" (17). This program was run only for the FWD data collected on June 23, 1981, on Road 2233. The outputted subgrade M_R result can be found in Table 3.

The second program, entitled DEFPTS (18), is based on Boussinesq theory and computes deflections at the pavement surface at various radial distances from the load application. By inputting M_R values, thicknesses, Poisson's ratio for each layer, and the appropriate loading configuration, a desk-top computer outputs deflections at any desired radii. This program was used with both Dynaflect and FWD deflections to estimate subgrade M_R through a process of trial and error. It should be noted that the loading used in the program for the Dynaflect was not two 500-lb (2.22-kN) loads but one 1,000-lb (4.45-kN) load over a load radius of 1.41 in. (3.58 cm). This was suggested and shown to be a reasonable configuration by Scrivner et al. (19); in testing DEFPTS, the accuracy of the suggested loading was confirmed.

The input values used in DEFPTS for the various layers are shown in Figure 14. The M_R for the asphalt concrete layers and bases were as determined

TABLE 3 Summary of Resilient Modulus Predictions from Moisture and Deflection

		Resilient Modulus (psi)				
		From Moisture		From Dynaflect Deflection		
Road	Date	Water Content	Suction	Treybig et al. *(15)*	Vaswani *(16)*	DEFPTS
2233	01/27/81	900	1,500	3,100	4,300	14,000
	04/20/81	3,700	4,100	3,900	5,000	14,000
	06/23/81			3,100	4,000	12,000
	07/14/81			3,700	5,000	11,500
	07/16/81	3,800	4,200			
2301	01/28/81	2,850	2,400	8,500	3,800	15,000
	04/21/81	3,800	4,000	6,700	3,800	18,000
	07/13/81			6,200	4,000	20,000
	07/16/81	3,750	4,050			

Note: On June 23, 1981, using FWD data: (a) ISSEM4 gave M_R = 6,000 psi, and (b) DEFPTS gave M_R = 6,300 psi.

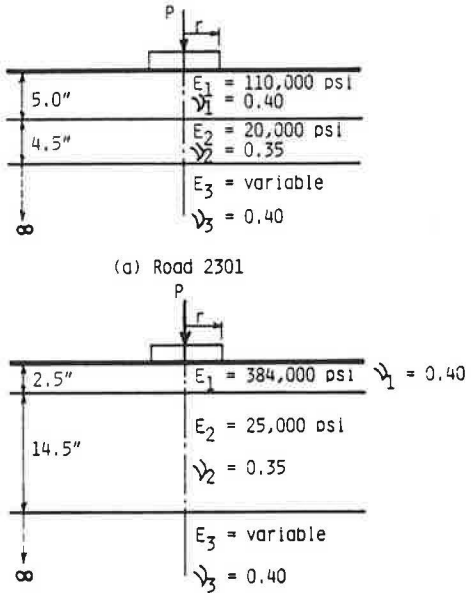

FIGURE 14 Pavement sections used for determining subgrade resilient modulus for both test sites.

from laboratory testing. The Poisson's ratios used were typical values suggested in several references (20,21), and in fact Poisson's ratio over a range of 0.35 to 0.45 for the layers made little difference in the calculated deflections. The results of the DEFPTS analysis are given in Table 3.

Comparison of Subgrade Modulus Predictions

Plots of deflection basin area are shown in Figures 15 and 16 for maximum and minimum deflection, from Dynaflect deflections, and also resilient modulus versus time for Roads 2233 and 2301, respectively. The values of M_R predicted by Vaswani's (16) technique were based on the deflection basin area, because such changes in actual measured values of area should be reflected by changes in M_R from Vaswani's technique, because increased area means increased deflections and implies decreased subgrade modulus or vice versa. From Figure 15 (Road 2233), the expected relationship between area and M_R was shown to hold between each successive measurement date. For Road 2301, the area did not provide as reliable an indicator of changes in M_R as it did for Road 2233.

The values of M_R predicted by Treybig's (15) technique are based on maximum deflection. To determine if changes in actual measured maximum deflections corresponded to expected changes in M_R, maximum deflection was plotted in Figures 15 and 16. In both figures the expected relationship between maximum deflection and M_R predicted by Treybig's technique existed; that is, if maximum deflection decreased between any successive measurement, M_R increased or vice versa.

To check the relative changes of M_R predicted by DEFPTS using Dynaflect deflections, which reflect changes in season, deflections measured by the outermost sensor were plotted in Figures 15 and 16 because the outer deflection sensors reflect the condition of the subgrade. For Road 2233 (Figure 15), the results were fair because, in general, increased deflection was reflected in decreased modulus or vice versa. For Road 2301 (Figure 16), the results were better because between successive measurements the minimum deflection and outputted M_R's related as would be expected.

When moduli predicted by moisture content and suction were compared with relative changes in area and maximum and minimum deflections, it was found that the relationships were generally mixed (e.g., in some cases the relative changes in M_R between successive dates were related as expected to area or deflection), whereas for other successive dates relative changes in M_R by suction and moisture con-

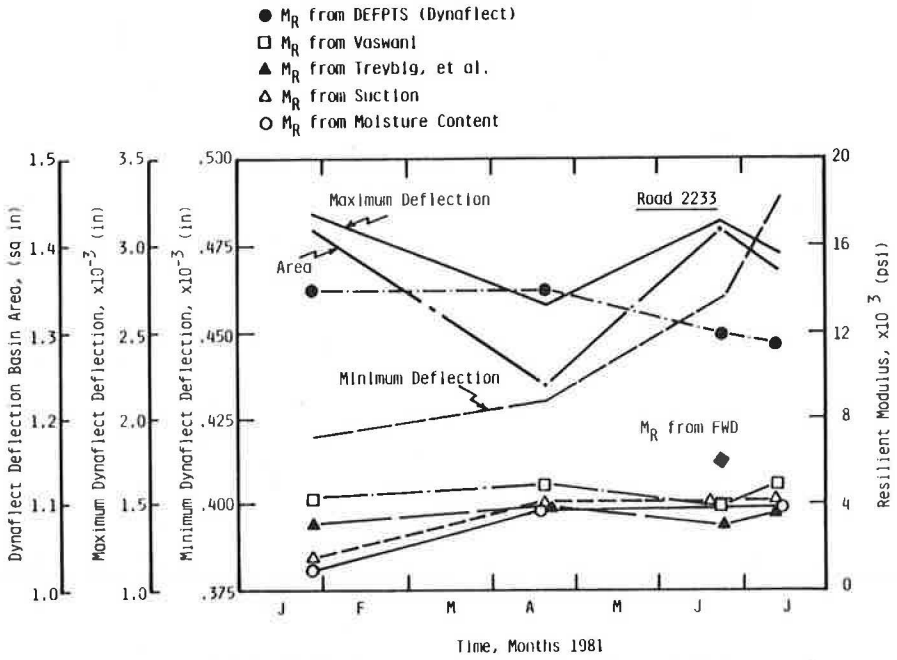

FIGURE 15 Plots of deflection basin area, maximum and minimum deflections, and resilient modulus versus time for Road 2233.

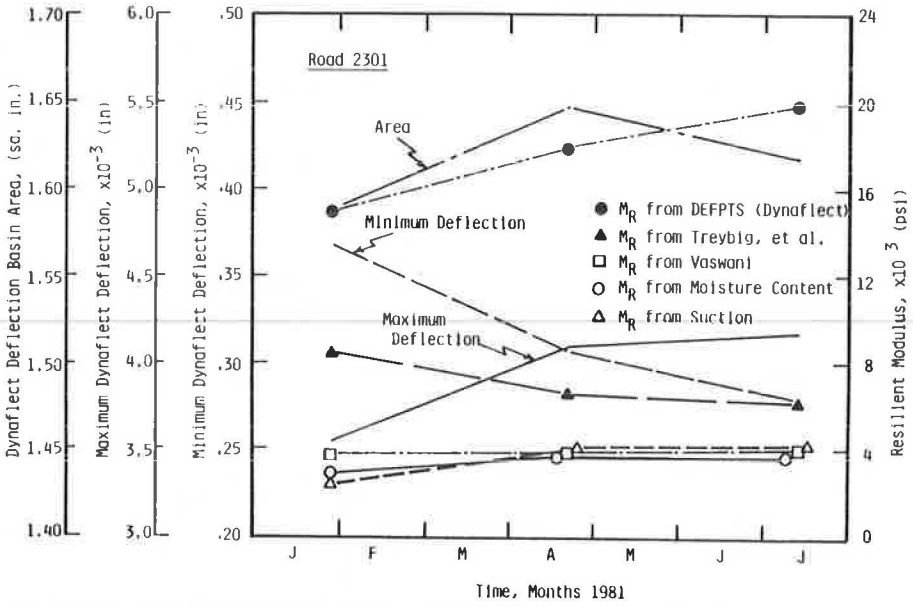

FIGURE 16 Plots of deflection basin area, maximum and minimum deflections, and resilient modulus versus time for Road 2301.

tent did not reflect expected changes in area (maximum or minimum deflections).

Also plotted in Figure 15 is the value of subgrade M_R, as determined by ISSEM4 and DEFPTS, for the measurement of deflection by an FWD on June 23, 1981. Note that the value of M_R predicted by the two programs was nearly identical, 6,000 psi (41.4 MN/m^2), and that the values were about 50 percent greater than those determined by nomograph techniques (15,16) based on Dynaflect measurements or from moisture and suction predictions. The values of M_R computed by ISSEM4 and DEFPTS from FWD deflections were probably closer to the in situ values of subgrade, because laboratory samples of Road 2233 subgrade did not appear to be as strong as the in situ material. This difference was associated with the difficulties of reproducing the observed field unit weight and moisture conditions in the laboratory, and implies that the M_R values in the field should be higher than those measured in the laboratory. This also implies that use of the FWD is more realistic than the Dynaflect, which is in accordance with Hoffman and Thompson (22) and Whitcomb (23). In conjunction with this, it was also believed that M_R determined from DEFPTS from the Dynaflect deflections was on the high side of the M_R in the field. It was suggested that the value of M_R determined by using DEFPTS and Dynaflect deflections, which was 3 times greater than laboratory values, was excessive. However, without undisturbed samples, it was impossible to accurately know the actual M_R value.

CONCLUSIONS

The salient conclusions resulting from this study are as follows.

1. It is possible to measure changes in pavement strength from deflection with changes in season even if subgrade freezing and subsequent thaw weakening do not occur.
2. A method for predicting resilient modulus using field-measured moisture content and suction was developed.
3. The M_R values from soil moisture, when compared with several published techniques for estimating subgrade M_R, generally resulted in M_R values of the same order of magnitude and also reflected similar changes in subgrade strength with changes in season.
4. The use of moisture content or suction to predict changes in subgrade resilient modulus yielded essentially identical values of M_R.
5. It appears that resilient modulus determined from deflection measurements using FWD data and computer analysis yields the best results of M_R.
6. Although M_R can be predicted from moisture content and suction, it would be much easier to only use deflections, which require only a minimum amount of laboratory testing, whereas using moisture content and suction required field installation and extensive laboratory testing.
7. The use of published techniques for predicting M_R yield reasonable values of M_R, reflect changes in season, and are fairly easy to use.

RECOMMENDATIONS

When using the approach of predicting subgrade resilient modulus from moisture content or suction, it is recommended that

1. More soil cells be installed over the test section to better define the resistances measured in a test section;
2. During site visits undisturbed samples (if possible) of the subgrade be obtained and brought back to the laboratory for resilient modulus testing;
3. After completing modulus testing on the undisturbed samples of subgrade, the moisture content be measured, a slice of the sample be taken, and suction on a suction plate be measured (these values would serve as a check on the field-determined values of moisture content and suction from the soil cells); and
4. Calibration of the soil cells for moisture content be done on larger samples than used in this project.

Further, if subgrade modulus is to be predicted by using moisture content or suction, it is recommended that moisture content be chosen because they both yield similar results. The laboratory equipment for measuring moisture content is readily available, whereas the laboratory equipment for measuring suction is complicated and is not available in many laboratories.

Finally, it is recommended that deflections be monitored and used for predicting subgrade modulus in any study of seasonal strength variations, and that an FWD should be the first choice in testing equipment, over a Dynaflect, should an FWD be available.

ACKNOWLEDGMENT

The study described herein was supported by Region 6 of the Forest Service, U.S. Department of Agriculture.

REFERENCES

1. A Guide to the Structural Design of Flexible and Rigid Pavements in Canada. Canadian Good Roads Association, Ottawa, Ontario, Canada, Sept. 1965.
2. F.H. Scrivner, R. Peohl, W.M. Moore, and M.B. Phillips. Detecting Seasonal Changes in Load Carrying Capabilities of Flexible Pavements. NCHRP Report 76. HRB, National Research Council, Washington, D.C., 1969, 37 pp.
3. W.C. Sayman. Plate-Bearing Study of Loss of Pavement Supporting Capacity Due to Frost. Bull. 111. HRB, National Research Council, Washington, D.C., 1955, pp. 99-106.
4. R.F. Bibbens. Effect of Season of Year on Pavement Response. Transportation Engineering Report 82-10. Department of Civil Engineering, Oregon State University, Corvallis, Oct. 1982.
5. K.T. Meyer. Summary of Work and Findings, NCHRP 1-10, Environmental Factors as Related to the Pavement System. Materials Research and Development, Inc., Oakland, Calif., Sept. 1967.
6. G.D. Aitchison and B.G. Richards. A Broad-Scale Study of Moisture Conditions in Pavement Subgrades Throughout Australia. In Moisture Equilibria and Moisture Changes in Soil Beneath Covered Areas: A Symposium in Print, Butterworths, London, England, 1965, pp. 184-225.
7. C.M.A. DeBruijn. Annual Redistribution of Soil Moisture Suction and Soil Moisture Density Beneath Two Different Surface Covers and the Associated Heaves at the Onderstepoort Test Site Near Pretoria. In Moisture Equilibria and Moisture Changes in Soils Beneath Covered Areas: A Symposium in Print, Butterworths, London, England, 1965, pp. 122-134.
8. E.K. Sauer and C.L. Monismith. Influence of Soil Suction on Behavior of a Glacial Till Subjected to Repeated Loading. In Highway Research Record 215, HRB, National Research Council, Washington, D.C., 1968, pp. 8-23.
9. Roadway Design in Seasonal Frost Areas. NCHRP Synthesis of Highway Practice 26. TRB, National Research Council, Washington, D.C., 1974, 104 pp.
10. S.A. Kidwai. Evaluation of the Resilient Properties of Selected Soils and Aggregates. Transportation Research Report 82-12. Department of Civil Engineering, Oregon State University, Corvallis, Aug. 1982.
11. B.J. Dempsey. Climatic Effects on Airport Pavement Systems: State of the Art. Final Contract Report 3-76-12. U.S. Army Corps of Engineers Waterways Experiment Station, Vicksburg, Miss., June 1976.
12. W. Vischer, G. Coghlan, and P. Heath. Siuslaw National Forest, Materials Report on the Forest Soils and Their Engineering Properties. Forest Service Report. Forest Service, U.S. Department of Agriculture, Corvallis, Oreg., Sept. 22, 1971.
13. J.L. Northrup. Seasonal Aggregate Thickness Design. Interim Report 1, Field Season 1978. Region 1, Forest Service, U.S. Department of Agriculture, Boise, Idaho, 1978.
14. L.D. Baver. Soil Physics, 3rd ed. Wiley, New York, 1956, Volume 1.
15. H.J. Treybig, B.F. McCullough, F.N. Finn, R. McComb, and W.R. Hudson. Design of Asphalt Concrete Overlays Using Layer Theory. Proc., 4th International Conference on the Structural Design of Asphalt Pavements, 1977, pp. 589-621.
16. N.K. Vaswani. Determining Moduli of Materials from Deflections. ASCE, Journal of Transportation Engineering, Vol. 103, No. TE1, Jan. 1977, pp. 125-141.
17. R.N. Stubstad. Mechanistic Evaluation of Existing Pavement Structures: The Dynatest Method. Proc., 5th International Conference on the Structural Design of Asphalt Pavements, 1982.
18. C.A. Bell. Use of the Boussinesq Equations in Analysis of Pavements. Oregon State University, Corvallis (in preparation).
19. F.H. Scrivner, C.H. Michalak, and W.M. Moore. Calculation of the Elastic Moduli of a Two-Layer Pavement System from Measured Surface Deflections. In Highway Research Record 431, HRB, National Research Council, Washington, D.C., 1973, pp. 12-24.
20. A.I.M. Claessen, C.P. Valkering, and R. Ditmarsch. Pavement Evaluation with the Falling Weight Deflectometer. Proc., Association of Asphalt Paving Technologists, Vol. 45, 1976.
21. N.K. Vaswani. Method for Separately Evaluating Structural Performance of Subgrades and Overlying Flexible Pavements. In Highway Research Record 362, HRB, National Research Council, Washington, D.C., 1971, pp. 48-62.
22. M.S. Hoffman and M.R. Thompson. Comparative Study of Selected Nondestructive Testing Devices. In Transportation Research Record 852, TRB, National Research Council, Washington, D.C., 1982, pp. 32-41.
23. W.G. Whitcomb. Surface Deflections and Pavement Evaluation--Equipment and Analysis Techniques. Transportation Engineering Report 82-4. Transportation Research Institute, Oregon State University, Corvallis, Jan. 1982.

Publication of this paper sponsored by Committee on Environmental Factors Except Frost.

Serviceability Loss Due to Roughness Caused by Volume Change in Expansive Clay Subgrades

BRENT RAUHUT and ROBERT L. LYTTON

ABSTRACT

It is common knowledge that pavements built on expansive clay subgrades will become rough whether heavily trafficked or not. Therefore it is obvious that much of the roughness that occurs on such roadways is caused by differential volume change in the subgrade, but this has been largely ignored in both analysis and design. Relatively little research effort has been expended to study this source of serviceability loss. Velasco and Lytton recently developed a multiple regression model to predict loss of serviceability with time caused by differential volume change in expansive clay subgrades. This model was developed from a limited data base that included present serviceability indices and various characteristics of the subgrade soils indicative of volume change potential. Applications of this model to four test sections in Texas and four in Colorado indicated that the effects of the independent variables on the loss of serviceability caused by expansive clay predicted by the model appeared to be reasonable. The predicted results for each test section are discussed with relation to known 18-kip equivalent single-axle loads and the characteristics of the subgrade clays. The assignment of responsibility for loss of serviceability between axle loads and differential volume change in the subgrade is explored and is discussed in detail.

A recent research effort (1) had as one of its goals the identification and application of predictive distress models for distresses significant to the generation of repair or rehabilitation of flexible pavements. Roughness caused by differential volume change in subgrades was identified as a significant distress and was studied during that project.

There are three known causes of volume change in subgrades. One is consolidation of subgrade materials in embankments or of natural subgrade materials in marshes or swamps. A second is the roughness induced by freezing of moisture in subgrade materials and subsequent thawing in the spring. The third is roughness due to differential volume change caused by seasonal or other moisture changes in expansive clay subgrades. There are no known models for predicting roughness caused by the first two and only one for predicting roughness caused by the third; therefore this third cause of roughness is the subject of this paper and is discussed in detail herein.

DIFFERENTIAL VOLUME CHANGE IN EXPANSIVE CLAY SUBGRADES

The mechanism involved relates to the relative ability of various clay soils to imbibe or relinquish moisture. The moisture migration from or to the clay depends directly on environmental conditions such as temperature, rainfall, and humidity, but the relative volume change depends on characteristics of the clay and soil mixture such as clay mineral type, the fraction of the soil mixture that is composed of clay minerals, and whether it was initially formed in freshwater or saltwater. A network of cracks in the subgrade is usually well established before construction of any roadway over clay soils, and these cracks apparently continue to offer convenient paths for moisture migration after the pavement is in place.

Because volume change in expansive clays has damaged structures worth billions of dollars worldwide, geotechnical engineers have studied this phenomenon for decades and much progress has been made in understanding it. Measurements have also been made of pavement surfaces over expansive clays, and a number of methods such as subgrade stabilization with lime or cement have been applied to limit the volume change. These studies have not directly contributed much to the prediction of the roughness that may be expected to occur in a specific environment and for a specific clay subgrade, but they did identify those parameters that should be considered as potential independent variables for empirical models to predict the occurrence of such roughness.

PREDICTING ROUGHNESS CAUSED BY DIFFERENTIAL VOLUME CHANGE IN EXPANSIVE CLAY SUBGRADES

Velasco and Lytton (2,3) recognized the need for models that would predict the reduction in present serviceability index (PSI) caused by expansive clay subgrades in pavements and developed an empirical model based on a limited data base in Texas. This equation was developed empirically by using regression techniques, with change in PSI as the dependent variable, and a range of independent variables intended to represent pavement structure, the effects of environment, and the nature of clay subgrades. Serviceability was obtained from 12 flexible and 5 rigid pavements in Texas through calculations based on measurements with a GM surface profilometer. Samples of the clay subgrades were obtained, and the required properties were derived from laboratory testing. The form of this equation was as follows:

$$\Delta SI = Ac^{B}n^{D} \quad (1)$$

Because the initial values of serviceability when the roadways were opened were unavailable, it was necessary to estimate initial values to calculate the difference considered to be the change in serviceability index (SI). The initial serviceability index was assumed to be 5.0, and the resulting regression coefficients A, B, and D were 2,675, 1.09, and 7.62, respectively. The values of c and n were also obtained through regressions as follows (2,3):

$$c = 0.0004\ Depth^{-0.81} Time^{0.49} AC^{-1.20} ESP^{0.12} \quad (R^2 = 0.77) \quad (2)$$

$$n = 0.79\ Depth^{0.09} CEC^{-0.16} Clay^{0.40} Range^{-0.16} \quad (R^2 = 0.83) \quad (3)$$

where

Depth = effective depth of pavement (in.) based on a moment of inertia I for the pavement section above the subgrade with its layer thicknesses weighted by layer stiffness relative to that of the surface layer (1,2), i.e.,

$$\text{Depth} = \sqrt[3]{12I/1\text{ in.}}$$

Range = range of values of Thornthwaite moisture index for a 20-year period (range is usually 50 to 90), smaller values generally apply in drier areas and vice versa;

Time = time since construction, or since last rehabilitation before the roughness was measured (years);

Clay = percentage of clay (grain size less than 0.002 mm), which is obtained from hydrometer grain size testing;

AC = activity [i.e., (Plasticity index/% clay)];

CEC = cation exchange capacity, where meg/100 gm ≈ (plastic limit)$^{1.17}$; and

ESP = exchange sodium percentage (approximately 2 for lacustrine deposits and 16 for saltwater deposits).

The test sections used for the development of this empirical relationship were specifically selected because they were essentially free of any load-induced distresses and because the only important observable distress was long wavelength unevenness. Further, the analyses made with the Fast Fourier transform method were for wavelengths of 10 ft or greater to essentially eliminate most of the effects of any load-induced damage. Therefore, it appears reasonable to assume that virtually all of the measured roughness remaining after the "filtering" previously described was caused by the expansive clay subgrades.

Although the data base for the development of this relationship was limited, it appeared to be reasonably well-founded, except that (a) the assumption of an initial PSI of 5.0 appeared to be much too optimistic for the known capabilities of the highway construction industry, and (b) the data base included measurements from five rigid pavements. It was decided to rerun the regressions using the more probable value of 4.2 for initial serviceability index and omitting the rigid pavements from the regression.

IMPROVEMENT OF THE MODEL

As discussed previously, it was decided to conduct a new regression analysis using only data from flexible test sections and using revised reductions in PSI based on an assumed initial PSI value of 4.2. This was done, and the result using the original equation form given in the previous section was as follows:

$$\Delta SI = 39{,}396\, c^{1.544} n^{9.59} \qquad (R^2 = 0.66) \tag{4}$$

The values for c and n may be obtained as described in Equations 2 and 3; their substitution into Equation 4 results in

$$\Delta SI = 0.02323\, \text{Depth}^{-0.387} \text{Time}^{0.757} AC^{-1.85} ESP^{0.185} CEC^{-1.53} \text{Clay}^{3.84} \text{Range}^{-1.53} \tag{5}$$

EVALUATION OF MODEL

To check the reasonableness of this model, predicted changes in SI were made for four Texas test sections and four Colorado test sections for which measured data were available. Data needed for the calculations are given in Tables 1 and 2. As most of the data needed was not available from records, estimates were made by using Equations 2 and 3.

Equation 4 was used for the calculations, and it calculated values of the independent variables. The resulting predictions of ΔSI due to expansive clay are given in Tables 3 and 4. Note that the measured changes in SI are also shown, and the difference shown is caused by traffic (although it could be due partially to other causes such as differential embankment settlement and so forth). Where the calculated predictions for change in SI due to expansive clay exceeded the measured changes, no change because of traffic is assumed.

The results in Tables 3 and 4 are plotted in Figures 1 and 2. The approximate 18-kip equivalent single-axle loads (ESALs) experienced by the test sections at an appropriate point in time are also shown. Note that the measured values of PSI (shown as filled circles) are somewhat erratic, and that the total changes are drawn in smoothly to represent the most probable values. Total changes have been extrapolated in some cases with dashed lines to allow approximate comparisons to predicted changes caused by expansive clays.

The predicted changes in SI caused by expansive clays are discussed by individual test sections.

TABLE 1 Available Data Collected for Texas and Colorado Test Sections

Test Section	Plastic Limit	Plasticity Index	% Passing No. 200	Thicknesses Surface	Base	Subbase	Year of Last Const. or Rehab.
TX-25-82(2971)	20	26	78	3.5	13.0	----	Oct 1961
TX-25-82(2853)	10	24	50-70	9.5	5.0	6.0	Oct 1970
TX-25-62(2895)	20	7	40-65	9.5	5.0	----	Nov 1972
TX-5-87(2675)	20	28	60-80	2.3	10.0	5.0	Mar 1967
CO-1-70(4-59)	22	31	95	9.0	24.0	----	Jun 1975
CO-3-70(114-19)	19	24	65	9.0	17.0	----	May 1965
CO-3-40(5-1-1)	23	21	95	9.5	----	----	Aug 1969
CO-96(1)	20	28	80	2.8	4.5	11.4	Jun 1965

TABLE 2 Approximate Values of Independent Variables for Calculating c and n

Test Section	Range	AC	ESP	% CLAY	DEPTH	CEC
TX-25-82(2971)	↑	.80	16	33	7.7	33.3
TX-25-82(2853)		1.0	16	24	11.4	14.8
TX-25-62(2895)		.80	16	9	10.0	33.3
TX-5-87(2675)	50	.80	16	35	9.5	33.3
CO-1-70(4-59)		.80	16	39	15.6	37.2
CO-3-70(114-19)		.80	2	30	12.6	31.3
CO-3-40(5-1-1)		.80	2	26	9.5	39.2
CO-96(1)	↓	.80	16	35	9.7	33.3

TABLE 3 Measured Changes in SI and Calculated Changes Caused by Expansive Clays for Texas Sections

Test Section	Time (Years)	c	$c^{1.544}$	n	$\lvert n \rvert^{9.59}$	Δ SI Total Measured	Δ SI Due To Expansive Clay	Δ SI Due to Traffic
TX-25-82(2971)	4	2.753×10^{-4}	3.18×10^{-6}	-1.173	4.634		0.58	
	8	3.866×10^{-4}	5.38×10^{-6}	-1.173	4.634		0.98	
	13	4.905×10^{-4}	7.77×10^{-6}	-1.173	4.634	0.7	1.42	
	16	5.430×10^{-4}	9.01×10^{-6}	-1.173	4.634	1.3	1.66	
	19	5.907×10^{-4}	1.04×10^{-5}	-1.173	4.634		1.89	
TX-25-82(2853)	2	1.091×10^{-4}	7.63×10^{-7}	-1.218	6.647	0.20	0.20	
	4	1.532×10^{-4}	1.29×10^{-6}	-1.218	6.647	0.10	0.33	
	6	1.869×10^{-4}	1.75×10^{-6}	-1.218	6.647	1.40	0.46	0.94
	8	2.152×10^{-4}	2.18×10^{-6}	-1.218	6.647		0.57	
	10	2.401×10^{-4}	2.6×10^{-6}	-1.218	6.647		0.68	
TX-25-62(2895)	2	1.395×10^{-4}	1.1×10^{-6}	-0.7144	0.0397	0.10	0.002	0.10
	4	1.959×10^{-4}	1.9×10^{-6}	-0.7144	0.0397		0.003	
	6	2.389×10^{-4}	2.6×10^{-6}	-0.7144	0.0397	0.20	0.004	0.20
	8	2.751×10^{-4}	3.2×10^{-6}	-0.7144	0.0397		0.005	
	10	3.069×10^{-4}	3.8×10^{-6}	-0.7144	0.0397		0.006	
	13	3.490×10^{-4}	4.6×10^{-6}	-0.7144	0.0397		0.007	
TX-5-87(2675)	2	1.653×10^{-4}	1.45×10^{-6}	-1.224	6.958		0.40	
	4	2.322×10^{-4}	2.45×10^{-6}	-1.224	6.958		0.67	
	6	2.832×10^{-4}	3.32×10^{-6}	-1.224	6.958	1.3	0.91	0.39
	8	3.261×10^{-4}	4.14×10^{-6}	-1.224	6.958	1.6	1.13	0.44
	10	3.638×10^{-4}	4.90×10^{-6}	-1.224	6.958	1.7	1.34	0.36
	13	4.137×10^{-4}	6.0×10^{-6}	-1.224	6.958		1.65	

TABLE 4 Measured Changes in SI and Calculated Changes Caused by Expansive Clays for Colorado Sections

Test Section	Time (Years)	c	$c^{1.544}$	n	$\lvert n \rvert^{9.59}$	Δ SI		
						Total Measured	Due To Expansive Clay	Due to Traffic
CO-1-70(4-59)	2	1.106×10^{-4}	7.79×10^{-7}	-1.313	13.64	0.4	0.42	--
	3	1.349×10^{-4}	1.06×10^{-6}	-1.313	13.64	0.5	0.57	--
	5	1.733×10^{-4}	1.6×10^{-6}	-1.313	13.64	0.7	0.86	--
CO-3-70(114-19)	2	1.024×10^{-4}	6.92×10^{-7}	-1.192	5.40	0.5	0.15	0.35
	4	1.438×10^{-4}	1.17×10^{-6}	-1.192	5.40	1.1	0.25	0.85
	6	1.754×10^{-4}	1.59×10^{-6}	-1.192	5.40	1.2	0.38	0.82
	8	2.02×10^{-4}	2.0×10^{-6}	-1.192	5.40	1.4	0.43	0.97
CO-3-40(5-1-1)	2	1.288×10^{-4}	9.86×10^{-7}	-1.059	1.73		0.07	
	4	1.809×10^{-4}	1.67×10^{-6}	-1.059	1.73	0.0	0.11	--
	6	2.207×10^{-4}	2.26×10^{-6}	-1.059	1.73	1.5	0.15	1.35
CO-96(1)	2	1.627×10^{-4}	1.41×10^{-6}	-1.226	7.084	0.1	0.39	--
	4	2.286×10^{-4}	2.39×10^{-6}	-1.226	7.084		0.67	
	6	2.788×10^{-4}	3.25×10^{-6}	-1.226	7.084		0.91	
	8	3.21×10^{-4}	4.03×10^{-6}	-1.226	7.084		1.12	
	10	3.58×10^{-4}	4.78×10^{-6}	-1.226	7.084	0.7	1.33	--
	13	4.07×10^{-4}	5.82×10^{-6}	-1.226	7.084	1.9	1.63	0.27

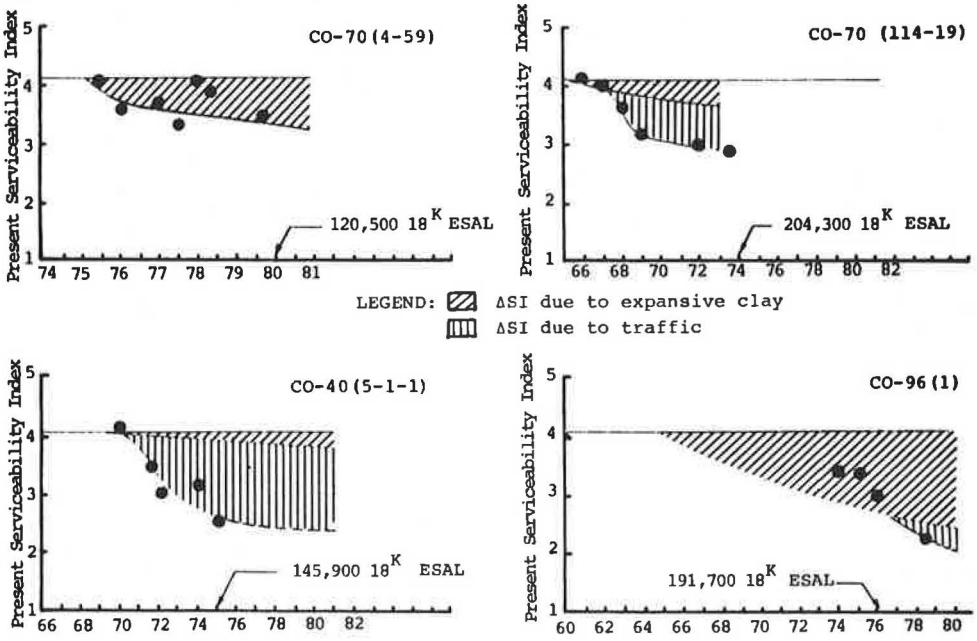

FIGURE 1 Measured changes in SI divided into predicted changes caused by expansive clay and traffic, Colorado test sections.

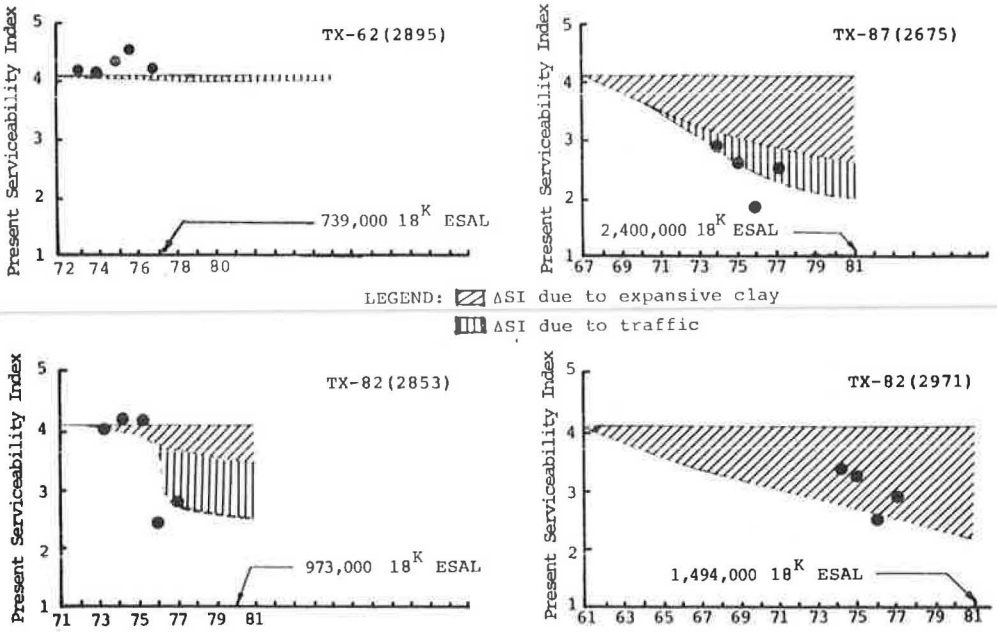

FIGURE 2 Measured changes in SI divided into predicted changes caused by expansive clay and traffic, Texas test sections.

1. TX-62(2895): There was virtually no measured change in PSI between 1972 and 1977, nor was there any measurable change predicted. The plasticity index of the subgrade was quite low, so no roughness caused by differential volume change in the subgrade would be expected.
2. TX-87(2675): Most of the measured change in PSI was attributed to the moderately expansive clay, but traffic loadings appear to have contributed to the measured changes after a few years.
3. TX-82(2853): The moderately expansive clay subgrade contributed to the loss of serviceability, but it appears that the majority of the loss was caused by traffic.
4. TX-82(2971): This pavement experienced relatively minor serviceability loss during the first 14 years after rehabilitation, but the rate increased after that. The model appears to have overpredicted the change in serviceability because of the moderately expansive clay subgrade in this case. It appears more likely that virtually all of the change was caused by differential volume change in the clay for the first 14 years, but that the increase in the rate of serviceability loss around that point was likely caused by traffic.
5. CO-70(4-59): The expansive clay subgrade is credited by the model for all of the serviceability loss. This appears logical, considering the changes in PSI with time and the relatively light traffic on the pavement.
6. CO-70(114-19): The moderately expansive clay appears to have contributed to the loss of serviceability, but the primary cause was considered to be traffic. The moderate prediction in this case is caused primarily by a relatively low estimated clay content.
7. CO-40(5-1-1): The clay subgrade was predicted to have caused little of the loss of serviceability. Most of the loss was believed to have been due to traffic or other causes.
8. CO-96(1): The model appears to have overpredicted the loss in serviceability because of the moderately expansive subgrade. It appears that the clay was the primary cause of roughness for the first 10 years after the pavement was overlaid, but the sudden increase in serviceability loss at that point was caused by traffic.

The effects of the independent variables on the loss of serviceability because of expansive clay, as predicted by the model, appear to be reasonable. The predictions appear reasonable, but they also appear to trend somewhat toward overpredictions where the clay content was relatively high.

It is recognized that the assignment of responsibility for relatively high changes in serviceability to differential volume change in expansive clay or shale subgrades will meet with strong opposition from many relatively knowledgeable researchers, especially those with close ties to the AASHO Road Test, who tend to ascribe virtually all pavement roughness to the effects of axle loads. This will be partly because there has been little effort to quantify roughness caused by expansive clay subgrades before the recent work of Velasco and Lytton. However, it is well-known by researchers who practice in areas that have expansive clays that pavements on expansive clays become rough fairly rapidly, even if traffic is nominal. It appears logical that early roughness is caused by the seasonal shrinkage and swelling of the expansive clays, which will never be uniform. The magnitudes of such movements are generally greater than those attributable to material variations and consequent differential compaction caused by repetitive wheel loadings. Also, it is becoming increasingly apparent from data collection on test sections around the country that rutting is often relatively nominal; thus differential rutting is not likely to induce much roughness. The primary effects of axle loads on increasing roughness in typical pavement structures appear to generally begin when surface cracking occurs and excess moisture infiltrates base and subgrade materials. If an unstable asphalt cement (AC) mix is used or other inadequate design or construction practices are applied, however, it is possible to experience roughness because of shoving, corrugations, differential consolidation of base, and so forth.

In limited support of the previous discussion, Florida test sections also studied during the proj-

ect reported by Rauhut et al. (1) reveal virtually no change in serviceability, even under heavy traffic (see Figure 3). This is partially due to the stiffness of the limerock base, but it is strongly believed that serviceability loss could be expected if these pavements were on expansive clay instead of on sand subgrades. It should also be noted that Texas test section TX-62(2895), the only one of the eight from Texas and Colorado with a subgrade having low plasticity, experienced almost no change in serviceability during the first 10 years after reconstruction.

New York test sections also had relatively nonexpansive subgrades, but they are silty and they undergo freezing and thawing that also cause important changes of serviceability (see Figure 4). Note that the cumulative 18-kip ESALs for these test sections were not especially high.

It is not the intent of this discussion to suggest that heavy axle loads do not cause roughness in pavements (as they certainly did at the AASHO Road Test), but there are strong reasons to believe that the results of the AASHO Road Test would have been quite different if conducted at lower traffic rates over a longer period in a no-freeze area with an expansive clay subgrade. Of course, they would also have been considerably different for flexible pavements if either conducted in a southern climate or as a long-term test with lower traffic rates.

SUMMARY

The model described herein for predicting changes in serviceability caused by differential volume changes in expansive clays is the only one known to exist.

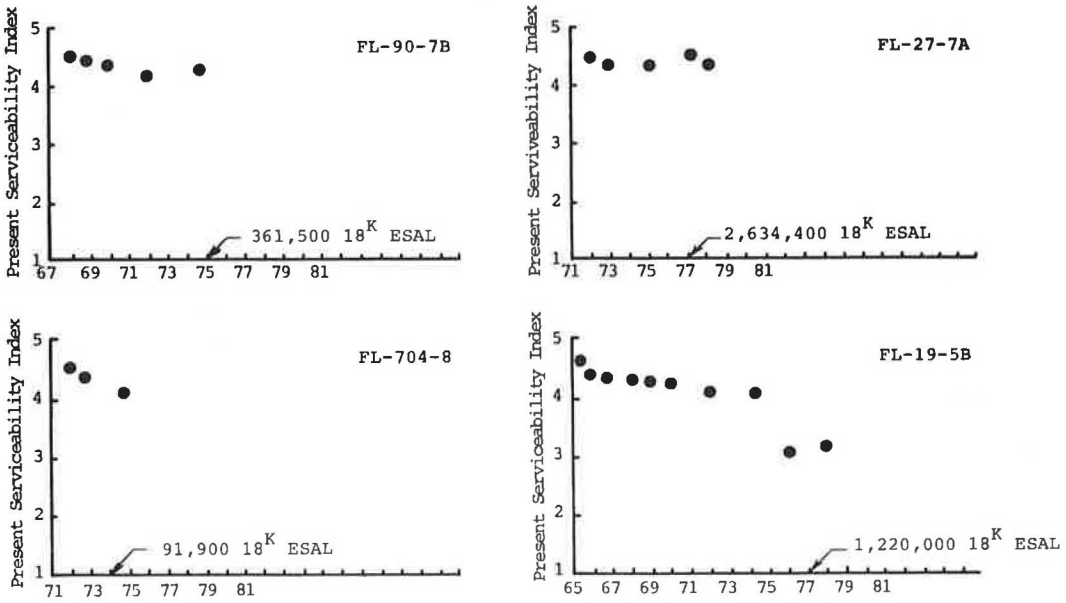

FIGURE 3 Measured PSI, Florida test sections.

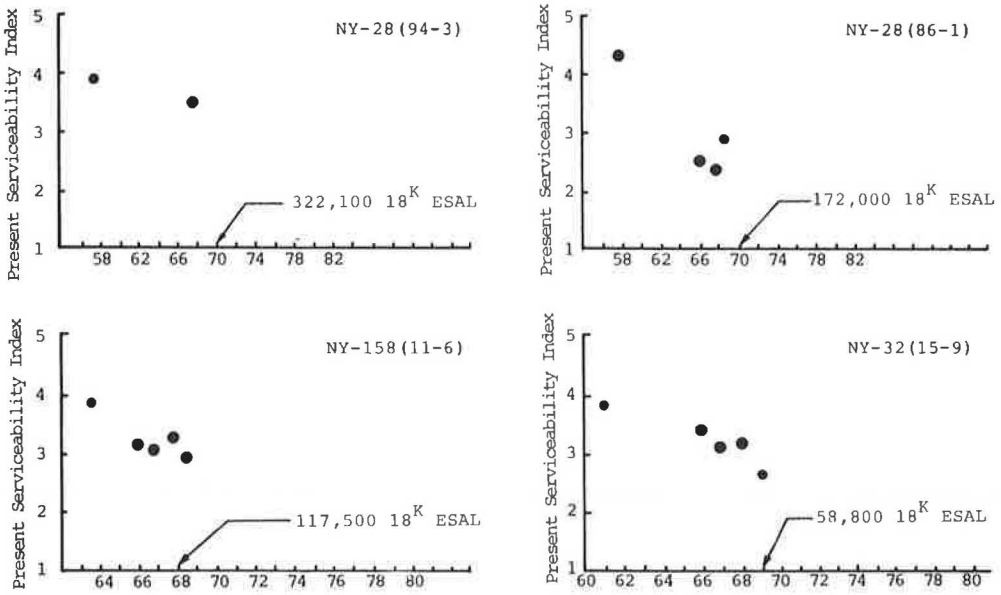

FIGURE 4 Measured PSI, New York test sections.

Its development is believed to have been well-founded but based on a limited data base, and it requires input data that are frequently not available and thus must be developed on the basis of approximate relationships. Even with these approximations, the model appears to generally provide reasonable predictions of serviceability loss. It is not clear whether the two overpredictions out of the eight examples studied were caused by a tendency toward overprediction by the models or caused by high estimates of clay content. It should be noted, however, that use of a clay content of 30 percent in lieu of 35 percent for test section CO-96(1) would have reduced the predicted ΔSI by 45 percent and resulted in a reasonable prediction. Similarly, a reduction of 5 percent in clay content from 33 to 28 percent for test section TX-82(2971) would have reduced the predicted SI by 47 percent and would also have resulted in reasonable predictions.

The overall evaluation of the proposed model is that it is likely as reliable as the other models available for predicting change in PSI, including the AASHO equation and those developed during the "cost allocations" project (1,4) for total change in PSI.

The approach to differentiating between load-induced serviceability loss and that caused by differential volume change because of expansive clay subgrades was to assume that the predicted change in serviceability from the VESYS III-B regression equations is the total predicted change in PSI (as it should be). That assignable to load-induced effects will be the total predicted change in PSI using the flexible pavement models, less that calculated by the expansive clay model. Where the serviceability loss caused by the expansive clay exceeds that predicted for the axle loads, the serviceability loss is assumed to be caused by the environment. As the serviceability loss caused by traffic increases with axle load applications and begins to exceed that attributable to the clay subgrade, the difference is attributed to the axle loads.

The approach adopted does not deal directly with combined roughness, but it is believed to be an advancement of the state of the art in understanding roughness in pavements and the consequent reduction in serviceability. The ability to divide sources of roughness more accurately between the environment and axle loads must await substantial future research.

ACKNOWLEDGMENTS

Support for this work was provided by FHWA, U.S. Department of Transportation, through contract DTFH61-80-C-00175 with Brent Rauhut Engineering, Inc., and by the Texas State Department of Highways and Public Transportation through support of Research Study 2-8-80-284 conducted by the Texas Transportation Institute. The authors are grateful for the valuable technical coordination provided by FHWA contract manager William J. Kenis of the Office of Research and Development.

REFERENCES

1. J.B. Rauhut, R.L. Lytton, and M.I. Darter. Pavement Damage Functions for Cost Allocation--Volume 1: Damage Functions and Load Equivalence Factors. Draft Final Report FHWA/RD-82/126. FHWA, U.S. Department of Transportation, July 1982.
2. M.O. Velasco and R.L. Lytton. Pavement Roughness and Expansive Clays. Interim Report FHWA/TX-80/282-2. Texas Transportation Institute, Texas A&M University, College Station, Oct. 1980.
3. M.O. Velasco and R.L. Lytton. Pavement Roughness and Expansive Clays. In Transportation Research Record 790, TRB, National Research Council, Washington, D.C., 1981, pp. 78-87.
4. J.B. Rauhut, R.L. Lytton, P.R. Jordahl, and W.J. Kenis. Damage Functions for Rutting, Fatigue Cracking, and Loss of Serviceability in Flexible Pavements. In Transportation Research Record 943, TRB, National Research Council, Washington, D.C., 1983, pp. 1-9.

Publication of this paper sponsored by Committee on Environmental Factors Except Frost.

Expansive Pyritic Shales

DEAN D. DUBBÉ, MUMTAZ A. USMEN, and LYLE K. MOULTON

ABSTRACT

Although much attention has been directed to the solution of problems created by swelling soils, relatively little effort has been devoted to the solution of problems created by expanding pyritic shales. This is a very real problem that has caused extensive damage to many structures in the United States and abroad. In an effort to call attention to this problem and to the need for further research directed at its solution, the current state of the art with respect to swelling pyritic shales is presented and discussed. The factors and mechanisms responsible for swelling of pyritic shales are identified; methods of testing and evaluating the potentially expensive shales are outlined; and ways of controlling or eliminating the problem are summarized. A number of case histories involving experiences with expansive pyritic shales are included to illustrate the potential seriousness of the problem and to underscore the need for additional research.

It has been reported that the average annual losses in this century from floods, earthquakes, hurricanes, and tornadoes have been less than one-half of the damages from expansive soils (1). Geotechnical engineers who deal with expansive soils or shales have been faced with the decision of either accepting a certain risk in view of the uncertain response of foundation materials to changing environmental conditions or choosing safe but generally expensive foundation systems. There has been a general reluctance to adopt the latter approach because it has appeared that strengthening the foundation can sometimes cost more than correcting the damages that can result from foundation heaving. It is important to note, however, that whereas considerable money has been spent to control floods, relatively little has been invested to develop and implement methods for controlling or mitigating damages associated with foundation heaving.

A family of expansive materials that has caused significant damage to many structures, but has been widely overlooked, is pyritic shale. In the past damage to structures by expanding pyritic shale was not readily identified. Consequently, damages were often attributed to differential settlement, frost heave, subsidence, or poor construction practices. More recently, however, the problems associated with expansive pyritic shales have been better recognized. Spanovich (2) suggests that part of the reason for an increased frequency of problems caused by expanding shale is a result of advances in powerful excavation equipment that can produce greater cuts and expose deeper fresh shale strata, and also as a result of the increased use of slab-on-grade construction (because of economic constraints) without providing crawl spaces to absorb heave.

Shale is a sedimentary rock formed by the compaction and cementation processes acting on clay, silt, and sand particles. Compaction shale is a transition material between soil and rock susceptible to significant weathering and slaking, whereas cemented shale exhibits the general characteristics of sounder rock (3). Because of its abundance (it constitutes about 50 percent of all exposed rock), shale is often used as an engineering material to build fills and embankments, highway bases in certain cases, and as a foundation for all types of structures, including bridges and other transportation structures. Extensive studies have been conducted on the evaluation of many shales for highway use (4-9), but little attention has been directed in these studies to pyritic shales either as a construction or foundation material.

The importance of understanding the nature of pyritic shale is two-fold. First, it is an expansive material for which the mechanism of expansion or swelling is different from what is known for ordinary shales or soils (10). The swelling phenomena observed in pyritic shales are primarily caused by the volume changes induced by the chemical alteration of sulfide minerals. Second, lechate from pyritic shale can attack concrete and cause deterioration. This phenomenon is known as "sulfate attack" (11) and also results from the chemical alteration of minerals, this time leading to volume changes in concrete.

The purpose of this paper is to summarize the existing information and knowledge on pyritic shales. Factors and mechanisms of swelling in pyritic shales and experimental methods of evaluating swelling potential are reviewed. A number of case histories related to heaving damage and concrete deterioration are presented and discussed. Finally, known methods of controlling the problem are described and research needs are identified.

FACTORS AND MECHANISMS OF SWELLING IN PYRITIC SHALES

Primary and Secondary Reactions

Heave observed in certain shales has been identified to be the result of the oxidation of sulfide minerals, the most common of which are pyrite and marcasite. Pyrite, or ferrous disulfide (FeS_2), is a yellowish mineral with a metallic glint that long ago earned the name of "fool's gold." Pyrite is generally regarded as stable or slightly reactive under normal conditions; however, on exposure to dampness for a long period in the presence of air, it oxidizes and expands. Pyrite is widespread, being the most common iron sulfide mineral. It occurs in rocks of all types and geologic ages, most often in metamorphic and sedimentary rock. Marcasite has the same chemical formula as pyrite, but X-ray analysis reveals a different atomic arrangement. Marcasite is generally gray in color and is more susceptible to oxidation than pyrite. However, it is less abundant than pyrite (12).

Crystallographically, the oxidation and expansion mechanisms of the sulfide minerals to sulfate are quite readily understood. The pyrite structure is stacking of close-packed hexagonal sheets of sulfide ions with iron occupying the interstices of the sulfide layer. The packing density of this configuration is related to the radius of the sulfide ion, which is 1.85 angstroms, producing a volume of 26.14 cubic angstroms. In the sulfate structure, each atom of sulfur is surrounded by four atoms of oxygen in

tetrahedral coordination. The packing density of the corresponding sulfate compounds will depend on the radius of the sulfate ion, which is 2.805 angstroms. This results in a volume of 94.4 cubic angstroms, which represents an approximate volume increase of 350 percent per packing unit (13). If calcium is present, gypsum may be formed, which may give rise to an eight-fold increase in volume over the original sulfide (14).

The primary oxidation reactions occurring in the sulfide alteration process are thought to be as follows (15):

$$2FeS_2 + 2H_2O + 7O_2 \rightarrow \underset{\text{ferrous sulfate}}{2FeSO_4} + \underset{\text{sulfuric acid}}{2H_2SO_4} \quad \text{(I)}$$

$$\underset{\text{ferrous sulfate}}{4FeSO_4} + O_2 + 2H_2SO_4 \rightarrow \underset{\text{ferric sulfate}}{2Fe_2(SO_4)_2} + 2H_2O \quad \text{(II)}$$

$$\underset{\text{ferric sulfate}}{7Fe_2(SO_4)_2} + \underset{\text{pyrite}}{FeS_2} + 8H_2O \rightarrow 15FeSO_4 + 8H_2SO_4 \quad \text{(III)}$$

Reaction I will normally proceed unaided, although the oxidation of the sulfide may be assisted by autotrophic bacteria. Reaction II is thought to be entirely due to the ferrobacillus-thiobacillus bacteria, because the reaction cannot proceed in an acid environment. This was shown by Goldhaber and Reynolds (16) in a series of experiments. Data obtained on samples drawn periodically and analyzed for total sulfur in solution, thiosulfate and sulfate, indicated that the rate of oxidation increased markedly as pH increased, particularly above a pH of 7. Reaction III oxidizes more pyrite by reacting with ferric sulfate, a strong oxidizing agent produced in Reaction II.

Gypsum is known to form from the reaction of sulfuric acid with calcite. Jarosite, another main reaction product, is essentially insoluble in water and forms most readily in an acid environment (12). Gillot et al. (17) stated that when lime is present, gypsum forms together with iron hydroxides, whereas jarosite and iron hydroxides appear to be the main reaction products when lime is absent.

Some secondary minerals are also formed from the chemical reactions (2). These minerals are (a) melanterite, an aqua to white mineral that will dissolve in groundwater; (b) rozenite, an aqua to white, stringy mineral that forms by the loss of bound water when sulfuric acid dehydrates melanterite; (c) coquimbite, composed of soluble, blue-green or white crystals that form with alternate wetting and drying of rozenite; (d) kaolinite, a white, powdery, stable clay mineral that remains in addition to jarosite; and (e) limonite, a rusty, red powder or stain that results from the further breakdown of jarosite.

The roles of the primary and secondary reaction products derived from the oxidation of sulfide minerals are somewhat controversial. This is particularly true in the case of gypsum. It is not thoroughly understood whether heave is caused by the formation of gypsum crystals or whether gypsum only exhibits a void-filling function. However, there is general agreement that the secondary minerals--jarosite, rozenite, coquimbite, kaolinite, and limonite--serve only to occupy voids formed during the expansion process.

Studies performed on black shales in Pennsylvania, West Virginia, and eastern Ohio have suggested that the expansion of pyritic shales is sometimes erroneously attributed to the formation of gypsum crystals that only inhabit voids vacated by dissolved minerals (17). However, Quigley et al. (18) and others (12,19-21) state that the growth of gypsum crystals within shale is the primary cause of heave. Resolution of this issue is of practical as well as theoretical importance. If heave is caused by the formation of gypsum, black shales that are essentially free of calcite would be considered safe from an engineering standpoint because the supply of calcium ions would be limited and the amount of gypsum formed would be small.

The chemistry of the formation of gypsum in pyritic shales appears to be rather straightforward, involving an attack on calcite by sulfuric acid formed by the oxidation of pyrite. The acid reacts with calcite to produce a calcium sulfate solution that may be transported to the site of crystallization. The alteration products (gypsum) are frequently located near existing pyrite, which indicate that they precipitate out of solution and begin to grow after traversing a short diffusion path (17). As crystallization proceeds, additional solution is brought in from surrounding areas by capillary action, and the growing crystals force the shale layers apart. This process is analogous to frost heave by ice lenses.

By the use of a scanning electron microscope on samples of weathered pyritic shale, Grattan-Bellew and Eden (22) found that gypsum can form in two morphologies: (a) bundles of fibers growing normal to the bedding planes of the shale, and (b) flat, blade-shaped crystals growing parallel to the bedding planes. Examination of large quantities of heaved shale has revealed that the major cause of heave is the growth of the bundles normal to the laminations. Why some of the gypsum forms bladelike crystals while others form bundles is not fully understood. It is speculated that the presence of iron salts and the physical conditions present during the crystallization may modify the morphology of gypsum crystals.

An interesting argument for the expansion of pyritic shales caused by the growth of gypsum crystals is presented by Coveney and Parizek (23). According to these researchers, gypsum, the chief host of sulfur in the weathered rock, is considerably less dense (specific gravity = 2.36) than pyrite (specific gravity = 5.02), the chief host mineral in the unweathered rock. The sulfur-bearing minerals in the weathered rock occupy nearly twice as much volume as that in the fresh rock. Thus gypsum formed by weathering occupies about twice the volume of pyrite, causing the shale to swell roughly 1.55 percent by volume. Because the shale is effectively confined at the bottom and the sides, this would result in thickening of the shale layers by that percentage, which would yield an average floor uplift of 0.8 in. for a 4- to 5-ft-thick pyritic shale layer. This alone would be too small to account for the observed heave in many cases. However, these calculations fail to consider that the gypsum crystals occupy only a small portion of the volume of the space they form. Observations of a polished surface of a typical veinlet show that only 27 percent of the plane surface area is occupied by gypsum crystals and the remaining 73 percent consists of voids. The pore space developed by gypsum growth thus amounts to a minimum of three times the space occupied by the gypsum. Taking this into account, an overall volume increase of 8 percent can be expected. This would correspond to a heave of about 4 to 4.5 in. for the same 4- to 5-ft pyritic shale layer, which is in general agreement with heave observed at some sites. The magnitude of the uplift force created by this mineral growth has not been accurately determined, but it has been suggested that heave pressures as high as 12,000 lb/ft^2 may develop (2).

Although melanterite is another possible reaction product that can contribute to the expansion phenomena in shales, it has not been possible to identify its role clearly. This is because it is unstable and reverts to an anhydrous powder form on exposure to normal room temperature and atmosphere (12). It is also extremely soluble; therefore, the usual sampling of the shale by core drilling would most likely dissolve and wash out the melanterite crystals, leaving little if any evidence that the mineral was present.

Role of Autotrophic Bacteria

Some controversy has arisen in the discussion of whether or not autotrophic bacteria are in part responsible for the expansion of pyritic shales. It is suggested by some researchers (15,18,21) that the bacteria play the role of a catalyst in the oxidation of sulfides to sulfates. As Berard (24) points out, however, the oxidation of the sulfide minerals will proceed without any bacteria assistance, but it is certainly catalyzed by oxidizing bacteria. In the case of unstable minerals such as pyrite and pyrhotite, bacterial action is not necessary to produce rapid oxidation. Given the right oxidation potential, which is often found in soils above the water table, these two sulfides will transform into lower free energy minerals.

The origin of the autotrophic bacteria can be most easily identified by observing the geologic origin of black shales. Black shales are believed to have formed in stagnant marine environments characterized by reducing conditions in which organic mineral collected and anaerobic bacteria were active. The common bacteria present were those whose role was to reduce sulfates to sulfides in the bottom muds. These bacteria play a role in the formation of black shale, whereas the oxidizing autotrophs of the thiobacillus type are functional in the heaving process (18).

The autotrophic bacteria grow and multiply using energy from the oxidation of inorganic compounds. Thiobacilli bacteria are probably most active in the early phases of the reaction, whereas ferrobacilli play a dominant role only later when there is a reduction in pH because of the production of sulfuric acid. Sulfuric acid is formed in the oxidation reactions and produces an environment favorable to the growth of this type of bacteria. According to Penner et al. (15), these bacteria require an acid environment with an optimum pH of 2.2. They are known to go into dormancy at a pH value greater than 4.5, and optimum temperature is thought to be around 95°F.

Additional Factors That Influence Heaving

In addition to the previously mentioned factors, there are still other factors that merit consideration and discussion. These include groundwater and site grading.

Groundwater

The exact role of groundwater in the heaving process is not clearly understood. Studies have indicated that if the sulfide-bearing stratum is totally submerged, the heaving process does not occur, most likely because of the absence of necessary oxygen (21). On the other hand, the oxidation of potentially exp nsive sulfide minerals will begin in an environment relatively free of water, such as that above the water table (24). Therefore, the lowering of the groundwater level by excavation or peripheral drains around the structure may help trigger the oxidation and consequently the expansion of the sulfide-bearing stratum.

Site Grading

The excavation of soil above strata that contain potentially expansive sulfide minerals may enhance the oxidation of sulfide minerals. First, grading may remove the weathered rock and thus expose fresh rock that contains a higher concentration of sulfide minerals (2). Second, removal of overburden pressure can cause slight rebounding and fracturing in the underlying strata, further exposing the sulfide minerals to air and moisture (25). Finally, a secondary effect of excavation is that the structure is placed closer to the sulfide layer, which may cause a loss of any insulation of the sulfide-bearing stratum from the heat of the structure. This insulation from heat given off by the structure is important. As emphasized by Berard (24), a temperature gradient is responsible for the upward migration of water and dissolved oxygen, which in turn causes the oxidation of the sulfide. In addition, Quigley and Vogan (21) suggest that a warmer, more humid environment caused by the higher temperatures is more favorable to the growth of bacteria.

TESTING AND EVALUATION OF SWELLING POTENTIAL

A number of testing schemes are available to evaluate the swelling potential of shales in general and pyritic shales in particular. These are the free swell test and the modified swell test (14,26), induced gypsum crystal growth (20), and total sulfur analysis (12). Although the results of these tests generally give a good indication of the amount and rate of swelling expected in situ, the reliability of quantitative predictions is not well established.

Free Swell Test

In the free swell test the rock core specimen rests on a pedestal mounted to the base of a rigid frame, as shown in Figure 1 (26), and is permitted to expand unrestricted in all directions. The amount of swelling is measured in the vertical direction with a dial gage, which is initially zeroed against a standard stainless-steel bar. As noted earlier, the expansion of shaley rocks is significantly larger in the direction perpendicular to the bedding planes

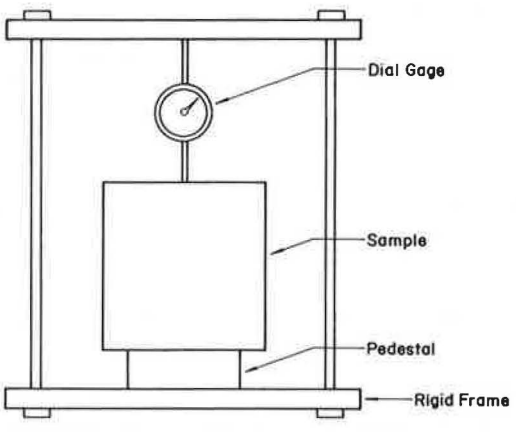

FIGURE 1 Free swell test apparatus *(26)*.

than in a direction parallel to the layering. The testing assembly is stored in a curing room under conditions of 100 percent humidity and is removed periodically to take readings. The strains calculated from these readings can be plotted as a function of elapsed time (log scale) to get an indication of the amount of swelling expected to occur in the field (14).

Modified Swell Test

The modified swell test is a semi-confined test in which the rock sample is submerged in distilled water and the strains are monitored in one direction by a dial gage, as shown in Figure 2 (14). A constant load is applied to the rock sample in the direction of measurement while deformation in other directions remains unrestricted. Again the test data can be analyzed by a semi-logarithmic plot of strain versus time. The average slope of such a plot gives an index of swelling potential, which indicates the tendency of the rock to expand on stress relief (14).

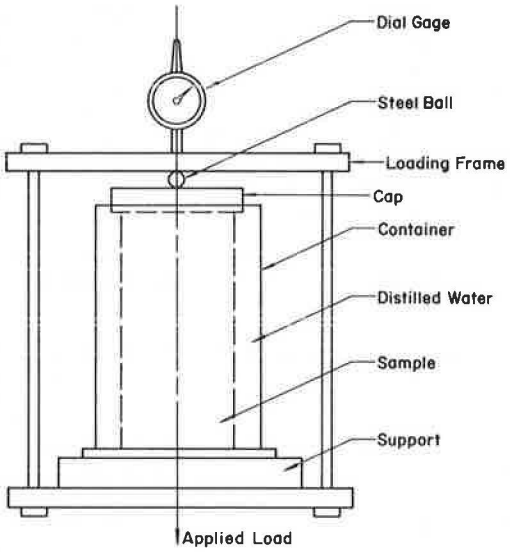

FIGURE 2 Modified swell test apparatus (14).

It should be noted that the modified and free swell tests are simple and inexpensive to carry out. For this reason it becomes easy to perform a large number of tests to aid in the evaluation of potential problems. The major drawback with these tests, however, is that they are time-consuming. Reactions that cause swelling generally take long time periods.

Induced Gypsum Crystal Growth

In the induced gypsum crystal growth test a modified one-dimensional consolidometer is used to monitor heave in shale while gypsum crystal growth is induced artificially (20). The testing device resembles a fixed-ring consolidometer used in soil testing with the addition of two fluid inlets and reservoirs located on opposite sides. Specimens are exposed to solutions of $CaCl_2$ and $(NH_4)_2SO_4$ induced simultaneously under the same head at opposite fluid inlets. The reaction to form gypsum crystals in this case is

$$CaCl_2 + (NH_4)_2SO_4 + 2H_2O \rightarrow \underset{\text{gypsum}}{CaSO_4 \cdot 2H_2O \downarrow} + 2NH_4Cl$$

The samples remain submerged during the entire period of testing, and volume change is monitored throughout the test. After completion of testing the samples are removed for photographing and are analyzed by a scanning electron microscope or by X-ray diffraction to monitor gypsum formation.

Total Sulfur Analysis

In total sulfur analysis the total sulfur content of a sample is assumed to consist of sulfate, pyritic sulfur, and organic sulfur. The amount of sulfate sulfur represents a measure of the degree of oxidation, and thus gives an indication of the amount of expansion that has taken place in the sample before sampling. The amount of pyritic sulfur represents the amount of potential expansion that can take place when all of the sulfides completely oxidize. The organic sulfur content, which is needed to complete the measure of total sulfur, is not believed to be involved in the expansive reaction (27). Total sulfur analysis is valuable in assessing probable ultimate heave values and percent heave to which a structure has already been subjected.

Sampling

Sampling for the tests previously described must be executed with great care. The usual types of samples tested for potentially expansive sulfide minerals are rock cores and samples removed by hand from excavations. If sampling is to be done at a site where heaving has occurred, no water should be used in the drilling operation, because the drilling water may wash out or dissolve some or all of the melanterite crystals. At sites where heaving has already occurred, test pits are a preferable method of investigation and sampling (12). Specimens for testing should be prepared for such testing as soon after sampling as possible. The rock cores or other samples should be wrapped in plastic immediately at the site to minimize changes in the natural moisture conditions.

In the case of testing the samples for autotrophic bacteria, extracts of water samples from boreholes should be incubated in a ferrous sulfate medium at a pH of 2 to 3 for 2 weeks on a rotary shaker to establish if microorganisms exist. The samples should then be examined microscopically for the presence of autotrophic bacteria of the thiobacillus ferroxidan and ferrobacillus ferroxidan types (17).

PROBLEMS RESULTING FROM PYRITIC SHALES: CASE HISTORIES

The following case histories illustrate factors that contribute to the expansion of pyritic shales and demonstrate the potential damaging consequences of such expansion. In addition, some of the case histories presented demonstrate that the oxidation of pyritic shales can lead to reaction products that can cause damage to structures through concrete deterioration, which could perhaps be more widespread and more devastating than the heaving problem. Methods of solving the problems illustrated in the case histories will be discussed in a general manner later in the paper.

West Virginia University Hospital and Basic Sciences Building

The investigation of the West Virginia University (WVU) Hospital and Basic Sciences Building was performed by Triad Engineering Consultants, Inc., of Morgantown, West Virginia, in September 1981 (28). The building exhibited signs of distress in the form of cracking in the non-load-bearing tile walls, along with noticeable heaving of the concrete floor slabs. Black carbonaceous shales containing pyrites were found in the rock strata below the building. An investigation was performed to see if the wall distress and floor heave could possibly be attributed to underlying expansive shales.

The distressed areas were found at various locations over the complete building site; however, the areas of greatest distress appeared to have occurred on the ground floor. Primarily, these distressed locations were most severe in areas that overlie the black shale strata located relatively near the edge of the excavation for the construction of the basement.

The evaluation of the expansive shales revealed that the black carbonaceous seam appeared to be the cause of heaving and cracking in the floors and walls. The shale seam generally lies below the ground floor elevation and above the basement floor elevation, and has a variable thickness ranging from 0.9 to 2.6 ft. When the basement area was excavated, most if not all of the black shale was removed from under the proposed basement floor. For this reason, the heave appeared only in the ground floor and not in the basement.

The total sulfur test was performed on samples obtained from areas of heave. In the black shale the percentage of total sulfur varied between 1.86 and 5.96, depending on location. The percentage of sulfate sulfur ranged from 0.03 to 1.61; however, the higher values were found on samples obtained from under areas where floor heaving and distress cracking were the severest. This conformed to previous research, which found that the expansion of the shales is caused by the reaction of the pyrites into various forms of sulfates. In general the movements occurred near the edge of the basement excavation, but just a few feet away from the edge of the excavation cut little or no movement occurred. Also, the percentage of sulfate sulfur was greater in the black shale nearest to the cut of the basement and decreased with increasing distance from the cut face.

It was suggested that the reason for increased swell next to the cut was because of the excavation. The excavation for the basement intersected the black shale seam that allowed air and aerated groundwater into the shale, which reacted with the pyrites.

The areas where expansion of the shales had already occurred had not undergone the total amount of expansion possible because considerable amounts of pyrites had not reacted. Because of the relatively short monitoring period, the amount of additional expansion could not be accurately determined; however, it appeared that the expansion at the time of testing had not yet reached 50 percent. Also, it was noted that as the heave continued the rate of expansion should increase because the rock strata becomes more fractured, which would allow access of more air and aerated water to unreacted pyrites.

Wheeling Hospital

Heaving of floor slabs, partitions, and column coverings was observed in portions of the basement of the Wheeling Hospital following flooding of the lower levels of the hospital on Labor Day 1975. In addition, the elevator shaft of the hospital also appeared to have heaved upward as observed by the cracking of the floor slabs adjacent to the elevator shaft in the upper floors.

The initial foundation investigation report for the hospital, which was completed in July 1970, indicated the presence of potentially expansive pyritic shales within the foundation and recommended protective measures to be taken to reduce or eliminate expansion. A later investigation in June 1980 reported the presence of these expansive shales and their reaction products beneath one of the most badly heaved areas of the basement floor slab. Later in 1980 a rather extensive set of elevation readings was taken on the floor slab, and heave monitoring positions were established to permit more precise measurements of heave to be made on a regular basis.

In June 1982 Triad Engineering Consultants, Inc. (27), was contacted to perform an independent investigation of the situation to verify the presence and areal extent of the expansive shale problem, to determine the potential long-term effects of the expansive shales in terms of how much additional movement can be expected and over what time period, and to suggest possible remedial measures to solve the problem. The investigation included damage inspection, borings, examination and testing (by total sulfur analysis) of soil and shale samples obtained from the distressed areas, and the correlation of the test results with heave measurements to predict the magnitude and rate of future heaving.

The foundation material was found to consist of a heterogenous fill containing silty clay, sand, gravel, pyritic shale, and coal fragments underlain by pyritic gray shales up to a depth of 11.5 ft below the basement level. No groundwater was encountered. Sulfur content tests indicated that total sulfur percentages varied from a low of 1.49 to a high of 4.84 in the gray shale. The sulfate sulfur contents varied between 0.01 and 2.70 percent, with higher values generally indicating good correlation with the amount of heaving observed. It was concluded that heaving was a direct result of expansion caused by the oxidation of sulfide minerals in the underlying soil and rock.

Based on the elevation readings provided, use of linear time-heave curves, and an average volume expansion factor calculated by dividing the apparent heave by the volume of sulfates formed to date, it was estimated that up to approximately 4 in. of heave had occurred through July 1982. The future or remaining heave was estimated as the product of the same expansion factor and the volume of the unreacted pyrites in the underlying strata; it was projected to be as much as 11 in.

In this instance the pyritic shales causing heaving of the basement floor were found to be mostly close to the surface, and therefore the most effective and economical type of remedial construction would involve the removal of the existing floor slabs, the excavation of the pyritic shales, backfill with well-compacted granular material, and the construction of new floor slabs. The only reasonable solution to the heaving problem for the elevator shaft appeared to be the installation of a system of rock anchors to prevent future heaving. However, the expected rates of heaving were relatively slow. Consequently, although these remedial measures will eventually be necessary, it was not recommended that they be undertaken immediately.

WVU Engineering Sciences Building

The Engineering Sciences Building consists of a 10-story tower section surrounded on three sides by

low-rise structures. Shortly after the building was constructed in 1959, some minor cracking and distress were observed in the floor slabs and non-load-bearing walls. Movements have continued until the present time, and maintenance has been performed periodically. Detailed maintenance records were not kept; however, it appears that expensive repairs were made twice and possibly three times during the 1960s. Since the summer of 1971, movements apparently accelerated according to maintenance personnel.

Level surveys of the building were conducted to determine the vertical direction of movement (i.e., heave or settlement) and to obtain an approximate measure of the amount of movement. The survey indicated that little or no movement has occurred under the tower section of the building. The section of the building where the basement floor is supported on grade had experienced the largest movements and the heaviest damage. Slabs on grade have heaved up to 2.5 in. and column foundations have heaved up to 3.0 in.

A subsurface investigation was conducted to determine the nature of the material causing the heave. Pyrites were encountered in all of the borings drilled as part of the geotechnical investigation. Borings and test pits, made from the level of the basement floor, found such sulfate minerals as gypsum and jarosite crystals and limonite staining on the bedding planes, all evidence of previous expansion of sulfide minerals.

Chemical analyses were performed on several of the rock samples to determine the sulfur content. It is suggested that a sulfide content as low as 0.5 percent is potentially expansive, and a sulfide content of greater than 1 or 2 percent is considered highly expansive (25). The test results indicated that the rock had high expansion potential as evidenced by both the total sulfur and the sulfide sulfur contents.

It appeared that the excavation for the building removed 30 to 50 ft of overburden soil, which allowed the joints and bedding planes to open slightly. The bedding planes are nearly horizontal, and the rock is relatively impervious in the direction perpendicular to the bedding. Therefore vertical penetration of air and moisture was restricted. Thus only surficial expansion of the rock, which is relatively small, was possible in the subbasement of the building where vertical penetration of air and moisture took place. This was not the case for the rock behind the retaining walls separating the subbasement and basement sections. Here the bedding planes are exposed to lateral infiltration of air and oxygen-rich water, which migrate horizontally with little resistance, including the chemical reaction leading to heave. As a result, approximately 7 to 10 ft of rock below the basement floor near the retaining walls is participating in the expansion, whereas probably only 2 or 3 ft of rock is participating in the expansion below the subbasement. Consequently, the heave is maximum near the retaining walls and decreases with increasing distance from the walls. In addition, it was found that, considering the sulfur content of the rocks below the Engineering Building and the thickness of the rock that might be involved in the heave, it is reasonable to expect that the ultimate heave might be twice the present magnitude.

A program of remedial construction designed to correct these problems will be undertaken in the near future. The heaved floor slabs will be removed and replaced with a structural floor system supported on columns founded below the expansive strata. Those column footings that have heaved will be tied down with rock anchors to prevent future heaving.

Three-Story Steel Frame Building in Pittsburgh

A three-story steel frame building in Pittsburgh (29) with masonry exterior was built on natural soil. Heavy concentrated column loads were supported by spread footings bearing the bedrock. The upper surface of bedrock was a thin layer of black carbonaceous shale about 18 in. thick. Beneath this was a layer of limestone 3 to 4 ft thick, and the next 4 ft were gray weathered clay shale interbedded with limestone.

The first portion of the building was built in 1931, and subsequently several additions were constructed. Crack damage was first reported in 1950 in the first floor walls and slabs. The damage spread through the second and third floors and increased slowly at a uniform rate. The concrete floor of the gymnasium heaved in 1954 and was 6 in. higher in the center than the perimeter. The floor was replaced in 1956, and during the next 15 years the gymnasium floor again developed a differential movement of 4 in.

Two test borings were drilled inside the building. The shale beneath the floor slabs and footings was examined petrographically and chemically. Iron sulfides and their alteration products from the oxidation of the sulfides were found in various mineral forms. It was concluded that air or moisture or both caused the alteration and expansion. Heat from a utility tunnel beneath the floor slabs around the perimeter of the building probably accelerated the reaction. The amount of sulfur and sulfate in the altered shale compared with the unaltered sample indicated that the oxidation would continue and that the amount of total expansion would be twice the amount that had already occurred.

Black Shale Heaving and Concrete Deterioration in Ottawa, Ontario, Canada

The Therapy Treatment Building of the Rideau Health and Occupational Center located in southeast Ottawa is a two-story building with basement areas, an area without basement, and a deep swimming pool, all founded on shale bedrock. The two-story portion without the basement and founded on intact rock experienced heave, whereas the basement area and the swimming pool were not affected. The concrete floor slab heaved up 3 in. between 1965 and 1969. The floor of the second story auditorium was also considerably warped, indicating that the interior columns also had heaved.

A concrete heating and service tunnel was constructed in a trench dug into rock around the perimeter of the two-story building. The central mass of the shale bedrock was not excavated and forms a horizontal rock plateau 6 to 7 ft above the bottom of the service tunnel. The interior columns of the building are founded on this rock plateau and are lightly loaded, as they support only the weight of the second floor auditorium. The ground floor slab consists of concrete poured over about 18 in. of granular material on top of the rock plateau. During the winter the service tunnels are hot (about 85°F). During the summer, when the heat is off, the rock is probably close to ambient rock temperature.

The important heave mechanism at this site was believed to be geochemical alteration of sulfides in the shale bedrock to secondary sulfates having a much greater volume. The amount of secondary gypsum

found in the core samples was noted to correspond to the amount of heave.

Quigley and Vogan (21) presented the following explanation for the secondary gypsum growth related to this case.

1. Secondary gypsum occurred above the water table in a zone that was probably partially saturated by capillary rise. The environment was humid because of the heat from the service tunnel, which was ideal for the growth of aerobic, oxidizing bacteria, which were confirmed to exist from cultures grown in the laboratory.
2. Chemical analysis confirmed the presence of sulfur in the black shale (as pyrite).
3. Autotrophic bacteria of the thiobacillus and ferrobacillus ferrooxidan types, found in the groundwater at the site, derived their energy from oxidizing pyrite or ferrous sulfate.

It was hypothesized that these bacteria catalyzed the oxidation of pyrite in shale, producing sulfuric acid. This sulfuric acid slowly dissolved the calcite in the rock, altering it to gypsum. The gypsum migrated in a much larger volume and exerted pressure on the structure above.

At the St. Luke Church in the New Edinburgh area of Ottawa, Ontario, extensive heaving was reported (22) in the basement floor, and it was suspected that this was caused by the expansion of pyritic shale. The building is underlain by a black carbonaceous shale that contains about 5 percent organic matter, 8 percent calcite, and 4.25 percent pyrite. The investigation also revealed an interesting secondary consequence of pyritic shale oxidation in the form of concrete deterioration caused by the attack by sulfate solution formed by the oxidation of pyrite in the underlying shale.

The church was constructed in 1913, but after 15 to 20 years the basement floor had to be repaired and was covered with a new layer of concrete at the time, because the original concrete, lying directly on the weathered black shale, was severely deteriorated. The uneven thickness of the new concrete suggested that the original floor had already heaved. The floor was reexamined in 1974 and the upward movement was estimated to be 2.5 in. It was confirmed through investigation that heaving had resulted from the growth of gypsum crystals between the bedding planes in the shale.

The mechanism and causes of heave were similar to those already discussed; however, deterioration of the concrete was also significant. Examination of the old concrete with a binocular microscope indicated that the cement had been largely removed, leaving large voids between the aggregate particles. According to Reading (11), when concrete is subjected to acid attack, it is usual for the soluble phases of cement to be removed, leaving a weak porous material, such as what was observed in this case. Calcite is usually a major constituent of old concrete; however, because of the acid attack, it had largely been removed in this case.

Concrete Deterioration in Oslo, Norway

For more than 60 years the construction industry in Oslo, Norway, has been plagued with the problems of concrete deterioration and foundation upheaval. The unstable forms of the iron sulfide mineral in the shales in the Oslo area are pyrite and pyrhotite ($FeS_{1.4}$). The rate of oxidation of pyrhotite is extremely rapid. In fact, in its natural state it can be kept in moist air for only a short while. It appears that pyrhotite can also accelerate the oxidation of pyrite.

Moum and Rosenqvist (30) report that normal sulfate attack may take several years to cause any noticeable damage, whereas water from the alum shale containing ferrous sulfate has caused considerable deterioration in a few months. For example, the concrete walls of an underground bomb shelter built in an alum shale area softened and deteriorated in about 9 months.

According to the authors, the mechanism of attack is closely related to the composition of sulfate solution entering into the system. In the alum shale the solution contains bivalent iron, which is later partially oxidized to trivalent iron. There are differences in the types of effects produced by sulfuric acid, sodium sulfate, and bivalent iron sulfate as they attack concrete. Sulfuric acid mainly attacks the surface of the concrete and dissolves the cement gel and paste. The sodium sulfate solution, on the other hand, may penetrate the concrete without immediate reactions at the surface, but the quantities of sulfate brought into the concrete may be much higher. In the interior of the concrete the sulfate will react with tricalcium aluminate (C_3A) in the cement to form ettringite crystals, which occupy a much greater volume than the C_3A. In contrast to these two types of attack, bivalent iron sulfate may penetrate the concrete in the same way as the sodium sulfate solutions, but may carry with it even higher concentrations of sulfate. In the interior of the concrete the solution has a tendency to decrease the pH rather than increase it, thus leading to either a typical sulfate attack or an acid attack.

With respect to the deterioration of special concrete, Moum and Rosenqvist (30) found that the alum shale solutions appear to attack air-entrained concrete more quickly than other concretes. However, sulfate-resistant concretes appear to perform well.

METHODS OF CONTROLLING THE PROBLEM

What can be done to deal with pyritic shales? Unfortunately, understanding the problem does not necessarily ensure the findings of an appropriate solution. However, a number of corrective measures have been suggested and used with some success. Some of the methods of controlling the problem include (a) avoiding the sulfide-bearing shale, (b) controlling or inhibiting the oxidation of the sulfide minerals, (c) site grading to remove or to deeply bury the sulfide carrier, (d) coating with impervious material such as bitumen, (e) oxidation of the layer before construction, (f) building a structural floor system, (g) rock bolting to pin down the floor, and (h) laying a limestone aggregate base.

Avoiding the sulfide-bearing material would solve the problem, but in many instances this is out of the question. It is necessary, therefore, that a solution be found to counteract or control the heaving problem.

Controlling or inhibiting the oxidation process has proved to be a method that provides a satisfactory prevention of expansion. Shales have been flooded with a potassium hydroxide solution in Ottawa (31). It is reported that such measures have effectively counteracted heaving. This basic solution stops the growth of autotrophic bacteria that catalyze the various stages of alteration of pyrite to gypsum. It was found that 0.01 and 0.1N KOH solutions caused swelling to cease, but 1N KOH actually accelerated the rate of swelling. Along the same lines, Dougherty and Barsotti (12) found that less

rapid swelling took place with a sulfuric acid solution (pH 3.5) than with distilled water (pH 7). The instability of pyrite under basic solutions suggests that the submergence of shales in strong KOH solutions may be counterproductive by raising the pH beyond the stability field of the pyrite. In view of this, it would appear preferable to flood the shales with neutral or even slightly acidic solutions to stop the swelling.

Site grading to remove the problem material or to bury the sulfide carrier is another viable solution. Changes in the grading plan have often been used effectively. At some sites the simplest scheme is to lower the grade to completely remove the expansive material or to raise the grade above the swell-prone material to allow swell to occur, with no damage to the structure (2). Obviously, in many instances this solution may be the simplest and most cost effective. However, in other cases the depth or thickness of the expansive layer may make site grading uneconomical.

Another possible means of controlling the problem has been bitumen coating to prevent oxidation of pyrite. For years contractors and builders in the Cleveland area have followed this procedure successfully where the presence of pyrite is known or suspected (32). As part of this procedure, the shale is cut 4 in. to 1 ft above its final grade, and the entire excavated area, including the walls of the cut, is immediately given a spray or brush coat of bitumen. After all other miscellaneous work is completed and the structure is ready for concrete work, the shale is then cut in sections to the proper subgrade depth. As each section is exposed it is concreted immediately. The principal reason for this procedure is to eliminate contact between the shale and air and water. Experiments by Dougherty and Barsotti (12), as well as actual field findings by Quigley and Vogan (21), suggest that the total submergence of shale in groundwater alone will accomplish the same effects because it effectively cuts off the much needed supply of oxygen to the sulfide mineral.

Deliberate acceleration of the oxidation before development is another possibility. However, it has been noted that it would be difficult, if not impossible, to determine the location and extent of all potentially expansive materials (12). Furthermore, even if accelerated greatly, the oxidation process may take too long, making this method uneconomical in terms of actual building time.

Dougherty and Barsotti (12) have also suggested a structural floor system as a solution in some cases. A space provided between the floor slab and the expansive material would actually allow the material to swell with no adverse side effects. The footings can be placed below the potentially expansive stratum or can be designed for a dead load that is sufficient to resist heaving. As noted earlier, a structural floor system will be constructed to correct the heaving problem in the WVU Engineering Sciences Building.

Finally, two other methods proposed by Dougherty and Barsotti (12) are rock bolts and laying a limestone aggregate base. For lightly loaded structures, rock bolts could be used where bolts would be drilled into sound rock below the stratum containing the potentially active sulfide minerals and would serve as an anchor to resist uplift. In laying a crushed limestone aggregate base placed beneath the floor, the thinking is that the limestone would retard the chemical reaction and formation of melanterite. However, gypsum might form from the downward leaching of calcium and might compound the problem.

RESEARCH NEEDS

Although the causes and mechanisms of swelling in expansive pyritic shales have been generally identified, insufficient research has been done on methods of controlling or eliminating the problem. Additional research in this area is warranted. Attention should be directed to how soon the reaction may start and at what rate it proceeds after excavation and construction. Further research should also focus on testing and analytical methods of predicting the problem materials and the extent and rate of expected expansion and associated damage. One area that deserves special attention is the morphology of gypsum crystals (i.e., bundles versus flat, blade-shaped crystals) and possible physical and chemical means of controlling the type of crystal formed.

Biochemical means should be explored as a possible way to control heave. If biogenic oxidation can be halted, this might break the chain of oxidation reactions that cause swelling. Possible ways of achieving that may include chemical disinfection to kill the bacteria or creating an unfavorable environment for bacteria growth.

The sulfate attack problem on concrete from pyritic shales should also be studied further. A related problem warranting research is the environmental impact of the leachate from pyritic shales.

REFERENCES

1. D.E. Jones and W.G. Holtz. Expansive Soils: The Hidden Disaster. Civil Engineering, Vol. 43, Aug. 1973, pp. 49-51.
2. M. Spanovich. Damage to a Structure Founded on Pyrite Shale. Presented at Engineering in Appalachian Shales Conference, West Virginia University, Morgantown, June 1969.
3. J.E. Bowles. Foundation Analysis and Design. McGraw-Hill, New York, 1973.
4. J.H. Shamburger, D.M. Patrick, and R.J. Lutton. Design and Construction of Compacted Shale Embankments--Volume 1: Survey of Problem Areas and Current Practices. Report FHWA-RD-75-61. FHWA, U.S. Department of Transportation, Aug. 1975.
5. G.H. Bragg, Jr., and T.W. Ziegler. Design and Construction of Compacted Shale Embankments--Volume 2: Evaluation and Remedial Treatment of Shale Embankments. Report FHWA-RD-75-62. FHWA, U.S. Department of Transportation, Aug. 1975.
6. R.J. Lutton. Design and Construction of Compacted Shale Embankments--Volume 3: Slaking Indexes for Design. Report FHWA-RD-77-1. FHWA, U.S. Department of Transportation, Feb. 1977.
7. W.V. Strohm, Jr. Design and Construction of Compacted Shale Embankments--Volume 4: Field and Laboratory Investigations, Phase III. Report FHWA-RD-78-140. FHWA, U.S. Department of Transportation, Oct. 1978.
8. W.E. Strohm, Jr., G.H. Bragg, Jr., and T.W. Ziegler. Design and Construction of Compacted Shale Embankments--Volume 5: Technical Guidelines. Report FHWA-RD-78-141. FHWA, U.S. Department of Transportation, Dec. 1978.
9. C.W. Lovell. Use of Shale in Highway Embankments. Proc., 67th Annual Road School, Engineering Bulletin of Purdue University, Engineering Extension Series, Purdue University, West Lafayette, Ind., March 1981.
10. J.K. Mitchell. Fundamentals of Soil Behavior. Wiley, New York, 1976.

11. T.J. Reading. Combating Sulfate Attack in Corps of Engineers Concrete Construction. American Concrete Institute, Detroit, 1975, pp. 346-366.
12. M.T. Dougherty and N.J. Barsotti. Structural Damage and Potentially Expansive Sulfide Minerals. Bull., Association of Engineering Geologists, Vol. 9, No. 2, 1972, pp. 105-106.
13. E.J. Fasiska, H. Wagenblast, and M.T. Dougherty. The Oxidation Mechanism of Sulfide Minerals. Bull., Association of Engineering Geologists, Vol. 11, No. 1, 1974, pp. 75-82.
14. K.Y. Lo, R.S.C. Wai, and J.H.L. Palmer. Time Dependent Deformation of Shaly Rocks in Southern Ontario. Canadian Geotechnical Journal, Vol. 15, 1978, pp. 537-547.
15. E. Penner, J.E. Gillot, and W.J. Eden. Investigation of Heave in Billings Shale and by Mineralogical and Biochemical Methods. Canadian Geotechnical Journal, Vol. 7, 1970, pp. 333-338.
16. M.B. Goldhaber and R.L. Reynolds. Experimental Study of Pyrite of pH 5-9.5. American Association of Petroleum Geologists, Vol. 61, Aug. 1977, p. 1379.
17. J.E. Gillot, E. Penner, and W.J. Eden. Microstructure of Billings Shale and Biochemical Alteration Products. Canadian Geotechnical Journal, Vol. 11, 1974, pp. 482-489.
18. R.M. Quigley, J.E. Zajic, E. McKyes, and R.N. Yong. Biochemical Oxidation and Heave of Black Shale. Canadian Journal of Health Sciences, Vol. 10, 1973, pp. 1005-1015.
19. N.R. Morgenstern. Discussion: Black Shale Heaving at Ottawa, Canada. Canadian Geotechnical Journal, Vol. 7, 1970, pp. 114-115.
20. N.C. Lutenegger, N.C. Wallenhaupt, and R.L. Handy. Laboratory Simulation of Shale Expansion of Induced Gypsum Growth. Canadian Geotechnical Journal, Vol. 16, 1979, pp. 405-409.
21. R.M. Quigley and R.W. Vogan. Black Shale Heaving at Ottawa, Canada. Canadian Geotechnical Journal, Vol. 7, 1970, pp. 106-112.
22. P.E. Grattan-Bellew and W.J. Eden. Concrete Deterioration and Floor Heave Due to Biochemical Weathering of Underlying Shale. Canadian Geotechnical Journal, Vol. 12, 1975, pp. 372-378.
23. R.M. Coveney and E.J. Parizek. Deformation of Mine Floors by Sulfide Alteration. Bull., Association of Engineering Geologists, Vol. 14, No. 3, 1977, pp. 131-156.
24. J. Berard. Discussion: Black Shale Heaving at Ottawa, Canada. Canadian Geotechnical Journal, Vol. 7, 1970, p. 113.
25. Investigation of Damage: Engineering Building, West Virginia University. D'Appolonia Consulting Engineers, Inc., Pittsburgh (undated).
26. E. Lindner. Swelling Rock: A Review. In Rock Engineering for Foundations and Slopes, ASCE, New York, 1976, Volume 1, pp. 141-181.
27. L.K. Moulton and J. Kent. Evaluation of Expansive Shales Below the Wheeling Hospital, Wheeling, W.Va. Triad Engineering Consultants, Inc., Morgantown, W.Va., 1982.
28. Evaluation of Expansive Shales Below West Virginia University Hospital. Triad Engineering Consultants, Inc., Morgantown, W.Va., 1981.
29. A.C. Ackenheil. Building Foundations on Appalachian Shales. Presented at Engineering in Applachian Shales Conference, West Virginia University, Morgantown, June 1969.
30. J. Moum and I. Rosenqvist. Sulfate Attack on Concrete in the Oslo Region. Journal of the American Concrete Institute, Proceeding 56, 1959, pp. 257-264.
31. E. Penner, W.J. Eden, and J.E. Gillot. Floor Heave Due to Biochemical Weathering of Shale. Proc., 8th International Conference on Soil Mechanics and Foundation Engineering, 1973, pp. 151-158.
32. Structures Don't Settle in This Shale: But Watch Out for Heave. Engineering News Record, Vol. 164, Feb. 4, 1960, pp. 46-48.

Publication of this paper sponsored by Committee on Soil and Rock Properties.

Rainfall Infiltration, Drainage, and Load-Carrying Capacity of Pavements

SHANG J. LIU and ROBERT L. LYTTON

ABSTRACT

A systematic analysis is presented that simulates rainfall infiltration into the base course, and subsequently the rate of drainage out the base course into the subgrade and into lateral drainage. The method incorporates the distribution of the amount of rainfall, probabilities of wet and dry days, infiltration of water into the pavement through cracks and joints, and the drainage of a base course. The effects of saturation on the resilient moduli of the base course and the subgrade are calculated. A Gamma distribution is used for describing the probability density function for the quantity of rain that falls, and a Markov chain model is applied for estimating the probabilities of wet and dry days. A new model that uses a parabolic phreatic surface and allows drainage through a permeable subgrade has been developed for computing the drainage of the pavement base and subgrade. Example results indicate that pavement performance is better in a high rainfall area that has a permeable subgrade when compared with the pavement performance in a low rainfall area that has an impermeable subgrade.

In estimating the long-term performance of pavements and in designing pavements to endure the effects of local climate, it is essential to be able to estimate the effect of rainfall on the modulus of the base course and subgrade. In this paper a comprehensive way of making such estimates is described, and the results of example calculations are given.

One cause of excess moisture content in the pavement is rainfall infiltration through cracks and joints. Methods for estimating the amount of rainfall and subsequent water infiltration through cracks and joints have been developed by Cedergren (1) and Markow (2), both of whom mention the lack of adequate field observation data on this subject. Markow simulated pavement performance under various moisture conditions by incorporating the amount of unsealed cracking in the pavement surface, the seasonal rainfall, and the quality of subsurface drainage into the model. His model is used in the EAROMAR system, which is a simulation model of freeway performance used by FHWA in conducting economic analyses of various strategies of roadway and pavement reconstruction, rehabilitation, and maintenance. Several improvements can be made on this model, as described later in this paper.

In this paper a stochastic model that consists of five main parts is described:

1. Estimation of the amount of rainfall that falls each day on a pavement,
2. Infiltration of water through the cracks and joints in the pavement,
3. Computation of the simultaneous drainage of water into the subgrade and into the lateral drains,
4. Dry and wet probabilities of the weather and pavement sublayers, and
5. Effect of water saturation on the load-carrying capacity of base courses and subgrades.

Groundwater sources and the side infiltration from pavement shoulders are not considered in this paper.

MODELS OF RAINFALL DISTRIBUTION AND FREQUENCY ANALYSIS

To estimate the quantity of rainfall that falls on a specific pavement and eventually enters the cracks and joints of that pavement, it is necessary to establish three items of information concerning local rainfall patterns:

1. The quantity of rain that falls in a given rainfall (the total quantity in each rainfall varies from one rainfall to the next, but historical records indicate that the quantity follows a probability density function),
2. The intensity and duration of each rainfall, and
3. The random occurrence of sequences of wet and dry days.

The methods that are used in estimating these quantities are described in the following subsections.

Probability Model of Quantity of Rainfall

Several theoretical probability distribution models of the total quantity of precipitation in a single rainfall have been presented in statistical climatology (3), in which the Gamma distribution has a long history of being used as a suitable theoretical model for frequency distributions of precipitation (4). Because the Gamma distribution has been well accepted as a general model as well as a fairly practical method, it is selected to represent the distribution of the quantity of rainfall.

The probability density function of the Gamma distribution is

$$f(R;\alpha,\beta) = [\beta^{\alpha}/\Gamma(\alpha)]\, e^{-\beta R} R^{\alpha-1}, \quad R \geq 0$$
$$0 \qquad R < 0 \tag{1}$$

where R is the precipitation quantity, and $\Gamma(\alpha)$ is the Gamma function, where $\Gamma(n+1) = n!$, $n = 0, 1, 2, \ldots$.

The parameters α and β may be estimated by the moments method:

$$\alpha = \bar{R}^2/S^2 \quad \bar{R} = \text{mean} = \Sigma R_i/n$$
$$\beta = \bar{R}/S^2 \quad S^2 = \text{variance} = \Sigma (R_i - \bar{R})^2/n \tag{2}$$

Models of Intensity and Duration of Rainfall

Storms and floods vary spatially and temporally in magnitude and are often characterized through their

peak discharges. The frequently used rainfall intensity-duration-return period equation (5,6) has often been expressed by

$$i = kt_p^x/t_R^n \quad (3)$$

where

t_R = effective rainfall duration (min),
t_p = recurrence interval (years),
i = maximum rainfall intensity (in./hr) during the effective rainfall duration, and
k,x,n = functions of the locality [for example, it was found that in the eastern United States n averaged about 0.75 and x and k were about 0.25 and 0.30, respectively (5)].

The unit hydrograph is a graph of rainfall intensity versus time with a volume of 1 in. of runoff resulting from a rainstorm of specified duration and areal pattern. Most of the storms of like duration and pattern are assumed to have the same shape, which is similar to the Gumbel distribution (3). In this model the normal distribution is used instead of the Gumbel distribution as a starting point for deriving the equation of the relationship between rainfall duration (t_R) and the quantity (R) (see Figure 1). The deviation between these two functions is fairly small for practical purposes.

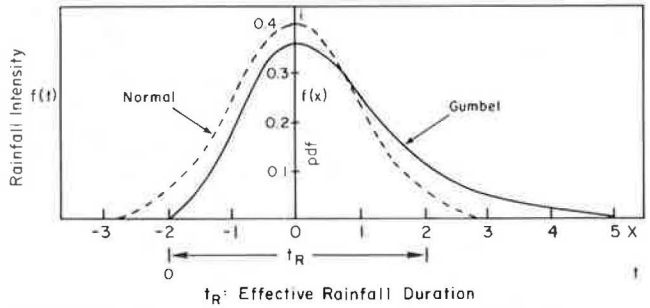

FIGURE 1 Comparison of normal and Gumbel distributions.

The equation relating the duration of rainfall and its quantity is derived as

$$t_R = (1.65R/kt_p^x)^{1/1-n} \quad (4)$$

Frequency Models of Rainfall: Markov Chain Method for Estimating Dry and Wet Probabilities

Several methods of estimating the probability distributions of the lengths of sequences of dry days and wet days on which the quantity of precipitation is greater than 0.01 in. have been used in a variety of weather-related research fields. However, the Markov process has been regarded as the basic general method. To simplify the modeling, the first-order Markov chain model was selected as an estimation of the rainfall occurrence probability.

A transition probability matrix generated with the Markov chain method for predicting weather sequences is represented by four elements, represented by the probabilities given in the matrix that follows. The matrix is known as a "transition" matrix:

$$P(t) = [p_{ij}(t)] = \begin{bmatrix} p_{00}(t) & p_{01}(t) \\ p_{10}(t) & p_{11}(t) \end{bmatrix} \quad (5)$$

where p_{ij} represents the probability that the Markovian system is in state j at time t given that it was in state i at time 0; the subscript 0 stands for dry, and a subscript of 1 stands for wet. Thus $p_{10}(t)$ represents the probability of having a dry day at time t when time 0 is a wet day; other elements of this matrix can be illustrated in a similar manner.

The transition probability matrix of the Markov chain model is derived from the assumption that the number of wet or dry days in a sequence follows a negative exponential distribution:

$$f(x) = \lambda e^{-\lambda x} \quad \begin{cases} x > 0, \lambda > 0 \\ x = \text{number of wet or dry days in sequence} \end{cases} \quad (6)$$

The variable λ is the reciprocal of the average dry or wet days per period: $\lambda_d = 1/\bar{x}_{dry}$ and $\lambda_w = 1/\bar{x}_{wet}$, where $\bar{x}_{dry}$ is the average number of dry days in a given period, and $\bar{x}_{wet}$ is the average number of wet days in that same period. Therefore, the transition matrix is derived as (7)

$$P(t) = [1/(\lambda_w + \lambda_d)] \times \begin{bmatrix} \lambda_w + \lambda_d e^{-(\lambda_w + \lambda_d)t} & \lambda_d [1 - e^{-(\lambda_w + \lambda_d)t}] \\ \lambda_w [1 - e^{-(\lambda_w + \lambda_d)t}] & \lambda_d + \lambda_w e^{-(\lambda_w + \lambda_d)t} \end{bmatrix} \quad (7)$$

Associated with the Markov chain model (Equation 7) is a recurrence relation for computing the probabilities of dry and wet days that was derived by Katz (8):

$$\begin{bmatrix} W_0(k;N) \\ W_1(k;N) \end{bmatrix} \begin{bmatrix} p_{00} & p_{01} \\ p_{10} & p_{11} \end{bmatrix} \begin{bmatrix} W_0(k;N-1) \\ W_1(k-1;N-1) \end{bmatrix} \quad (8)$$

Transition Matrix

where W_0 (k;N) is the probability of k wet days during N consecutive days when the 0th day is dry (the subscript 0 stands for when the 0th day is dry and the subscript 1 stands for when the 0th day is wet), and the transition matrix is derived from the Markov chain method (Equation 7). Because the recurrence relation is applied on a daily basis, the time t is set at 1 day in the transition matrix. Also, the probability of occurrence of a given number of wet days in a period of time is formulated as (8)

$$W(k;N) = (1 - p_0)W_0(k;N) + p_0 W_1(k;N) \quad (9)$$

where W(k;N) is the probability of having k wet days during N consecutive days, and p_0 is the initial probability of having a wet day in a season or a year (e.g., if there are usually 45 wet days during a 92-day fall season, p_0 is 45/92 or 0.49).

An example of the probabilities of having k wet days in 5 consecutive days is given in Table 1. Based on the data for May 1970 from the Houston Intercontinental Airport, the probability of having 5 consecutive dry days is 0.264, that of having 1 wet day is 0.301, that of having 2 wet days is 0.236, and so forth.

In summary, the Gamma distribution is used for the rainfall quantity probability density function, the Markov chain and Katz's recursive model are applied to evaluate the probabilities of having dry and wet days, and Equation 4 is used to estimate the duration of rainfall. The Gamma distribution leads to an estimate of the distribution of the amount of rainfall that falls on a pavement. Estimation of rainfall duration is used for evaluating the total amount of precipitation that infiltrates into the

TABLE 1 Katz's Model for Computing the Wet Probabilities Associated with Markov Chain Model

N	k	$W_0(k;5)$	$W_1(k;5)$	$W(k;5)$
5	0	0.290	0.199	0.264
5	1	0.305	0.290	0.301
5	2	0.228	0.257	0.236
5	3	0.121	0.161	0.133
5	4	0.045	0.072	0.053
5	5	0.010	0.021	0.013

Note: Data are from Houston Intercontinental Airport for May 1970. $p_0 = 0.71$, $p_{00} = 0.78$, $p_{01} = 0.22$, $p_{10} = 0.54$, and $p_{11} = 0.46$, where N = number of consecutive days, k = number of wet days, W_0 = wet probabilities when 0th day is dry, W_1 = wet probabilities when 0th day is wet, W = probability of having k wet days in 5 consecutive days, p_{ij} = transitional probabilities from Markov chain model, and p_0 = initial wet probability.

base, and the Markov chain method and Katz's recursive model are adopted for computing the probabilities of having dry periods during which a pavement can drain out all of the excess water. These results are used for further analysis, as described subsequently.

INFILTRATION OF WATER INTO A PAVEMENT THROUGH CRACKS AND JOINTS

Ridgeway (9) and Dempsey and Robnett (10) conducted research in determining the amount of water entering pavement structures. Ridgeway's studies and Dempsey and Robnett's field observations are selected as the basis for the analytical model presented herein.

Ridgeway's Studies

Ridgeway (9) made measurements in Connecticut of free water infiltration rates on portland cement concrete and bituminous concrete pavements using several methods. He concluded that

1. The cracks and joints of pavements are the main path for free water because both portland cement concrete and asphalt concrete used in a pavement surface are virtually impermeable, and
2. An infiltration rate of 0.1 $ft^3/hr/ft$ of crack (100 $cm^3/hr/cm$) can be used for design purposes.

In this analysis the following average infiltration rates are chosen: for cracks in bituminous concrete pavement, 100 $cm^3/hr/cm$ of crack (0.11 $ft^3/hr/ft$ or 2.64 $ft^3/day/ft$), and for cracks and joints in portland cement concrete pavements, 28 $cm^3/hr/cm$ of crack or joint (0.03 $ft^3/hr/ft$ or 0.72 $ft^3/day/ft$).

Dempsey and Robnett's Observations

Dempsey and Robnett (10) conducted a study to determine the influence of precipitation, joints, and sealing on pavement drainage for concrete in Georgia and Illinois. Subsurface drains were installed, and all drainage outflows were measured with specially designed flow meters. The rainfall data were obtained from nearby weather stations.

Regression equations were obtained from their field studies for both sealed and unsealed conditions in the test area. To make a conservative evaluation of infiltration through cracks and joints, the highest regression coefficient from one of the linear regression equations, which is measured under the unsealed condition, is chosen. The resulting equation is

$$PO = 0.48PV + 0.32 \quad (10)$$

where PO is the pipe outflow volume (m^3), and PV is the precipitation volume (m^3).

Nonetheless, Dempsey and Robnett (10) pointed out that the infiltration rates predicted by their regression analyses were considerably less than those estimated by using Ridgeway's tests. In the simulation model used in this paper, Ridgeway's model is furnished as an analytical tool if data on the length of cracks and joints are provided by the user. If no data for cracks and joints are provided, the alternative is to use Dempsey and Robnett's model to estimate the free water amount for the pavements where the cracks and joints are not sealed.

DRAINAGE OF WATER OUT OF BASE COURSE

The subject of base course drainage has received considerable attention during the past three decades. Casagrande and Shannon (11) made field observations on several airfields in the United States to determine the environmental conditions under which base courses may become saturated. In addition, Casagrande and Shannon performed a simplified theoretical analysis of base course drainage. They assumed the phreatic surface is a straight line and the subgrade is impervious.

It was noted in the paper by Casagrande and Shannon (11) that as the slope of the pavement became flatter or the depth of the base became greater, their theoretical predictions differed more widely from actual observations. The differences between theory and field results are primarily caused by the assumptions (i.e., a linear free surface and an impermeable subgrade) in their model. This model is used in the Highway Subdrainage Design manual (12).

The theoretical analyses reported by Wallace and Leonardi (13) indicate that the phreatic surface assumes a shape closer to a parabolic rather than to a straight line. Dupuit's assumption, as used in related drainage problems by Polubarinova-Kochina (14), also suggested that a parabolic phreatic surface would yield more realistic results for drainage calculations.

To develop better analytical procedures for pavement drainage design, a parabolic phreatic surface and a permeable subgrade were used to derive a new model (15,16). This model is called Texas Transportation Institute (TTI) drainage model, and the analyses appear to fit the field data better than Casagrande and Shannon's model. The TTI drainage model is applied to compute the rate of drainage of water out of the base course into the subgrade and into lateral drainage.

The degree of drainage (U) that is used in the previous sections of this paper can be readily converted to the saturation level. The relationship between saturation (S_a) and the degree of drainage is

$$S_a = 1 - P.D. \times U \quad (11)$$

where P.D. is a percentage indicating the amount of water that can be drained from a sample, which is determined by the mixture of materials [Table 2 (17)].

A drainage time of 5 hr to a saturation level of 85 percent is set for an acceptable material based on studies done at the Georgia Institute of Technology and the University of Illinois (17). A drainage time between 5 and 10 hr is marginal, and greater

TABLE 2 Drainability of Water in the Base Courses from a Saturated Sample (*17*).

	Drainability (%) by Amount and Type of Fines								
	<2.5 Percent Fines			5 Percent Fines			10 Percent Fines		
	Inert Filler	Silt	Clay	Inert Filler	Silt	Clay	Inert Filler	Silt	Clay
Gravel[a]	70	60	40	60	40	20	40	30	10
Sand[b]	57	50	35	50	35	15	25	18	8

Note: Gap-graded material will follow the predominant size.
[a]Gravel, 0 percent fines, 75 percent greater than No. 4: 80 percent water loss.
[b]Sand, 0 percent fines, well graded: 65 percent water loss.

than 10 hr is unacceptable. A base course with granular materials that are classified as unacceptable will hold more water and allow excessive deformations and pumping in the pavements.

EFFECT OF SATURATION ON LOAD-CARRYING CAPACITY OF BASE COURSE AND SUBGRADE

Effect of Saturation on Base Course Properties

Haynes and Yoder (18) performed a laboratory investigation of the behavior of the AASHTO Road Test gravel and crushed stone mixtures subjected to repeated loading. A series of repeated triaxial tests was performed on the crushed stone and gravel base course materials. Their studies indicated that the degree of saturation level was closely related to the material strength of the base course (Figure 2), especially when saturation is greater than 85 percent, where total deformation begins to increase, thus accelerating fatigue damage.

In the simulation model presented here, the moduli of different base course materials must be furnished. In simulating the influence of the degree of saturation on the base moduli, the lower part of Figure 2 is applied. In the range of degree of saturation from 0 to 60 percent, the elastic moduli are assumed to be constant. Between 60 and 85 percent saturated the slope between deflection measurements and saturation levels is 0.24. At degrees of saturation greater than 85 percent, the slope is 3.5. To estimate the average base modulus during any specific season, the cumulative probabilities of each section of the elastic modulus, as well as the dry and wet probabilities of the base course, are incorporated into the model.

Effect of Saturation on Subgrade Properties

Thompson and Robnett (19) conducted research identifying and quantifying the soil properties that control the resilient behavior of Illinois soils. They concluded that the degree of saturation is a factor that reflects the combined effects of density and moisture content. Their analyses indicated a highly significant relation between the resilient modulus and the degree of saturation of the subgrade. A set of regression equations was developed for various soil classification groups. The equations developed are used to predict the resilient moduli of different soil groups.

The depth of the base course and subgrade is assumed to be 70 in. in order to evaluate the degree

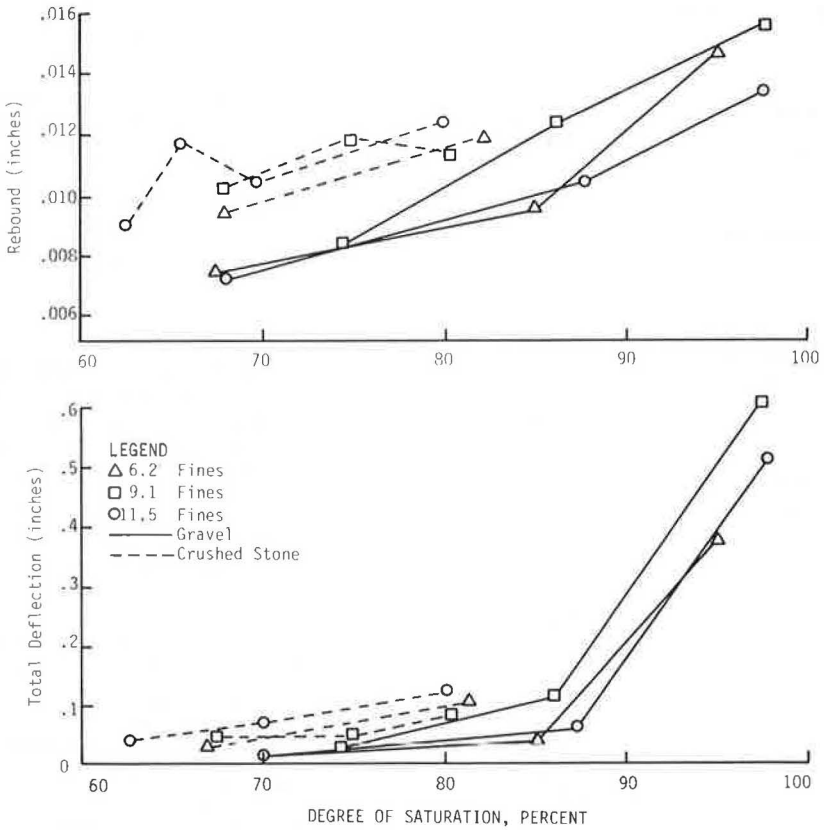

FIGURE 2 Effect of degree of saturation on the repeated-load deformation properties of AASHTO granular materials.

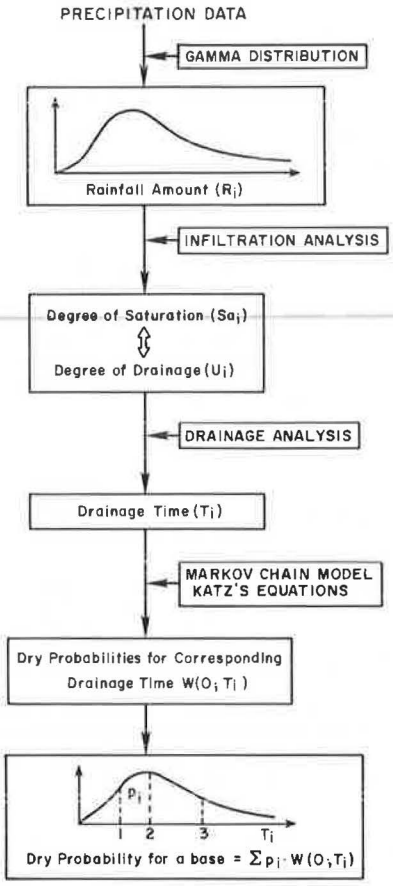

FIGURE 3 Synthesis of models used in systematic analysis of rainfall infiltration and drainage analysis of a pavement.

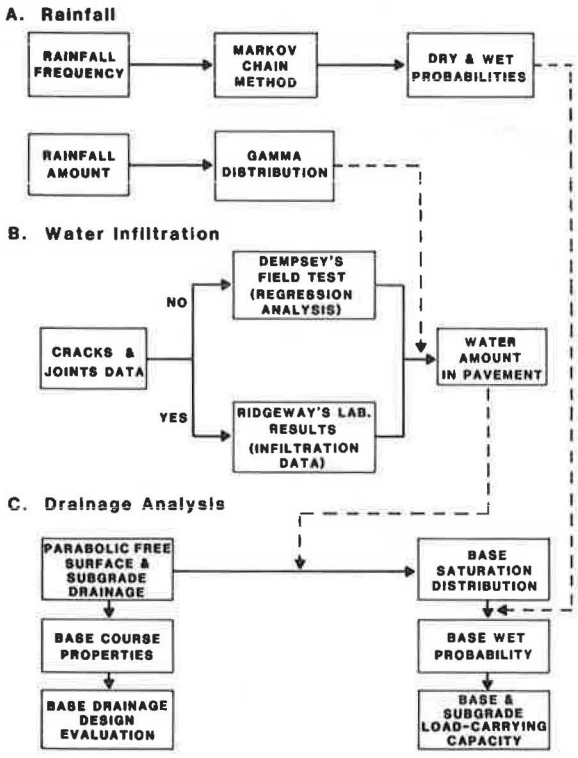

FIGURE 4 Flowchart for conceptual model of rainfall infiltration and drainage analysis of pavements.

TABLE 3 TTI Drainage Model for Analysis of a Houston Pavement

Drainage (%)	Hours	Drainage (%)	Hours
5.0	0.202E 00	55.0	0.198E 02
10.0	0.760E 00	60.0	0.256E 02
15.0	0.165E 01	65.0	0.323E 02
20.0	0.282E 01	70.0	0.403E 02
25.0	0.426E 01	75.0	0.499E 02
30.0	0.595E 01	80.0	0.620E 02
35.0	0.788E 01	85.0	0.779E 02
40.0	0.101E 02	90.0	0.100E 03
45.0	0.125E 02	95.0	0.137E 03
50.0	0.151E 02	100.0	0.187E 03

Note: The data in this table are from an analysis of a pavement in Houston in May 1970. The data for the system analysis of rainfall infiltration and drainage are as follows: length = 50.00, height = 0.50, slope% = 1.50, perm.1 = 10.00000, perm.2 = 0.00100, poro.1 = 0.2000, and poro.2 = 0.0500 (note that 1 and 2 stand for base course and subgrade, respectively). The analysis in this table is based on parabolic phreatic surface plus subgrade drainage.

TABLE 4 TTI Drainage Model for Evaluation of a Drainage Design of a Houston Pavement

Parameter	Value
Water drained due to gravel (%)	80.00
Gravel in sample (%)	70.00
Water drained due to sand (%)	65.00
Sand in sample (%)	30.00
Water that will be drained (%)	75.50
Critical degree of drainage (%) (85 percent saturation)	19.87
Draining time for 85 percent saturation (hr)	2.79

Note: This drainage design is satisfactory.

TABLE 5 Markov Chain Model and Katz's Recurrence Equations for Dry Probabilities Versus a Drainage Curve of a Houston Pavement

Time (days)	Drainage (%)	Probability (consecutive dry days)
1	58.72	0.710
2	74.08	0.554
3	83.32	0.432
4	89.17	0.338
5	98.02	0.264
6	95.57	0.206
7	97.30	0.161
8	100.00	0.125

TABLE 6 Stochastic Models for System Analysis of Rainfall Infiltration and Drainage Analysis of a Houston Pavement: Parameters of Gamma Distribution and Markov Chain Model

Parameter	Value
Rainfall, average per wet day (in.)	1.649
Variance of rainfall amount	2.341
Alpha of Gamma distribution	1.161
Beta of Gamma distribution	0.704
Lambda of dry days (Markov process)	0.409
Lambda of wet days (Markov process)	1.000
Sum of lambda of dry and wet days	1.409
Probability of dry days	0.710
Probability of wet days	0.290
Water-carrying capacity of base (ft^2)	5.000
Average degree of drainage per hour (%)	3.303
Overall probability of saturated base	0.225
Dry probability of base course	0.817
Wet probability of base course	0.183

Note: The analysis for water entering pavement is based on Dempsey's field equation.

TABLE 7 Stochastic Models for System Analysis of Rainfall Infiltration and Drainage Analysis of a Houston Pavement: Probability Distribution of Modulus of Base Course

Parameter	Saturation Level (%)									
	10	20	30	40	50	60	70	80	90	100
Water in base (ft^2)	0.50	1.00	1.50	2.00	2.50	3.00	3.50	4.00	4.50	5.00
Rainfall quantity (in.)	0.19	0.44	0.69	0.94	1.19	1.44	1.69	1.94	2.19	2.44
Rain duration (hr)	0.00	0.06	0.35	1.21	3.09	6.62	12.54	21.76	35.31	54.37
Base moduli (ksi)	64.60	64.60	64.60	64.60	64.60	64.60	29.36	19.00	5.07	2.14
Ratio of dry modulus	1.00	1.00	1.00	1.00	1.00	1.00	0.45	0.29	0.08	0.03
Subgrade moduli (ksi)	30.71	30.71	29.61	29.01	28.36	27.18	25.68	23.61	20.17	12.70
Probability density	0.48	0.46	0.41	0.37	0.32	0.27	0.24	0.20	0.17	0.15
Probability	0.08	0.12	0.11	0.10	0.09	0.07	0.06	0.05	0.05	0.04
Cumulative probability	0.08	0.20	0.31	0.41	0.50	0.57	0.63	0.69	0.74	0.78

TABLE 8 Evaluation of Rainfall Effect on Pavement Performance of a Houston Pavement

Distribution Characteristics of Rainfall Effect	Value
Average free water in base (ft^2)	0.92
Duration of average rainfall amount (hr)	0.040
Average rainfall amount per day (in.)	0.403
Average base course modulus in wet state (ksi)	41.45
Average base course modulus (ksi)	60.36
Average subgrade modulus (ksi)	30.31

of saturation in the subgrade. The average wetting front of water penetration from the base course into the subgrade is calculated by estimating the proportions of water in the base flowing into the subgrade from the TTI drainage model. The average subgrade modulus is determined by the average rainfall during that season that will infiltrate into the subgrade from the base.

The subgrade modulus is calculated by (20)

$$E_s = (E_1 d_1^3 + E_2 d_2^3)/d^3 \quad (12)$$

where

E_s = calculated total subgrade modulus;
d = depth of a subgrade ($= d_1 + d_2$);
E_1 = subgrade modulus under 100 percent saturated condition, which is evaluated from Thompson and Robnett's equations (19);
d_1 = average depth of water penetrating into subgrade from the base course;
E_2 = subgrade modulus under dry conditions; and
d_2 = average depth of dry portion of the subgrade.

SYNTHESIS OF METHODS OF RAINFALL INFILTRATION, DRAINAGE, AND LOAD-CARRYING CAPACITY OF A PAVEMENT

The following models are used as analytical procedures to estimate rainfall infiltration, drainage analysis, and load-carrying capacities of base courses and subgrades:

1. The Gamma distribution (4) for the distribution of rainfall quantity;
2. Dempsey and Robnett's (10) regression equations as well as Ridgeway's (9) results are used for infiltration analysis together with an estimate of the amount of rainfall that, in turn, permits an estimate of the duration of the rainfall;
3. The TTI drainage model (15)--the parabolic phreatic surface with subgrade drainage--as developed for base course and subgrade drainage analysis;
4. Markov chain model (7) and Katz's (8) recurrence equations for the calculation of dry and wet day probabilities; and
5. Evaluation of base course (18) and subgrade moduli (19) as they are affected by moisture contents in the materials.

A synthesis of these various models into a systematic analysis of rainfall infiltration and drainage analysis of a pavement is shown in Figure 3, and a conceptual flowchart is shown in Figure 4 for a clear profile of the entire model.

A series of sample calculations from the computer program is given in Tables 3-8. The rainfall data are for Houston Intercontinental Airport for May 1970, and a pavement structure is assumed for illustration. The pavement is 100 ft wide on one side, the base course is 6 in. thick, and the subgrade is permeable. The data in Table 3 give the degree of drainage and the draining time under the given base materials by using the TTI drainage model. The evaluation of a drainage design (17) is given in Table 4.

Based on the weather data and pavement structure, the drainage time, degree of drainage, and corresponding probabilities are calculated in Table 5. The characteristics of the probability distributions and related material properties under local rainfall conditions are given in Tables 6 and 7, and data on the effect of rainfall on the base and subgrade moduli are given in Table 8.

APPLICATION TO SYSTEMATIC ANALYSIS OF RAINFALL INFILTRATION, DRAINAGE, AND LOAD-CARRYING CAPACITY OF A PAVEMENT

An example is presented of the effects of the amount of rainfall and subgrade drainage on the load-carrying capacity of a pavement. It is assumed that a base course is 70 percent gravel and 30 percent sand, 100 ft wide, 6 in. deep, 1.5 percent slope, the coefficient of permeability of the base course is 10 ft/hr, the drainable porosity is 0.1, and the subgrade is assumed to be impermeable. The drainage design used is considered marginally acceptable because the drainage time of 6.35 hr that is required to reach a saturation level in the base is less than 85 percent.

This same design of a base course is used in two climatic regions: Abilene and Houston, Texas, which represent low and high rainfall areas, respectively. Daily rainfall data from 1970 were entered into the simulation model to compare the results for these cities. The results (Figure 5) indicate that the

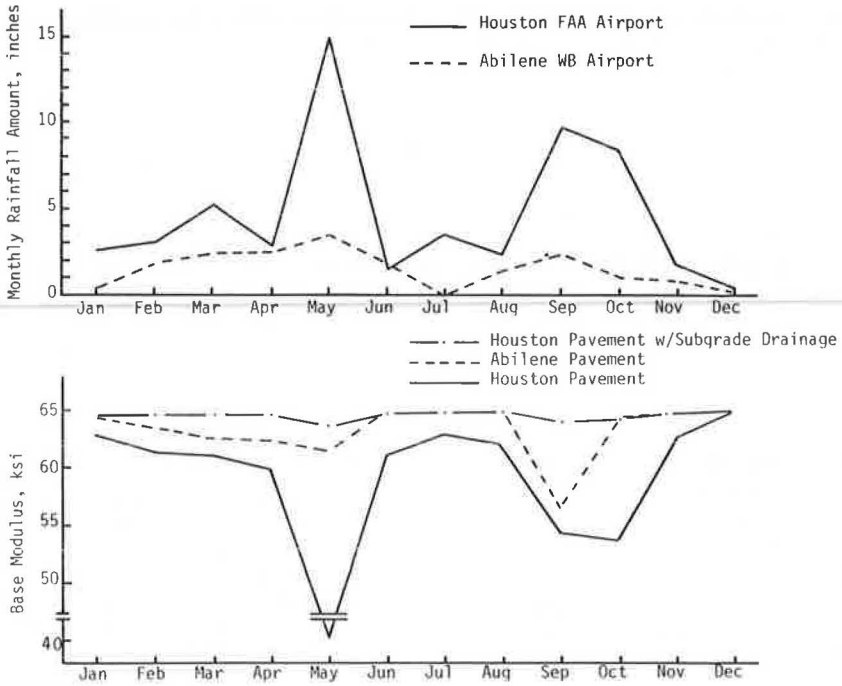

FIGURE 5 Effects of rainfall quantity and subgrade drainage on load-carrying capacity of pavements.

precipitation quantity affects the elastic moduli of the base course. If the water in the base course can drain into a subgrade with a permeability of 0.01 ft/hr and a porosity for freely draining water of 0.01 in a higher rainfall area (i.e., Houston), the load-carrying capacity could be improved significantly. It indicates that the pavement performance may be better in a high rainfall area that has a permeable subgrade, when compared with the pavement performance in a low rainfall area where there is an impermeable subgrade.

CONCLUSIONS AND RECOMMENDATIONS

A systematic analysis of rainfall infiltration into and drainage from a base course is constructed that incorporates a probability distribution of the amount of rainfall, the probabilities of dry and wet days, estimates of water infiltration into pavements, drainage analysis of pavements, and load-carrying capacities of base courses and subgrades. This comprehensive analysis of the effect of rainfall on pavement structures is recommended as an effective approach for future evaluation of the climatic effects on pavements.

ACKNOWLEDGMENT

This research has been funded by FHWA, U.S. Department of Transportation, and by a subcontract from the University of Illinois at Urbana. The authors gratefully acknowledge the support received from these sources.

REFERENCES

1. H.R. Cedergren. Drainage of Highway and Airfield Pavements. Wiley, New York, 1974.
2. M.J. Markow. Simulating Pavement Performance Under Various Moisture Conditions. In Transportation Research Record 849, TRB, National Research Council, Washington, D.C., 1982, pp. 24-29.
3. K.T. Kottegoda. Stochastic Water Resources Technology. Wiley, New York, 1980.
4. E. Suzuki. A Summarized Review of Theoretical Distributions Fitted to Climatic Factors and Markov Chain Models of Weather Sequences, with Some Examples. In Statistical Climatology, Elsevier, Amsterdam, Netherlands, 1980, pp. 1-20.
5. R.K. Linsley, Jr., and J.B. Franzini. Elements of Hydraulic Engineering. McGraw-Hill, New York, 1955.
6. R.G. Kazmann. Modern Hydrology. Harper and Row, New York, 1965.
7. H.A. Taha. Operations Research, 2nd ed. Macmillan, New York, 1976.
8. R.W. Katz. Computing Probabilities Associated with the Markov Chain Model for Precipitation. Journal of Applied Meteorology, Vol. 13, 1974, pp. 953-954.
9. H.H. Ridgeway. Infiltration of Water Through the Pavement Surface. In Transportation Research Record 616, TRB, National Research Council, Washington, D.C., 1976, pp. 98-100.
10. B.J. Dempsey and Q.L. Robnett. Influence of Precipitation, Joints, and Sealing on Pavement Drainage. In Transportation Research Record 705, TRB, National Research Council, Washington, D.C., 1979, pp. 13-23.
11. A. Casagrande and W.L. Shannon. Base Course Drainage for Airport Pavement. Proc., ASCE, Vol. 77, June 1951.
12. L.K. Moulton. Highway Subdrainage Design. Report FHWA-TS-80-224. FHWA, U.S. Department of Transportation, 1980.
13. K. Wallace and F. Leonardi. Theoretical Analyses of Pavement Edge Infiltration and Drainage. Research Report 6. Department of Civil Engineering, James Cook University of North Queensland, Townsville, Australia, 1975.
14. P. Ya. Polubarinova-Kochina. Theory of Ground Water Movement (translated by J.M. Roger De

Wiest). Princeton University Press, Princeton, N.J., 1962.
15. S.J. Liu, J.K. Jeyapalan, and R.L. Lytton. Characteristics of Base and Subgrade Drainage of Pavements. In Transportation Research Record 945, TRB, National Research Council, Washington, D.C., 1983, pp. 1-10.
16. S.J. Liu and R.L. Lytton. A Simulation Model for Rainfall Infiltration, Drainage Analysis, and Load-Carrying Capacity of Pavements. Texas Transportation Institute, Texas A&M University, College Station, Aug. 1983.
17. S.H. Carpenter, M.I. Darter, and B.J. Dempsey. A Pavement Moisture Accelerated Distress (MAD) Identification System--Volume 2. Report FHWA-RD-81-080. FHWA, U.S. Department of Transportation, 1981.
18. J.H. Haynes and E.J. Yoder. Effects of Repeated Loadings on Gravel and Crushed Stone Base Course Materials Used in the AASHTO Road Test. In Highway Research Record 39, HRB, National Research Council, Washington, D.C., 1963, pp. 82-96.
19. M.R. Thompson and Q.L. Robnett. Resilient Properties of Subgrade Soils. ASCE, Journal of Transportation Engineering, 1979, pp. 71-89.
20. R.L. Lytton and C.H. Michalak. Flexible Pavement Deflection Equation Using Elastic Moduli and Field Measurements. Research Report 207-7F. Texas Transportation Institute, Texas A&M University, College Station, Aug. 1979.

Publication of this paper sponsored by Committee on Subsurface Drainage.

Implementation of Internal Road Drainage Design and Application

GEORGE S. KOZLOV

ABSTRACT

As a result of more than 5 years of research, which culminated in the construction of two experimental, internally drainable road sections, it is now possible to present engineers with procedures for the design, construction, and maintenance of adequately drainable roads. These procedures are offered as a guide until their further application would provide additional data for improvements. It is suggested that adequate surface drainage, combined with appropriate internal drainage, is the most advantageous solution to the problem of water buildup beneath a roadway.

Research by the New Jersey Department of Transportation (NJDOT) has established that improved pavement durability can be realized if water is not allowed to accumulate within the structural section of a pavement. Therefore use of a drainage layer immediately below the lower bound layer of a pavement has been found to be the most effective means of achieving the necessary degree of internal drainage. This system is designed to handle surface infiltration water only.

However, groundwater drainage systems will be used only when groundwater is deemed to be a problem. It can be in the form of longitudinal or transverse drains to intercept flow, or drainage blankets or well systems to lower the water table and relieve pore water pressure. In this way the two internal water drainage sources previously mentioned call for two totally and distinctly different drainage approaches and solutions.

SUMMARY OF SUPPORTING RESEARCH

As part of the research study, a field investigation of the existing underdrainage conditions of New Jersey highways was performed. The field surveys indicated a definite need for better internal drainage solutions. Subsurface drainage failure under portland cement concrete pavements was found to be manifested by pumping, cracking, and eventual disintegration of the surfacings. Water-related deterioration of bituminous concrete pavements appeared to occur no less often; however, the relationship was often not visually apparent. It appeared that the type of surfacing had little effect on the moisture conditions immediately below a pavement.

The survey of New Jersey highways included a performance evaluation of several previous subsurface drainage solutions. The conclusion, in essence, was that longitudinal pipe drains, after-the-fact solutions, or even initial installations apparently are not adequate to handle the subsurface drainage of infiltrated roofwater. Thus the objective of this project became the development of the pavement design process.

Specifically, it was intended that the research formulate the design methods and the construction

and maintenance procedures for a drainage system that would control water within New Jersey pavements. To this end, an exhaustive study of the state of the art, extensive laboratory investigations, and some experimental field installations were conducted. To minimize the amount of surface water entering a pavement, it is obvious that every effort should be made to have a fully effective surface drainage system. Therefore, as part of the study, a practical surface drainage guide was prepared for use with the small drainage areas typically encountered in highway design (1). For subsurface drainage of the water that does get into a pavement, the literature review and results of the field surveys indicated that solutions proposed by Cedergren et al. (2) offered some promise for success.

The most important element of the Cedergren approach is the drainage layer. Such a system can be achieved if a drainage layer is provided that satisfies three basic requirements: It must be open enough to drain water in a reasonable length of time, yet with low enough flow rates to prevent internal erosion; it must be dense enough to support traffic loads; and it must possess filtration characteristics compatible with base and subbase materials. The development of materials that satisfied these requirements proved to be extremely difficult and became the object of a significant portion of the literature assessments and most of the laboratory work.

To design an effective drainage layer it was first necessary to identify flow theories for open-graded materials. Darcy's flow equation, even though only applicable to laminar conditions in fine grain soils, appeared somewhat useful in developing upper bounds on horizontal flow rates in an open-graded layer. In the end, horizontal flume tests had to be undertaken to confirm that the final drainage layer materials would perform effectively.

The actual design of the drainage layer began with an attempt to satisfy the requirement of removing infiltrated water in a reasonable time period. To preclude water freezing within a drainage layer and to avoid extensive periods of saturated pavement materials, achieving 50 percent drainage within 24 hr was concluded to be more appropriate for highways. For a selected drainage layer thickness of 4 in. and considering New Jersey's climatic conditions, probable rainfall, and possible infiltration rates, the 24-hr criterion led researchers to establish a needed minimum permeability of 1,000 ft per day within the drainage layer. However, from subsequent laboratory evaluations of available drainage layer materials, it was found more appropriate to establish a desired permeability range of 1,000 to 3,000 ft per day. With this restricted permeability range it was possible to isolate materials that also had adequate stability and filtration properties.

Several field construction trials were used to help direct and verify the laboratory efforts at developing adequate drainage layer materials. From these combined activities it was possible to formulate materials and construction specifications for nonstabilized open-graded (NSOG) and bituminous-stabilized open-graded (BSOG) layers.

PROCEDURES FOR DESIGN, CONSTRUCTION, AND MAINTENANCE

Design of Drainage for Surface Water Infiltration

The validity of the design procedures presented in this paper depend on the accuracy and completeness of the design and application requirements. The solutions developed by this research are as realistic as possible, while still retaining engineering integrity.

The requirements for the design and application of the subsurface drainage can be placed in the following categories:

1. The geometry of the flow domain,
2. The properties of the materials,
3. The application of the drainage facilities and the means for applying them, and
4. The climatological data.

The geometry of the flow involves the geometric design of the highway, related subsurface drainage geometry, and prevailing conditions. The fundamental properties of the drainage material, such as permeability, density, geological characteristics, and particle shape, define the performance of the material. To perform properly, drainage material must transmit the flow of water, properly support loads, and, most important, retain these characteristics for a reasonable life span of a road. Proper use of such characteristics in the design and application of the drainage facilities also requires suitable lifetime maintenance. The climatological data provide insight into the fundamental source of all subsurface water and the potentially adverse effects of frost action.

Highway and Subsurface Geometry

Almost all of the geometric design of subsurface features of a highway can exert some influence on the analysis and design of subsurface drainage. Therefore, before attempting to undertake such work, the designer should be armed with as much information as possible on these features. Included should be sufficiently detailed profiles and cross sections to permit assembly of the following data for each section of roadway under consideration: longitudinal grades; transverse grades (including superelevations); widths of pavement and shoulder surface, base, and subbase; required thickness of pavement elements based on normal structural design practice for the particular area under consideration; depths of cuts and fills; recommended cut and fill slopes; and details of ditches and other surface drainage facilities. In addition, it is considered desirable to have a topographic map of the highway corridor on which the final highway alignment has been superimposed.

The flow of water in the structural section (drainage layer) of the pavement is largely controlled by the longitudinal grade of the roadway and its cross slope. When the profile of a road is relatively flat, water entering the drainage layer will flow laterally by virtue of the cross slope of the layer and empty into the longitudinal drainage trenches. However, when there is a profile grade, the water will also flow somewhat in the direction of the grade.

For a particular roadway site, a good estimate of the flow path length for a single lane of pavement can be obtained by using the equations that follow. Also, an equation is provided for distance of flow parallel to the grade that is helpful in establishing the actual station locations of any needed cross drains.

$$S_l = \sqrt{S_{cross}^2 + S_{long}^2} \quad (1)$$

$$L = W\sqrt{1 + (S_{long}/S_{cross})^2} \quad (2)$$

$$L_G = W(S_{long}/S_{cross}) \quad (3)$$

where

S_{cross} = highway lane cross slope (ft/ft),
S_{long} = highway lane longitudinal slope (ft/ft),
S_1 = slope of the underdrain layer (path) (ft/ft),
W = width of drainage layer (lane width) (ft),
L = length of flow path (ft), and
L_G = distance water has traveled in the direction parallel to the grade (ft).

Transverse drains must be used at each underdrain outlet to convey water from the longitudinal drains to the outlet facility. Except for vertical sag and superelevated curve conditions, transverse drains should be placed at about a 45-degree angle to the longitudinal pipe line. In hilly terrain the cross drains should be required wherever needed to prevent the flow paths from exceeding approximately 150 ft.

The location of outlets will often be dictated by topograhpic and geometric features and overall drainage pattern; nevertheless, as a general rule, the spacing of outlets should not exceed 500 ft.

Normally the outlet pipes should be daylighted. If this is not possible, then they should be drained into the nearest inlet structure. When the latter is the case, it is imperative that the flow line of the subsurface drainage system pipe be at least 6 in. higher than the maximum predicted water surface in the inlet to avoid storm water backing up into the subsurface drainage system.

Design of Subsurface Drainage Layer

The infiltration of water into the pavement has been practically resolved so as not to require the knowledge of the water movements, as will be shown later. The drainage layer developed by NJDOT has the capacity to drain off the water in a reasonably short time, that is, before it can cause jeopardy to the structural capacity of the pavements. As already indicated and shown on standard details (Figures 1-4), the drainage layer should be located immediately below the bound layer of a pavement under a minimum of 6 in. of confinement. Figures 1 and 3 give the cross-sectional view of a drainage layer, its edge drains, and a typical cross drain for a generalized highway pavement. Figure 1 provides an alternate whereby the longitudinal edge drains are positioned at the edge of the pavement, whereas Figure 2 shows the same drains located at the edge of the shoulder. The alternave shown in Figure 2 is preferred, but if construction costs are of major concern or if the design considerations require, the approach shown in Figure 1 can be used. Figures 1 and 2 have the cross slopes and grade breaks of the drainage layer mirroring the pavement surface. Details in Figures 3 and 4 are basically duplicates of Figures 1 and 2, except that a constant cross slope is required of the drainage layer. From a long-term performance standpoint, construction in accordance with the details shown in Figures 3 and 4 are best. However, for ease of construction, but not necessarily for minimized installation costs, the configuration shown in Figures 1 and 2 will frequently be found more appropriate. Of course, variations of Figures 1-4 are entirely feasible as long as they are appropriately developed.

Principles of Subsurface Drainage

The roofwater drainage layer developed in this research is open enough to drain water in a reasonable amount of time, yet its flow is close to laminar. Also, this layer is dense enough to support traffic loads, while possessing filtration characteristics compatible with the base or subbase materials. Be-

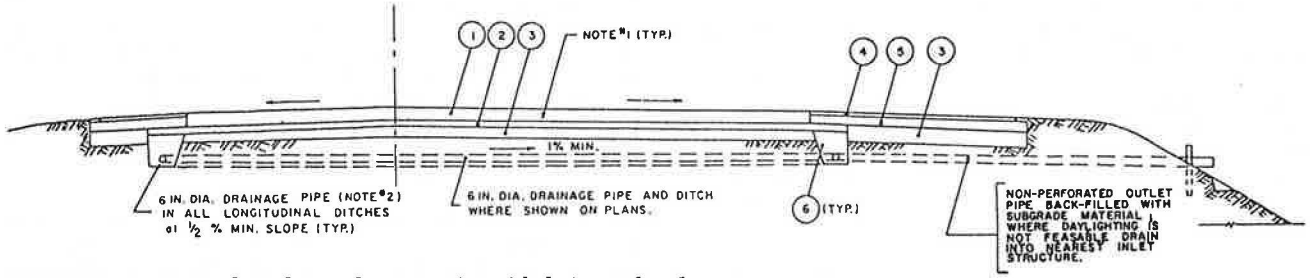

FIGURE 1 Internally drainable road cross section with drains at the edge of pavement.

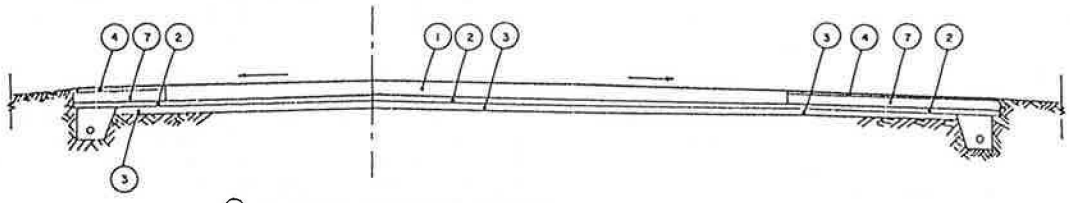

1. B.C. OR P.C.C. PAVEMENT, MIN. 6 IN. THICK
2. 4 IN. B.S.O.G. OR N.S.O.G. DRAINAGE LAYER
3. BASE OR SUBBASE LAYER.
4. B.C. SHOULDER
5. SOIL AGGREGATE OR DENSE GRADED AGGREGATE BASE LAYER.
6. 8 OR 57 COURSE AGGREGATE
7. L.F.A. PLANT MIXED STABILIZED BASE COURSE OR NONSTABILIZED BASE COURSE OVER FILTER FABRIC.

NOTES 1. USE PRIME COAT ON THE TOP OF THE NSOG LAYER.

2. DRAINAGE PIPE SHALL BE PERFORATED OR SLOTTED CORRUGATED METAL, PVC OR PE PLASTIC OR POROUS WALL CONCRETE PIPES.

FIGURE 2 Internally drainable road cross section with drains at the edge of shoulder.

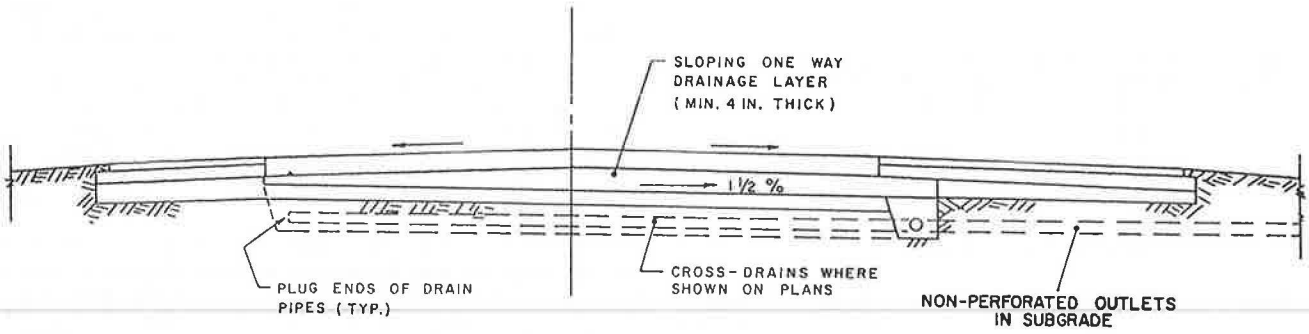

FIGURE 3 Road cross section drainable to the edge of pavement collector.

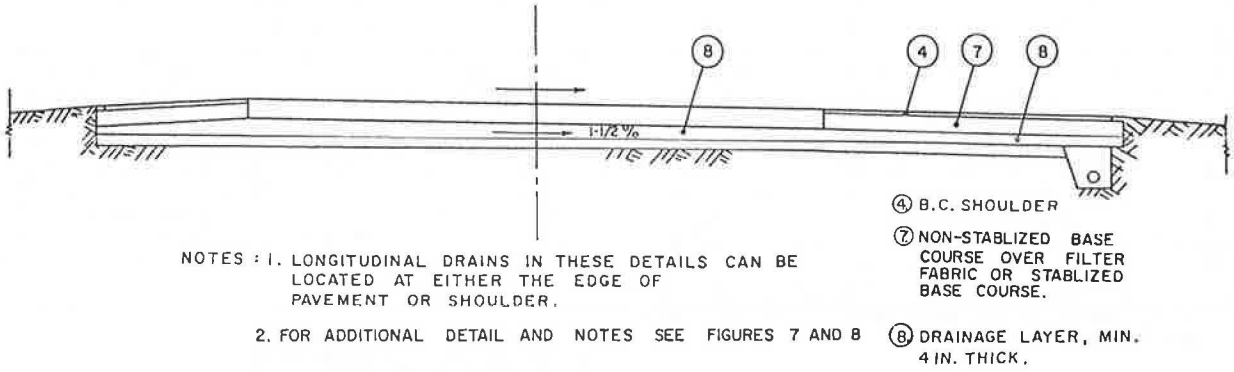

FIGURE 4 Road cross section drainable to the edge of shoulder collector.

cause there is practically no way to prevent the penetration of roofwater into pavements nor is it practical to drain this water any other way but horizontally, a drainage layer invariably should be used in all roads if the problems associated with water in pavement are to be solved.

As already indicated, the principles of subsurface drainage that have been adopted here suggest that only the drainage capacity of the drainage layer determines the quantity of water to be drained. This quantity of water will generally be less than the capacity of the drainage pipes in the longitudinal edge drains. Therefore, the capacity of a drainage layer can then be calculated by Darcy's equation:

$$Q = KAi \quad (4)$$

where

- Q = discharge quantity (ft^3/day) per foot of longitudinal drainage pipe length,
- K = permeability constant (ft/day),
- $i = H_o/L$ = hydraulic gradient (ft/ft),
- A = H x 1.0 cross-sectional area of drainage layer (ft^2) per unit width of the layer,
- L = length of flow path through the soil (ft),
- H = thickness of open-graded layer (ft),
- $H_o = H + L \tan\alpha$ (ft), and
- $\tan\alpha$ = slope of the base layer.

The next parameter of importance is the time of drainage. To keep structural water damage at an absolute minimum, the total removal of water within a reasonable time span is desirable. If the amount of water to be drained is given by n_eAL, the Darcy fundamental equation, when solved for time t, yields

$$t_{total} = n_eL^2/[K(H + L\tan\alpha)] \quad (5)$$

where t_{total} is the time of total drainage of the free moisture a layer can drain (days), and effective porosity (n_e) = (volume of voids that can be drained)/(total volume).

Most investigators agree that the subsurface drainage must be capable of removing within a short enough time span 50 percent of unbound moisture it can drain. This requirement prevents the freezing effect of the water from damaging the pavement structure. Using Casagrande's (3) flow equations for time, the 50 percent drainage point is expressed as

$$t_{50} = n_eL^2/[2K(H + L\tan\alpha)] \quad (6)$$

where t_{50} is the time of drainage of 50 percent of the unbound moisture a layer can drain (days). Effective porosity has been found to equal approximately 80 percent of the absolute porosity (n) for granular type materials.

With flow conditions of open-graded materials bordering on the turbulent, the flow rates will be lower than those predicted by Darcy's fundamental law. The magnitude of the flow rate in this instance would be a matter of conjecture, because little work has been done in studying turbulent flow in soils. In any case, because of possible turbulent conditions, there needs to be an extremely stable grain structure in the drainage layer.

Application of Open-Graded Drainage Layer

In any internal road drainage design, either the NSOG or the BSOG layers can be used with the appropriate collector system. Initially, the NSOG material was developed primarily for use in rigid pavement designs, whereas the BSOG drainage layer was meant for use in flexible pavements. It was originally theorized that for the unbound NSOG material, rigid pavement would provide better and more uniform load

distribution, whereas the BSOG layer, with its stability provided by asphalt, would be more compatible with flexible pavements. Thus far the NSOG material has been found to be somewhat better from a structural performance standpoint. However, BSOG is easier to construct. Currently, it does not appear that there will be a great differential in cost between the two material types. For structural design purposes, both NSOG and BSOG can be assumed to have a structural index equivalent to NJDOT dense-graded aggregate base (SN = 0.14).

It is imperative that both materials are applied with some type of barrier, be it some form of soil stabilization, filter cloth, or filter-type soils under, above, or adjacent to the open-graded layer and drainage trenches. Although the use of soil stabilization or filter fabric might increase the cost of drainable pavement if materials compatible with filter requirements (such as the subbases typically specified for New Jersey roadways) are placed under the open-graded layer, no additional cost should be incurred. If structural strength advantages were ascertained in flexible pavement design, the use of lime-fly ash soil stabilization could provide considerable cost savings.

NSOG Material Properties and Laboratory Procedures

The NSOG material must comply with the gradation band shown in Figure 5 and the composition of the mixture given in the following table. The material for this layer shall consist of crushed aggregate conforming to the following gradation requirements:

Sieve Size	Allowable Percent Passing
1.5 in.	100
1 in.	95-100
0.5 in.	60-80
No. 4	40-55
No. 8	5-25
No. 16	0-8
No. 50	0-5

The material can be made of a 50/50 blend of No. 57 and No. 9 stone or might be produced as a new standard size mix of coarse aggregates. Even though only three specific stone sources (limestone, trap rock, and gneiss) could be tested, these materials are representative of the predominant stone types available for NJDOT construction work. However, because these were not all-inclusive tests and were laboratory rather than field investigations, caution is suggested when using crushed stone from other sources. There are many stone sources and even a few other stone types that are currently acceptable for New Jersey projects. The producer of NSOG material, therefore, is required to submit for approval a particular target gradation that is within the band and can be produced with his aggregate sources. The permeability testing and density and gradational stability evaluation with the Burmister vibratory table are essential, and submission of samples for such purpose is required. The final approval of the material is based on the target gradation having permeability of 1,000 to 3,000 ft per day and a stable voids system. Gradational stability does not imply the structural strength of a material, but rather it is based on visual aspects (i.e., minimum of voids, degree of migration, and segregation; hence a stable voids system). When a sample is compacted into a Plexiglas mold it is visually evaluated for low void content and absence of segregation, and then density is measured directly in the mold. If No. 57 and No. 9 stone are mixed, they must individually meet grading specifications and in any case be of the same source (i.e., stone type) because mixing of stone types might impair the performance of the drainage layer.

To assure that adequate conditions are achieved in the field, in-place gradations are required to be close to the target gradation. The density of the material, while being close to that achieved in the Burmister mold, must be the maximum attained in the control strip test.

To ascertain that the requirements previously mentioned and specified in the NSOG construction and

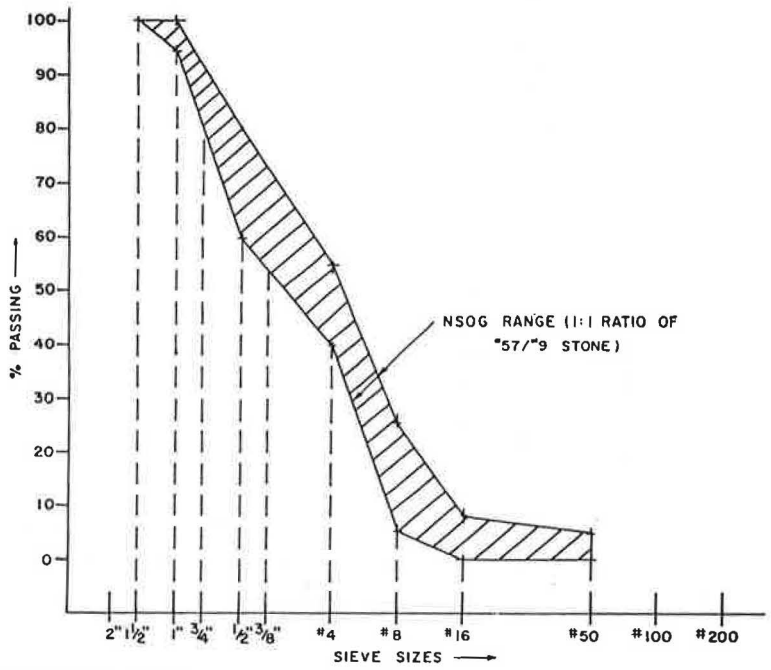

FIGURE 5 NSOG gradation range.

material specification are met, new falling head permeability and modified compaction tests are provided (4). The specified permeameter served well throughout the research study. The equipment can be used with confidence on materials that have a K factor ranging from 100 to 20,000 ft per day. This permeameter gives reasonable repeatability, and the permeability constant K values are probably slightly conservative, and hence applicable to the subject engineering problems. When used as a permanent piece of equipment, it should be improved and standardized for manufacturing purposes.

To duplicate field compaction conditions, laboratory compaction procedures for NSOG material were developed and provided by the specification (4). ASTM specification D2049 provides Burmister vibratory table test procedures for compaction of cohesionless soils. The Burmister equipment was modified for testing the open-graded materials, as it is described in specifications (4). A Plexiglas mold was used to allow viewing of the samples for evaluation of their gradational stability and density measurements. The relatively large Plexiglas cylinder mold, capable of holding 15 lb of uncompacted NSOG materials, proved to be essential for obtaining representative density results. For permeability tests, a 4-in. metal mold is used with a 1600-g specimen for compatibility with the permeameter. This equipment should also be standardized for manufacturing purposes.

It should be noted here that wet stone densities were lower than dry stone, on the average by approximately 8.5 percent. Also, there appears to be no migrations of the fine material to the bottom of the sample, although considerable migration of fines could be observed in dry samples. The presence of water appears to decrease the density and lessen the migration of fines. Therefore, although wet stone will be used in the field to minimize segregation, in laboratory compaction only dry stone must be tested.

BSOG Material Properties and Laboratory Test Procedures

The BSOG material must comply with the gradation band shown in Figure 6 and the composition of the mixture given in the following table. The BSOG material shall consist of bitumen, antistripping agent, and aggregate that conform to the following gradation requirements:

Sieve Size	Allowable Percent Passing
1 in.	100
0.75 in.	95-100
0.5 in.	85-100
0.375 in.	60-90
No. 4	15-25
No. 8	2-10
No. 16	2-5
No. 200	-

[Note that for the No. 200 sieve, 2 percent (by weight of total mix) mineral filler should be added. Also note that the bitumen content shall be 3 ± 0.5 percent by weight of dry aggregate and mineral filler.] This gradation, made of No. 8 stone size, is modified by the addition of some large size aggregate to lower material cost. Because the material passing the No. 4 screen and retained on the No. 8 screen controls the permeability, the BSOG gradation specifications of the No. 4 screen are also tightened.

The asphalt content for the BSOG material should always be set at 2 to 3.5 percent. The lower limit of this range was determined on the basis of a thorough coating of the stone particles. The upper limit, on the other hand, was established when the excess of the asphalt content begins to drain. Admixing of an antistripping agent to the asphalt is required for field applications. Also, a small amount of mineral filler (2 percent) is used to

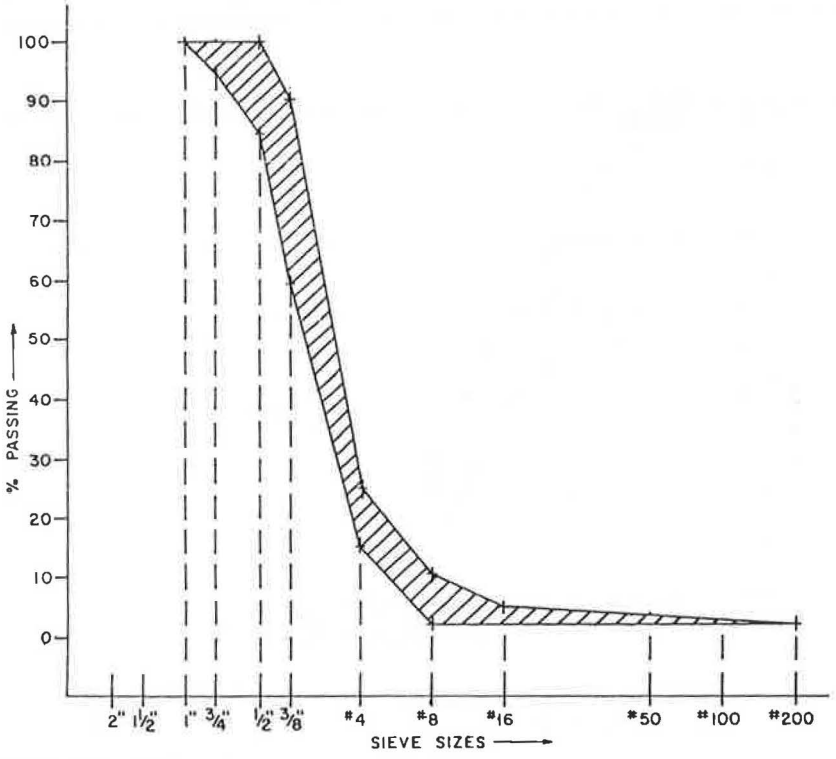

FIGURE 6 BSOG gradation range.

stiffen the asphalt cement, to reduce asphalt drain off, and to improve mixture cohesion.

As in the case of the NSOG material, the contractor is required to submit for approval a particular target gradation that is within the band. The design approval is based on the NJDOT laboratory test of mixture permeability. The compaction of the BSOG material is achieved with a Universal testing machine at pressures of 1,000 psi for trap rock and gneiss and 600 psi for limestone materials. This provides permeabilities within the required range of 1,000 to 3,000 ft per day. Field permeabilities should be somewhat higher than the laboratory values because the compaction process with the Universal testing machine tends to create a more closed surface than that achieved in the field.

It should be recognized that the laboratory compaction data can serve as a guide for field densities. Because the laboratory compaction pressures evolved from an attempt to match achievable field densification, the laboratory densities could be used as a rough indication of the probable field density. However, it could not be used as a target because maximum density achieved on a control strip should be the only acceptable target. Nevertheless, a general equivalency between laboratory and control strip field data offers some assurance that permeability levels in the field are somewhat comparable with laboratory values.

To assure compliance with the requirements and the specifications previously given, permeability tests and modified Universal testing machine compaction procedures are provided. ASTM specification D1075, as used in the Immersion Compression Test, was modified to suit the specific needs of BSOG material compaction. The major modification for testing drainage layer materials consisted of decreasing the compaction pressure specified in the test. This was done to minimize the effect of the apparent crushing of particles, which had caused considerable changes in gradation--a phenomenon that did not occur in the field. Again note that because the researcher could look only at a limited amount of New Jersey sources, caution must be exercised when new sources or stone types are being introduced.

Design of Water-Collection Systems

General

Some of the features of water-collection systems were already discussed in the subsurface geometry analysis. Basically, physical features such as the use of longitudinal and transverse drains, the angle of outlets, daylighting or draining the outlets into the inlet structures, and the like were discussed. The geometric analysis of the location, spacing, and arrangement of collectors was also made.

At this point two factors concerning internal drainage collection should be mentioned. One is vertical drainage, and the other is daylighting of the drainage layer instead of draining it into the edge drains. The vertical drainage of the infiltration water is impractical because of the impervious nature of the subbase and the complexity and cost of the solution for determination of the drainage characteristics of the subgrade. On the other hand, the daylighting principle, at a glance, appears tempting mainly because it is so much cheaper. However, it is a generally well-known fact that it is not uncommon for this type of outlet to become clogged and cease to function. This would mean a water buildup under the pavement resulting in a rapid deterioration of the pavement structure. Thus a drain that contains a pipe is the only positive mode of water collection that appears to be sufficiently practical and reliable.

Longitudinal Transverse Collectors and Outlets

Figures 7-11 provide typical details of longitudinal and transverse collector designs and outlets that are either daylighted or terminated in inlets. Factors that affect collector design basically are

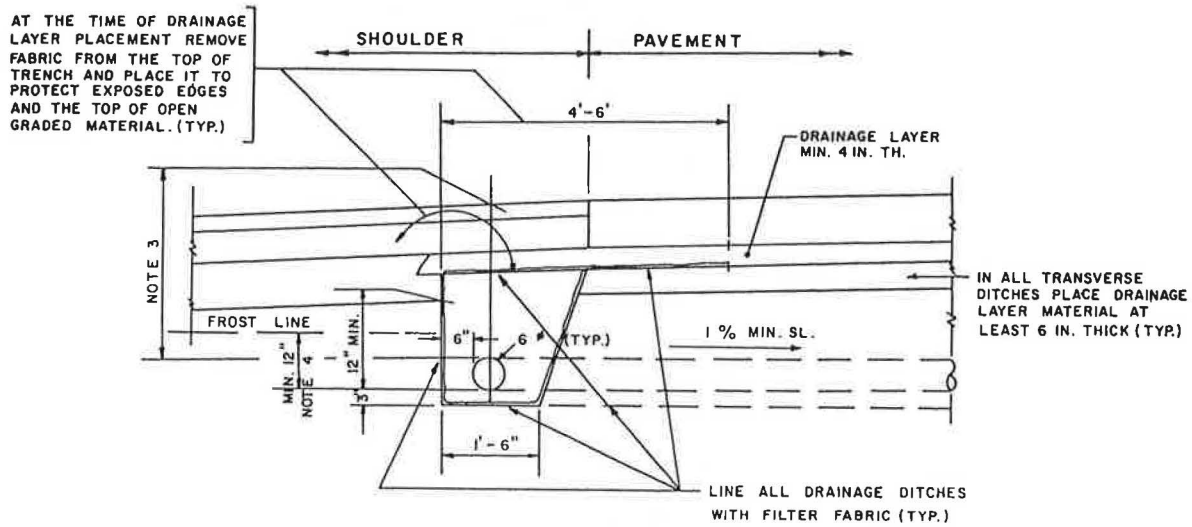

NOTE: 3. FOR ALL TYPES OF PIPES TOTAL MIN. COVER SHALL BE 30 INCHES, BUT NO LESS THAN 12 INCHES OF SOIL SHALL BE PLACED ON TOP OF A PIPE. COMPACTION SHALL BE IN 6 INCH LIFTS BEGINNING WITH FIRST 12 INCHES OF MATERIAL PLACED OVER THE PIPE.

4. IF A SHALLOW COLLECTOR DRAIN IS DESIRED DISREGARD MIN. DEPTH BELOW THE FROST LINE.

FIGURE 7 Typical detail of the edge of pavement subsurface drainage collectors.

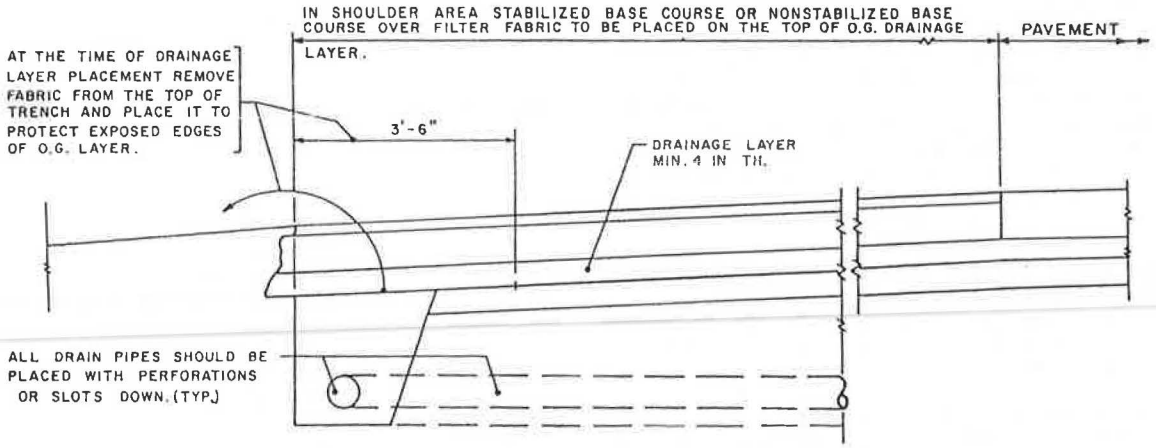

NOTE: FOR ALL ADDITIONAL DETAILS AND NOTES SEE FIGURE #7

FIGURE 8 Typical detail of the edge of shoulder subsurface drainage collectors.

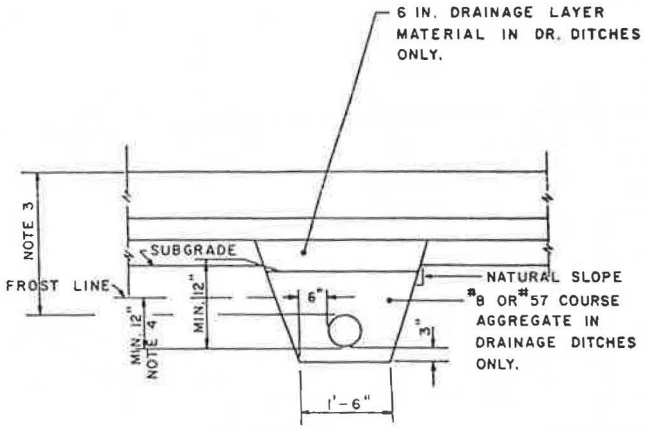

NOTE 3 FOR ALL TYPES OF PIPES TOTAL MIN. COVER SHALL BE 30 INCHES, BUT NO LESS THAN 12 INCHES OF SOIL SHALL BE PLACED ON TOP OF A PIPE. COMPACTION SHALL BE IN 6 INCH LIFTS BEGINNING WITH 12 INCHES OF MATERIAL PLACED OVER THE PIPE.

4. IF A SHALLOW COLLECTOR DRAIN IS DESIRED DISREGARD MIN. DEPTH BELOW THE FROST LINE.

FIGURE 9 Typical transverse ditch detail.

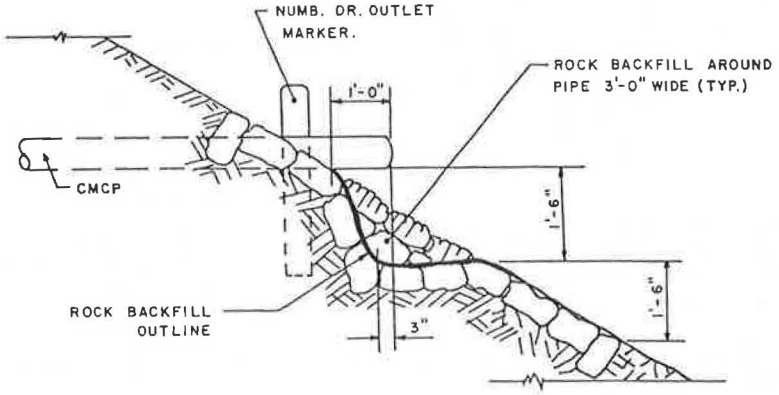

FIGURE 10 Typical detail of drainage outlet with rock backfill.

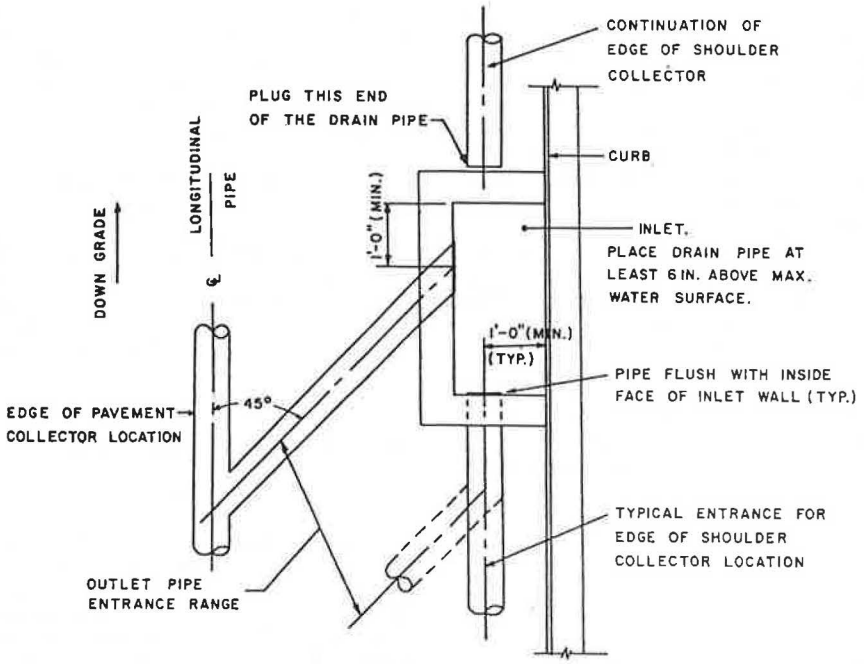

FIGURE 11 Typical outlet pipe entrance detail.

drainability, susceptibility to frost effects, and structural integrity. Drainability is, of course, the purpose of such a system; however, frost or structural instability could jeopardize its functionality. For this reason a collector must be carefully designed and constructed, as shown in Figures 7 and 8. The minimum requirements should be such that a 6-in. clearance is provided between the trench walls and the side of the pipe. In addition, the trench must be deep enough to keep the bottom of the drain pipe on a 3-in. bedding, at least 12 in. below the top of the subgrade, and under minimum structural cover required by the pipe designs.

There appears to be some controversy concerning location of a drain pipe in relation to the frost depth. Theoretically, a functional pipe is not going to have enough water to freeze. However, for reasons not fully substantiated, there are reports of frozen collectors impairing drainage functions. There are enough grounds to believe that situations might arise whereby the function of a collector might be impeded by frost. So the question is, How real a problem is the freezing of a collector system? It is the belief of this researcher that, in lieu of adequate knowledge, the possibility of such a calamity calls for an engineering judgment, and it is suggested that the requirements offered by U.S. Army manual TM5-820-3 (5) and shown in Figures 7-9 be used.

Because a drainage trench is located within a subgrade usually containing a large quantity of fines, a filtration medium such as a filter fabric lining is advisable, especially because the crushed-stone trench backfill must have drainage characteristics exceeding the drainage layer material and particle sizes compatible with the pipe perforations. A No. 8 or No. 57 stone fits well into the situation, whereas the No. 57 and No. 9 mixture has enough No. 9 stone size particles that might easily migrate into the pipe and permanently impede its function. To protect the trench backfill from contamination by fines from adjacent soils, a sufficient length of filter fabric flap should cover the trench during construction. This should be left in place until the placement of the drainage layer, at which time the flap should be removed and placed to protect the edges of drainage material.

The same requirements and procedures are necessary for transverse ditches, except that to increase the structural integrity, the top 6 in. of the pipe backfill is replaced by regular drainage layer material.

As note 3 in Figures 7-9 indicates, porous wall, corrugated metal, and polyvinal chloride (PVC) and polyethylene (PE) plastic pipes can be used in such applications. Although the first two types of pipe material have been used successfully for a long time, the application of plastic materials in such a manner is relatively new.

At this point the importance of only 3 in. of pipe bedding and good compaction of the pipe backfill must be mentioned. Experience has demonstrated that the use of more than 3 in. of bedding provides too much undrainable space below a drain pipe, and the structural strength, especially with plastic pipes, in large measure depends on the proper compaction of the backfill material. Improper handling of either criterion could impede the structural integrity of the collector.

DESIGN OF GROUNDWATER DRAINAGE

The analysis and solutions of the groundwater drainage problems can be found in publications by Moulton (6) and by Kozlov (4).

A groundwater control system refers to subsurface drainage specifically designed to remove or control the flow of groundwater. Such a subsurface drainage system may perform a number of the following functions:

1. Intercept or cut off the seepage above an impervious boundary, and
2. Draw down or lower the water table.

Often such a system may apply to more than one function, such as the interceptor drain not only cuts off the flow but it also draws down the water table. Such subdrainage systems are commonly identi-

fied in terms of their location and geometry. Contrary to infiltration water drainage systems, the groundwater drainage system will be used only when and where it is needed. This means it must be designed to fit each case individually, and in most cases it will consist of some form of interceptors. Furthermore, the quantity of flow and the means of its disposal must be known for a groundwater drainage system to be adequately functional.

In most cases little or no water gets into the pavement section from this source. However, in cases of a high water table or artesian flow, the water drawdown that is required often can be accomplished by a properly designed drainage blanket of high permeability. Normally it is located beneath the subbase on the top of the subgrade so as to keep water from saturating the pavement foundation. This layer, in variance to a drainage layer for the removal of roofwater, must be designed and constructed so as to remove all water as soon as it is reasonably possible.

CONSTRUCTION AND MAINTENANCE

General

The limited experience in building internally drainable roads has demonstrated the relatively easy constructability of such systems under portland cement concrete and bituminous concrete pavements. The experience has also revealed the possible pitfalls that can occur when a less-than-concerned attitude exists on the part of the road builders. Attempting to build such systems with inadequate, unsuitable, and dilapidated equipment is bound to be fraught with difficulties. In addition, constructing only part of the underdrainage system and leaving it, for example, over the winter to be completed next spring is totally unacceptable. Even neglecting it during the construction season is extremely ill-advised and will make it prone to considerable damage and probably even early failure at a later date because of possible contamination and degradation. Proper design and strict enforcement of drawings and specifications are absolutely essential. Because such requirements must also apply to the construction of any elements of a highway, the enforcement of said requirements should not cause increased costs when a reputable contractor is involved.

Thus the constructability of BSOG and NSOG drainage layers with proper equipment and in accordance with the procedures appears to cause few, if any, problems. However, if other than the specified equipment and procedures are used, placement of these materials can be somewhat problematic. The performance of such layers under rigid or flexible pavements, when proper confinement is provided, indeed appears to be adequate. When an asphalt-stabilized base is placed over a drainage layer, the BSOG material provides an adequate construction platform, whereas the NSOG layer, under adverse circumstances, might be somewhat unstable. The problems encountered with the NSOG layer appear to occur when adverse construction conditions require an unusual amount of manipulation by trucks delivering the mix to the paver. The end result might be a certain amount of rutting (0.5 to 1.0 in.) of the open-graded layer. If normal rutting is not tolerable, use of the BSOG drainage layer is recommended. However, if the NSOG material is used, careful construction practices (e.g., a laborer with a rake or a small compactor-roller) can keep the surface in an adequate shape.

The best means for including the special underdrainage in roadways is first to construct all subbases. If required, the top of the subbase is then stabilized or the filter cloth barrier is placed to provide a construction platform and to prevent the intrusion of fines into the overlying drainage layer. This is followed by the construction of the collection system. Finally the drainage layer is placed.

Irrespective of the proper design and construction of a subsurface drainage system, some maintenance will be required to ensure the continuous operation of the system. To the extent possible, all features of the system should be designed for minimum maintenance. Nevertheless, a program of continuing regular inspections, preventive-type maintenance, and repair-type maintenance must be anticipated.

Construction of Collection Systems

For drainage trenches the procedure should be to excavate through the subbase to a prescribed depth. Then the trench should be lined with filter cloth by unrolling it by hand, keeping it about 30 ft ahead of the backfilling operation. While two laborers hold the edges, a third man should walk the filter fabric, conforming it to the dimensions of the trench. After that a drainage pipe should be placed on 3 in. of No. 8 stone bedding and backfilled with No. 8 stone. Beginning 12 in. above the top of the pipe, the backfill in the trenches must be compacted in 6-in. lifts by three to four passes of a vibratory plate compactor.

The construction of outlet ditches is similar, except solid (nondrainable) pipes and regular subgrade soils for bedding and the backfill must be used. The outlet pipes should either be daylighted or terminated in the surface drainage inlet structures.

The procedure for trench construction that is acceptable for a small job requires the use of a Grad-All for trench excavation, a front loader for placement of the backfill, and regular trucking for material transportation. Although 1,000 ft per day of such trench construction might be achieved, considerably better progress on the order of 2,000 to 3,000 ft per day should be possible if more appropriate equipment and construction scheduling were used. For example, a significant increase in the efficiency of the trenching operation could be realized if a trenching machine, such as a Ditch Witch, and modified trucks to funnel stone into the ditch were used. All this, coupled with adequately scheduled removal of the excavated material and supply of pipe and backfill, would considerably improve construction progress.

Construction of NSOG and BSOG Drainage Layers

Placement of the open-graded layer (both NSOG and BSOG) can be best accomplished with an asphalt paver. Whether or not a stone spreader for placing an NSOG layer is usable depends on the degree of precision the equipment is capable of; it must be at least equivalent to the precision of an asphalt paver with automatic grade control. For placing NSOG and BSOG materials, the use of a tracked paver is recommended. Additional fine grading with a grader should be nil. Slightly moist (about 2 percent moisture) NSOG material can be handled by an asphalt paver with no modification or damage to the equipment. The NSOG material should be compacted by a vibratory roller, whereas the BSOG layer can be compacted with standard static rollers (three-wheel breakdown roller followed by tandem finishing

roller). The vibratory asphalt rollers could possibly be used on the BSOG material, but the temperature would have to be appropriately lower to prevent edge shoving.

Considering that the BSOG mix appears to be somewhat unstable when hot (excessive spreading has been observed at the edges during compaction), it is advisable for compaction to commence at a temperature of about 210°F. For permeability reasons, the mix is rather open with few fines, if any, in it. Thus the asphalt tends to act more as a lubricant, aiding compaction with this mix more than with a dense-graded mixture. The lower compaction temperature permits the asphalt viscosity to increase and its bonding ability to take over to achieve a more stable mix for compaction.

The test strip approach for compaction control of the open-graded layers appears to work well. Because this approach relies only on relative density measurements, a nuclear gauge operated in whatever mode, be it in the backscatter position with or without surface preparation or in the direct transmission mode, should be adequate. A nuclear gauge is thus used to monitor the increasing densities at the same three locations within a control strip between successive roller passes. As the compacted material approaches the maximum density achievable in the field, the average difference between any two consecutive passes approaches zero. Under the direction of the engineer, rolling must continue until this average density difference is less than or equal to 0.5 lb/ft^3. At this point maximum density is inferred because the observed density failed to increase with additional passes. Based on statistical data from the experimental installations, it is expected that most BSOG strips will require approximately 6 passes, and less than 5 percent of the control strip applications should require more than 10 passes. For NSOG control strips the average number of required passes should be approximately five.

As already stated, construction of pavement courses above the open-graded layers should not be difficult if proper equipment is used. After it has cooled, the BSOG material hardens into a very firm layer, which represents an adequate construction platform for both the portland cement and bituminous concrete surfacings. For the NSOG layer, only conventional paving procedures are necessary for placement of the concrete.

No shrinkage cracks in the concrete road slabs and little infiltration of the concrete into the open-graded layers has been observed. The latter case should dispel fears of excessive friction between underlying open-graded material and the pavement slabs.

MAINTENANCE OF SUBSURFACE DRAINAGE SYSTEMS

Irrespective of the proper design and construction of a subsurface drainage system, some maintenance will be required to ensure that the system continues to operate in a satisfactory fashion. In other words, no action or lack of action should be allowed to reduce the efficiency of the system. To the extent possible, all features of the system should be designed for minimum future maintenance. However, every operating condition for the system cannot always be anticipated. Thus a program of continuing regular inspections, preventive-type maintenance, and repair-type maintenance must be anticipated.

Cleaning of Collector Pipes

It might be anticipated that sediment could be deposited in collector pipes because of inadequate pipe gradients, uneven settlement of the system, or a heavy sediment load. In anticipation of such a possibility, clean-out boxes or risers at various locations within the pipe network could be designed into the system and, of course, the pipes also can be cleaned from the outlets. In addition, the pipe network should be designed in such a way that right angle turns are eliminated.

Maintenance of Outlets

The outlet system must be maintained in a free-flow condition throughout the life of the facility. With respect to pipe outlets, the principal concerns would be the blockages caused by weed growth, siltation of the adjacent ditch, debris from the roadway or slope, and activity of animals or man. Only through periodic inspection can these circumstances be identified and subsequently rectified. Such inspections should be made before seasonal periods of heavy rainfall, as well as following particularly heavy rainfall events or at least once every 3 months.

Also, outlet markers should be maintained in good condition. Damaged markers should be repaired or replaced immediately. Any marker destroyed or damaged during other construction or maintenance activities should be immediately reported for replacement or repair.

Miscellaneous Maintenance and Other Considerations

Careful periodic inspections are the key to adequate maintenance of the subsurface drainage system. However, other related maintenance activities associated with the pavement--pavement shoulder, surface drainage system, ice and snow control and removal, right-of-way mowing, and so forth--can all have an impact on the operation and maintenance of the subsurface drainage system. Although the maintenance of the subsurface system might not take precedence over one of the aforementioned activities, it must not be relegated to an insignificant status. For example, although mowing is an essential maintenance activity, it has a potentially detrimental effect on the outlet system. That is, the mowing machines could damage the outlets through impact with the outlets during the mowing operations. If the likelihood of such an occurrence is high, use of erosion control aprons or chemical weed control could be used in lieu of mowing.

Maintenance that ensures the efficient collection and removal of surface water will also generally improve the operation of the subsurface drainage system. Timely repairs of damage to surface drainage structures, pipes, ditches, and so forth will contribute to the proper operation of the subsurface drainage system. Likewise, timely and cautious repairs of damaged pavement and shoulder sections will be beneficial to the underdrain system.

Those responsible for the care of the subsurface drainage systems should maintain detailed as-built plans of the systems to facilitate subsequent repairs and replacements. In addition, a separate record of the location of drainage facilities, particularly outlets, should be maintained so that these facilities can be easily located by maintenance personnel. Inspection records should be kept along with records of each maintenance activity required by the system. If these records are kept in a continuous fashion, they may suggest the need for some more substantial efforts to prevent the recurrence of some continuing maintenance problem. The information concerning the modification of conditions adjacent

to the subsurface drainage system must also be diligently gathered and assessed. Any modification or change that would adversely affect the operation of the subsurface drainage system should be corrected promptly to mitigate potentially detrimental effects.

SUBSURFACE DRAINAGE AND PAVEMENT REHABILITATION

Adequate attention should be given to the performance of existing subsurface drainage sytems or to the construction of new or extended systems in conjunction with pavement rehabilitation projects.

Conventional rehabilitation techniques on pavements, where the foundation was undermined by inadequate subsurface drainage, only postpone the inevitable further disintegration of the pavement structure, resulting to a large degree in useless expenditures. Nevertheless, the internal drainage solution was developed for and should be used only for the purpose of resolving internal drainage problems of roads. Therefore, in no way is it just an alternate approach to currently available road pavement designs. Therefore, to assure the resolution of internal drainage on new construction, there is no choice but to apply the methods offered in this paper exclusively; for rehabilitation efforts this solution must be used selectively (i.e., only if road conditions warrant it). It goes without saying that the rehabilitation of roads damaged by other causes than subsurface water should be accordingly performed because their drainage probably already is functional by some natural means, such as permeable enough subgrades.

DESIGN GUIDELINES FOR REHABILITATION OF PAVEMENTS

An effective approach that can be offered for pavement rehabilitation proposes constructing an overlay consisting of 4 in. of BSOG material directly on the existing pavement surfacing and draining it into drainage trenches and outlets, as detailed in this paper. Because of adversities of the construction, NSOG material is not suggested for use in such a rehabilitation effort. The drainage layer, of course, will have to be overlaid by a minimum of 3 in. of bituminous-stabilized base course (BSBC) and 3 in. of medium aggregate bituminous concrete (MABC) surfacing. The proposed solution most probably will mean higher initial cost compared with the present, rather inadequate, conventional rehabilitation methods. This solution, however, appears to be a viable approach to the problems induced by internal drainage because it has the potential for alleviating water-related damage. An illustration of the economic aspects that are involved is available in the NJDOT files (7).

As in the construction of new pavements, the recommended subsurface drains are designed to handle water that infiltrates the pavement area only. It is assumed that the surface drainage is functioning and that the runoff from the surrounding areas will be drained by it.

Where groundwater is an expected problem, an investigation of the water-bearing strata should be made, including depth and permeability of the strata and the amount of water carried by it. This investigation will allow the designer to increase the pipe size to ensure adequate capacities for all sources of water.

CONCLUSIONS

In this paper solutions of the internal drainage problems of roads are provided in a rather condensed (so to speak) "cookbook" form. This became possible only because in this research effort an attempt was made to produce a well-organized, practical, and relatively simple approach to this problem without, however, jeopardizing engineering integrity. Such an approach makes it possible to present an engineer with complete enough procedures for building and maintaining adequately drainable roadways.

In the meantime, future monitoring of the already existing experimental drainable road sections should furnish enough controlled data to detect and, if need be, to remedy deficiencies that might surface.

ACKNOWLEDGMENT

The author is grateful to the personnel of the New Jersey Department of Transportation for their assistance in gathering and evaluating the data necessary for presentation of this paper.

REFERENCES

1. G.S. Kozlov. Road Surface Drainage Design, Construction, and Maintenance Guide for Pavements. New Jersey Department of Transportation, Trenton, June 1981.
2. H.R. Cedergren, K.H. O'Brien, and G.A. Arman. Guidelines for the Design of Subsurface Drainage Systems for Highway Structural Sections. Report FHWA-RD-72-30. FHWA, U.S. Department of Transportation, June 1972.
3. A. Casagrande. Base Course Design for Airport Pavements. Proc., ASCE, Vol. 77, June 1951.
4. G.S. Kozlov. Improved Drainage and Frost Action Criteria for New Jersey Design--Volume III: Road Subsurface Drainage Design, Construction, and Maintenance Guide for Pavements. New Jersey Department of Transportation, Trenton, Aug. 1983.
5. Drainage and Erosion-Control Structures for Airfields and Heliports. Technical Manual TM5-820-3. Department of the Army, Washington, D.C., July 1965.
6. L.K. Moulton. Highway Subdrainage Design. Report FHWA-TS-80-224. FHWA, U.S. Department of Transportation, Aug. 1980.
7. G.S. Kozlov. Rehabilitation of Pavements Damaged by Inadequate Subsurface Road Design. New Jersey Department of Transportation, Trenton, March 1979.

Publication of this paper sponsored by Committee on Subsurface Drainage.

Study of Factors Influencing Deflections of Continuously Reinforced-Concrete Pavements

WAHEED UDDIN, ALVIN H. MEYER, and W. RONALD HUDSON

ABSTRACT

The results of an investigation of the effects of temperature and location variables on Dynaflect deflections measured on rigid pavements are presented. All the experimental work described in this paper was carried out during the fall and summer of 1981 on a new 10-in.-thick, continuously reinforced-concrete pavement near Columbus, Texas. Dynaflect deflections and the top and bottom temperatures of the concrete slab were analyzed by using analysis of variance and multiple linear-regression techniques. The findings of this study are included in a procedure recommended for making Dynaflect measurements and for applying suitable temperature corrections to deflections measured near the pavement edge.

Nondestructive evaluation of existing pavements was carried out to assess their structural adequacy and rehabilitation needs. The Dynaflect, a steady-state vibratory device, is widely used for nondestructive evaluation of asphalt and rigid pavements. The response of a pavement to an external test load is measured in terms of surface deflection, which is indicative of the load-carrying capacity of the pavement. Dynaflect deflection data are used for in situ characterization of pavement layers and subgrade as a basic step in several current overlay design procedures. In the case of rigid pavements the distress manifestations indicate other deficiencies and problems, such as inadequate subgrade support conditions, existence of voids beneath the concrete pavement, and insufficient load transfer across transverse cracks and joints. A major rehabilitation program for an existing rigid pavement may include rectification of these deficiencies plus an overlay for the structural strengthening required for future design axle load applications. Dynaflect deflection data can also provide diagnostic information related to the evaluation of load transfer and detection of voids.

According to the available structural models based on the plate theory, the deflection of rigid pavements is influenced by the position of the applied loads. Furthermore, daily variations of temperature create a cycle of temperature differential in the concrete slab, which results in curling (1).

OBJECTIVES AND SCOPE OF STUDY

Several factors influence any deflection measurement made on a specific slab. Two of these are temperature and load position. In the case of a rigid pavement, these effects are significant. A temperature gradient through the thickness of the slab induces thermal stresses and, subsequently, curling. The deflection measurements may therefore be affected by temperature, particularly at the slab edge.

The principal objectives of this study are to

1. Identify temperature effects and other factors related to load position across the test section that may influence the Dynaflect deflections in rigid pavements,
2. Investigate the influence of these factors on measured Dynaflect deflections,
3. Develop, if necessary, a procedure for correcting the measured deflections to remove the effects of temperature, and
4. Recommend the most suitable placement of the Dynaflect for making deflection measurements for characterizing placement or for detecting voids beneath pavements in place.

The experimental program carried out on a continuously reinforced-concrete (CRC) pavement, the summary data, and the results of statistical analyses are described in this paper.

DEFLECTION BEHAVIOR OF RIGID PAVEMENTS

Environmental Variables

Temperature Effects

The average temperature of a concrete slab varies daily and yearly. Concrete pavement adjusts to yearly seasonal variations in temperatures by contraction or expansion over a considerable period of time. The major effect of seasonal variations in temperature is the development of frictional forces between the concrete slab and the underlying layer.

Daily temperature variations within the concrete slab are more important to deflection measurements because (a) there is a large deviation in temperature on the concrete surface in a daily cycle, and (b) the temperature gradient between the top and bottom of the concrete slab can vary considerably during a 24-hr cycle. The temperature gradient through a concrete slab causes surfaces to warp. For example, if the top of the slab is warmer than the bottom (e.g., near noon on a sunny day), the slab corners will tend to curl downwards. Upward curling will occur when the top surface is cooler than the bottom, such as late on a cool night. A parameter commonly used to study the effect of temperature gradient is temperature differential (DT), the algebraic difference between the temperatures of the top and the bottom of a concrete slab. DT is a positive value when the temperature of the top of the slab is higher than the temperature of the bottom, and it is negative when the bottom of the slab is warmer than the upper surface. The temperature differential is the result of the slow conduction of heat in concrete and therefore is a function of the thermal properties of concrete and the thickness of the concrete slab. Maximum temperature differentials occur during the day in the spring and summer. During the present study the maximum temperature differential (24.6°F) was observed in August 1981 for

the 10-in. concrete slab. The 1965 deflection study on CRC pavements reported by McCullough and Treybig (2) revealed an inverse relationship between temperature differential and the edge deflection (Benkelman beam) measured at the crack position.

Seasonal Effect

Any seasonal changes in deflections are generally the result of seasonal variations of moisture in the unbound base layer and the subgrade. The seasonal effects on deflections on rigid pavements are thoroughly discussed elsewhere (1,3). Metwali (4) described the results of analysis of variance (ANOVA) applied to the Dynaflect deflection data collected during fall and spring on different rigid pavement test sections. Metwali concluded that jointed-concrete pavements and asphalt pavements demonstrated statistically significant changes in the maximum Dynaflect deflections because of seasonal variations. CRC pavements did not experience appreciable seasonal variations in their deflection contrast. The findings by Metwali (4) are interesting and somewhat in conflict with current data and belief. Further research is needed, especially for CRC pavements.

Location Variable

The type of shoulder support at the pavement edge and the Dynaflect position with respect to the pavement edge and the locations of cracks or joints are also important factors that influence the deflection behavior of rigid pavement. These factors are discussed in the following sections.

Effect of Pavement Edge

Pumping in underlying unbound layers eventually results in the creation of voids under the pavement edge. Voids may also result from any movement in the subgrade or natural material, such as swelling or uneven settlement. The presence of voids beneath a pavement will result in relatively higher deflections. Birkhoff and McCullough (5) recommended a deflection survey along a pavement section to detect voids under the pavement edge. An important assumption in pavement design--that there is uniform ground support--is violated in the presence of voids. The voids will result in higher load stresses and eventually lead to deterioration of the pavement. Therefore a rehabilitation program should include a deflection survey to identify void areas.

Effect of Edge Support Conditions

The type of edge support will have a marked influence on the deflection behavior near the pavement edge. It is known from Westergaard's solutions that, for the case of edge loading, stresses at the pavement edge are much higher than stresses resulting from interior loading, and, because deflection is proportional to load stress, a larger deflection occurs at the pavement edge. For a concrete shoulder, deflection can be expected to be less than for a gravel shoulder. Another possible effect of a shoulder is the restraint offered to any lateral movement of the concrete slab by the edge support.

Effect of Cracks

Transverse cracks in CRC pavements are usually tightly held, but a loss in the load transfer will result in deflections larger than those measured between cracks (midspan position). Deflection at a crack will increase as the crack width increases. For material characterization, the midspan deflection (interior condition) is preferred. However, measuring the deflection at a crack position will give valuable information about load transfer efficiency and an indication of any excessive distress.

DESCRIPTION OF SETUP FOR DYNAFLECT AND TEMPERATURE MEASUREMENTS

A testing scheme was designed for making Dynaflect deflection and temperature measurements to investigate the effects of temperature and of the Dynaflect position. A newly constructed CRC pavement on the Columbus bypass of SH-71 was selected as the test site. Columbus, Texas, is located about 90 miles southeast of Austin and 70 miles west of Houston. Three test sections were selected on the southbound lanes. The first measurements were made on August 6 and 7, 1981, and resulted in four cycles at each test location (Figure 1). The pavement consists of a 10-in. concrete surface layer, a 4-in. asphalt

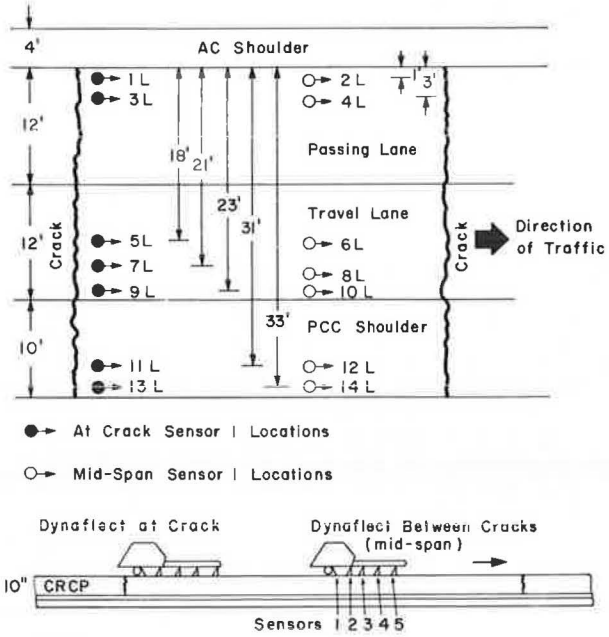

FIGURE 1 Layout plan of selected test locations, sections 1, 2, and 3.

base, and a 6-in. lime-treated subgrade overlaying the natural subgrade.

The second set of Dynaflect deflection data and slab temperatures were obtained on November 30 and December 1, 1981. Because of muddy conditions of the soil beyond the concrete shoulder, Dynaflect deflection data could not be acquired on locations 13L and 14L in all three sections. The deflection measurements were made smoothly and resulted in eight complete cycles. During summer measurements, average crack spacings were 11.3, 14.2, and 10.1 ft in test sections 1, 2, and 3, respectively, when the road was not opened to traffic. However, during the fall tests the average crack spacings were 7.4, 8.1, and 8.3 ft in test sections 1, 2, and 3, respectively, as a result of the occurrence of more cracks. The average crack width, as measured on the surface in fall 1981, was approximately 0.06 in.

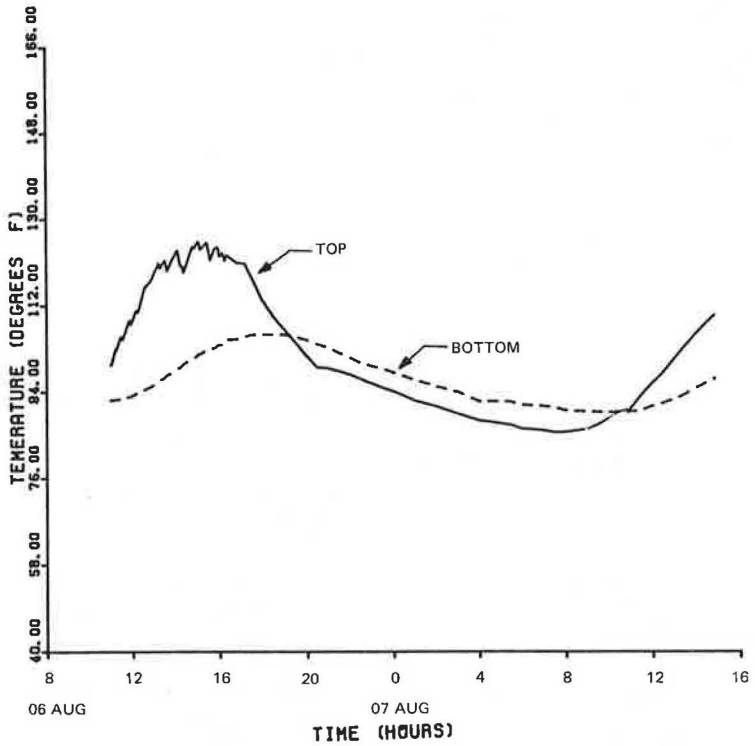

FIGURE 2 Temperature of top and bottom of concrete slab versus time, summer 1981.

The temperature block was placed in a preselected position so that the temperature of the concrete block could stabilize and be representative of the temperature conditions in the CRC pavement. Figure 2 shows the temperature records for the top and the bottom of the concrete block. The plot indicates that the temperatures in the concrete slab vary as a sinusoidal function of time, with the temperature at the bottom lagging behind the temperature at the top of the slab. This time lag occurs because of the low thermal conductivity of concrete. Details of the deflection measurements and a record of the temperatures at the top and bottom of the concrete slab are given elsewhere (1).

ANALYSIS AND DISCUSSION

The data setup for the statistical analysis is shown in Figure 1. For the comparison of means, only locations 1L and 12L are considered, forming 72 nonempty cells. The factors and their levels considered in the analysis are

1. Section (SEC) at three levels: SEC 1, SEC 2, SEC 3;
2. Season (S) at two levels: summer and fall;
3. Position with respect to the transverse crack (C) at two levels: near the crack (N) and midspan (M); and
4. Distance from the pavement edge (D) at six levels (Figure 1).

Analysis of Variance

Statistical Model

The following model was used in the analysis of variance of the deflection data:

$$W_{1ijklm} = \mu + SEC_i + S_j + C_k + D_\ell + \epsilon_{(ijlk)m} \quad (1)$$

where

W_{1ijklm} = mth Dynaflect deflection at sensor 1 measured at the lth location in the kth test position with respect to the crack in the jth season at the ith test section;
μ = overall mean;
SEC_i = effect of the ith test section;
S_j = effect of the jth season;
C_k = effect of the kth test position;
$\epsilon_{(ijkl)m}$ = random error caused by the mth test at the ith test section in the jth season on the kth position at lth distance from the edge [NID $(0, \sigma^2)$];
D_ℓ = effect of the lth distance from the pavement edge;
ℓ = 1, 2, 3, 4, 5, 6;
m = replications in each cell;
i = 1, 2, 3;
j = 1, 2; and
k = 1, 2.

The results of the ANOVA are given in Table 1. It can be concluded that the mean deflection is significantly different at different levels of all the factors, except season. For season, the null hypothesis cannot be rejected, which leads to the conclusion that the difference in mean deflections taken in summer and fall is not statistically significant. Figure 3 shows the effect of the Dynaflect position with respect to the transverse crack on the mean deflection W_1, thus indicating the significant difference, as found earlier from ANOVA. The significant influence of the distance of the Dynaflect from the edge on the mean deflection W_1 is shown in Figures 3-5. Figures 4 and 5 show the mean

TABLE 1 Summary of ANOVA

Source of Variation	Sum of Squares	DF	Mean Square	F	Significance of F
Within cells	0.295	360	0.001		
Constant	35.415	1	35.415	43183.36	0[a]
SEC	0.4048	2	0.202	246.78	0[a]
S	0.0000	1	0.000	0.01	0.915[b]
C	0.0426	1	0.043	51.95	0[a]
D	0.2498	5	0.050	60.93	0[a]

[a]Significant (i.e., reject the null hypothesis).
[b]Not significant.

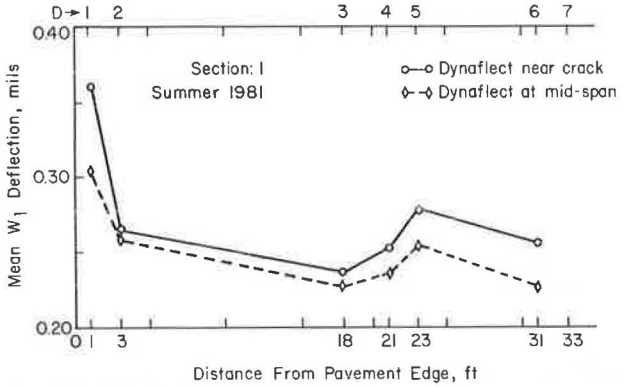

FIGURE 3 Variation in mean W_1 deflections at midspan and near crack as a function of distance from the pavement edge.

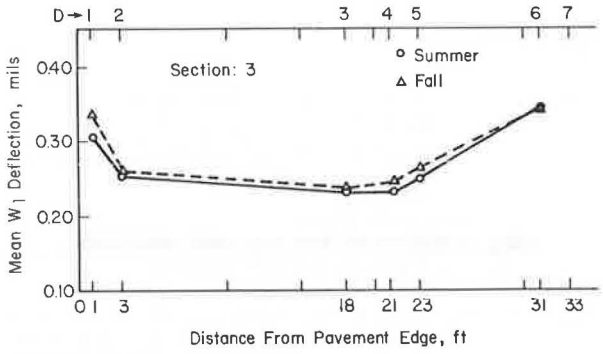

FIGURE 4 Effect of season on mean W_1 deflection at locations near transverse cracks.

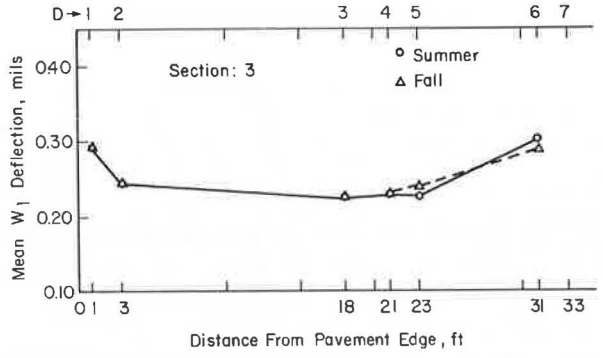

FIGURE 5 Effect of season on mean W_1 deflections at midspan locations.

deflection W_1 for summer and fall measurements, thus indicating no significant difference.

Consideration of Full Factorial Design

ANOVA was also performed considering all the possible interaction terms in addition to the main effects. It is concluded that

1. Except for season, the levels of all factors significantly influence sensor 1 deflections;
2. The effects of most of the two-, three-, and four-way interaction terms on sensor 1 deflection are not significant; and
3. The two-way interactions that significantly affected deflections are SEC with C and SEC with D; these interactions are shown in Figures 6 and 7.

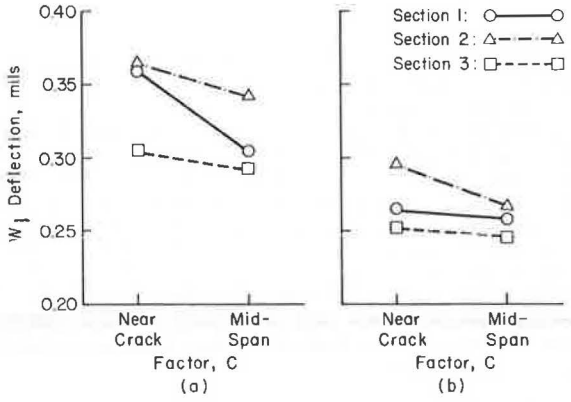

FIGURE 6 Graphical illustrations of two-way interaction SEC by C, summer 1981 data.

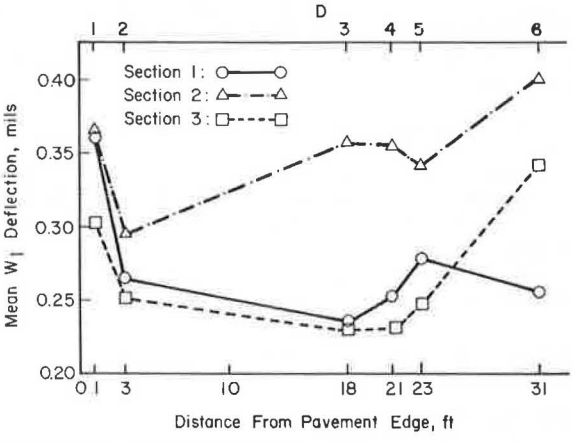

FIGURE 7 Graphical illustration of two-way interaction SEC by D, summer 1981 data.

TABLE 2 Summary of Analysis of Covariance

Source of Variation	Sum of Squares	DF	Mean Square	F	Significance of F
Within cells	0.269	359	0.001		
Regression	0.026	1	0.026	34.19	0[a]
Constant	17.670	1	17.670	23532.25	0[a]
SEC	0.411	2	0.205	273.66	0[a]
S	0.000	1	0.000	0.57	0.452[b]
C	0.042	1	0.042	56.54	0[a]
D	0.250	5	0.050	66.69	0[a]

Note: DT is the covariate.

[a]Significant (i.e., reject the null hypothesis).

[b]Not significant.

ANOVA on Log (Variance)

The basic assumption in ANOVA of the homogeneity of variance was checked by specifying Bartlet's test (6), which led to the rejection of the null hypotheses of homogeneous variance. ANOVA was also performed on log (variance) data. The results are as follows:

1. There is a significant influence of the levels of the factors SEC (sections), C (position with respect to the crack), and D (distance from the pavement edge) on the variance of the observed W_1 deflections.
2. The differences in variances of the observed W_1 deflections are not statistically significant with respect to season.
3. The plot of cell means versus cell variance indicated that four data points were associated with comparatively high variances. These correspond to summer data. The two in the top right-hand corner were in sections 2 and 3 at location 11L on the concrete shoulder. The other two correspond to location 1L in sections 1 and 2 [1 ft from the asphalt concrete (AC) shoulder]. These four points can be considered as outliers. Further investigation indicated that these large variances were caused by temperature differential.

Analysis of Covariance

DT in the concrete slab has a marked influence on the deflection measurements, as discussed earlier and in the report by Uddin et al. (1). An analysis of covariance was, therefore, performed in which DT was used as a covariate in conjunction with the factors considered in Equation 1. The model considered for the analysis of covariance is

$$W_{1_{ijklm}} = \mu + B(DT_m) + SEC_i + S_j + C_k + D_\ell + \varepsilon_{(ijkl)m} \quad (2)$$

where B is the regression coefficient.

In this model the regression procedure is used to remove the variation in the dependent variable caused by the covariate (6). The summary of the results is given in Table 2. The conclusions are essentially the same as those discussed for the ANOVA, as summarized in Table 1.

Effect of Temperature Variables on Dynaflect Deflections

The analyses performed thus far indicate that

1. W_1 deflections in summer and fall could be lumped together,
2. W_1 deflections are significantly different in each test section,
3. W_1 deflections near cracks are significantly different from those measured in the midspan position, and
4. W_1 deflections vary significantly with respect to the distance of the Dynaflect from the edge.

Therefore, the deflection measurements at each location should be treated as a sample from the individual population. The multiple linear-regression approach was used to identify the significant variables that could explain the variation in the measured W_1 deflections at each location (1). The explanatory variables considered in this study are (a) continuous variables and (b) dichotomous variables. The continuous variables are DT, mid-depth temperature (TMID), and spacing of the adjacent transverse cracks (CS). Mid-depth temperature is an average of the temperature of the top and the bottom of the slab. The dichotomous or dummy variables are used to represent the following qualitative variables:

1. Season (S): summer and fall, and
2. Section (SEC): sections 1, 2, and 3.

The results are given in Table 3. The following are the major findings (1).

TABLE 3 Effect of Removing Temperature Variables on R^2 of the Resulting Regression Equations for W_1 as Response Variables

	Dependent Variable (W_1)			
	Analysis A[a]		Analysis B[b]	
Location	Temperature Variables	R^2	R^2	Reduction in R^2[c] (%)
1L	DT	0.65	0.18	72.3[d]
2L	DT	0.68	0.40	41.2[d]
3L	DT	0.41	0.34	17.1[e]
4L	DT	0.49	0.40	18.4[e]
5L	TMID, DT	0.93	0.89	4.3[d]
6L	DT	0.71	0.61	14.1[d]
7L	TMID, DT	0.91	0.90	1.1[f]
8L	DT	0.79	0.65	17.7[d]
9L	-	0.67	0.67	0.0
10L	DT	0.71	0.61	14.1[e]
11L	DT	0.82	0.62	24.4[d]
12L	DT	0.90	0.82	8.9[d]
13L	DT	0.65	0.25	61.5[e]
14L	DT	0.83	0.55	33.7[d]

[a]All independent variables were considered in regression.

[b]Temperature variables were removed from the independent variables list before applying stepwise regression.

[c]Reduction in R^2 values of the resulting regression equations from analysis B as compared with the R^2 values of analysis A.

[d]Significant at 1 percent α level.

[e]Significant at 5 percent α level.

[f]Not significant.

1. The effect of DT on Dynaflect deflections varies with the position of the Dynaflect.
   (a) For the Dynaflect located in the midspan position (between transverse cracks) in the wheelpath or at the centerline of the slab, the measured deflections indicate a direct relationship with DT.
   (b) For the Dynaflect positioned anywhere near the pavement edge, the measured deflections exhibit an inverse relationship with DT (Figure 8).

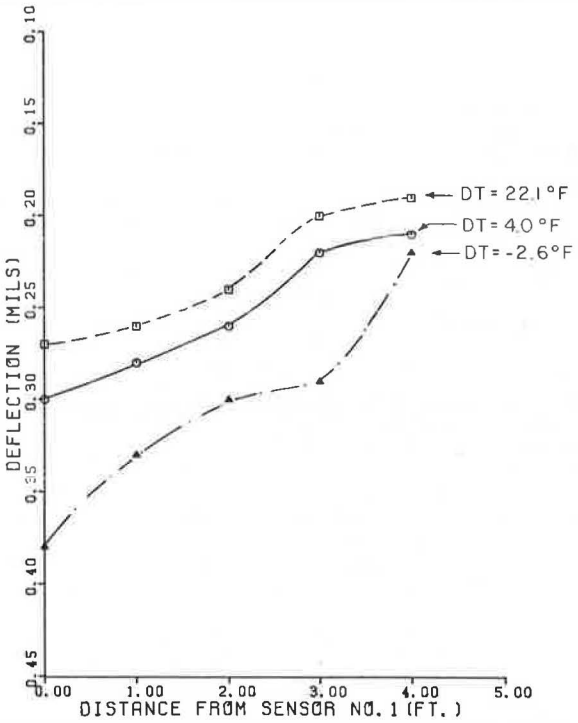

FIGURE 8 Deflection basins measured near pavement edge at different temperature differentials.

2. In the case of 1(a), the Dynaflect position corresponds to the interior condition. The errors caused by a very high positive DT (expected at the Columbus site) on measured deflections and the back-calculated elastic moduli of the pavement layers are practically negligible.

3. In the case of 1(b), the errors in measured deflections caused by a positive DT greater than 10°F are significantly high. This effect is more pronounced when the edge support is an asphaltic concrete shoulder or a gravel shoulder, as compared with a portland cement concrete shoulder.

These findings are also shown in Figure 9. Figure 10 is an example of daily variation of DT at the test site. The DT of a concrete slab is zero about 2 hr after sunrise on a clear day. The maximum DT occurs in the afternoon, about 2:00 or 3:00 p.m. It is important to recognize that DT will cause changes in the mean and variance of the deflections near the pavement edge.

TEMPERATURE CORRECTION PROCEDURE

A procedure for applying a temperature correction to the Dynaflect deflections measured at or near the edge of a rigid pavement is described in this section. As discussed earlier, DT in the slab is the most important temperature parameter that influences the deflections measured at the pavement edge. The deflection measured at any DT should be corrected to bring it to zero DT. The step-by-step procedure is as follows:

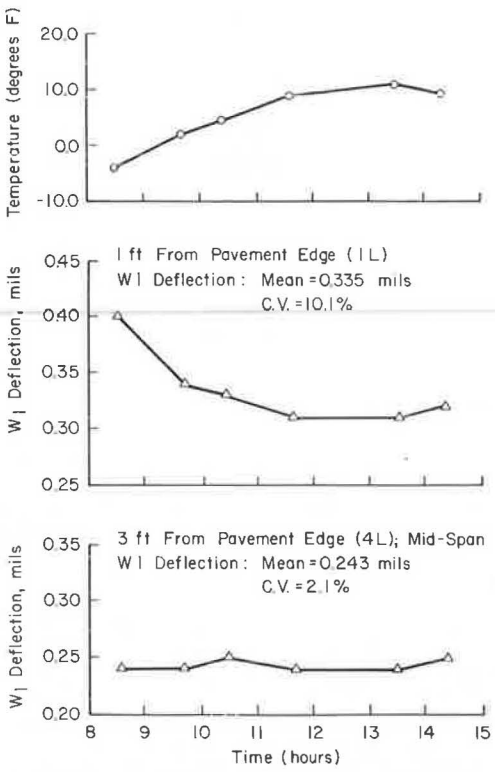

FIGURE 9 Variations in temperature differential and Dynaflect deflections with time (12/1/81) on section 3 at Columbus bypass SH-71, Texas.

1. Collect replicate Dynaflect deflection measurements at a location at or near the pavement edge.
2. Measure the temperatures of the top and the bottom of the concrete slab at the same time as the deflection measurements. Use the data to estimate the corresponding DT. An estimate of the hourly distribution of the DT can also be made by using the predictive model described by Uddin et al. (1) and by making use of the climatological data for the test location.
3. Develop a simple linear-regression equation with sensor 1 deflection, W_1 as the dependent variable, and DT as an independent variable.
4. Use the slope of the best-fit line to calculate the required amount of correction to the measured deflection (W_1). In the case of a positive DT, the corrected deflection will be larger than the measured deflection; in other words, the correction will be additive. The corrected deflection corresponds to zero DT.

An example is presented (1) to illustrate how the measured W_1 deflections were corrected to a zero DT condition. The data for W_1 and DT correspond to location 1L. Each data set corresponds to 12 replicate deflection measurements for sections 1, 2, and 3, respectively. The corrections were applied as explained in the preceding section. Figure 11 shows the best-fit lines for the measured and corrected deflections. As expected, the regression lines for the corrected deflections are practically horizon-

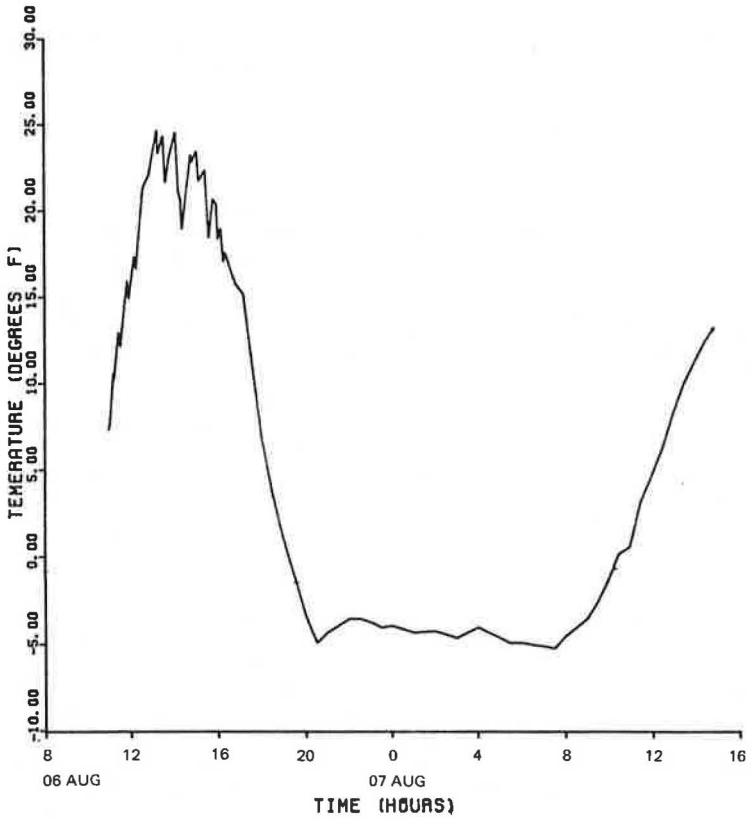

FIGURE 10 Temperature differential versus time relationship, summer 1981.

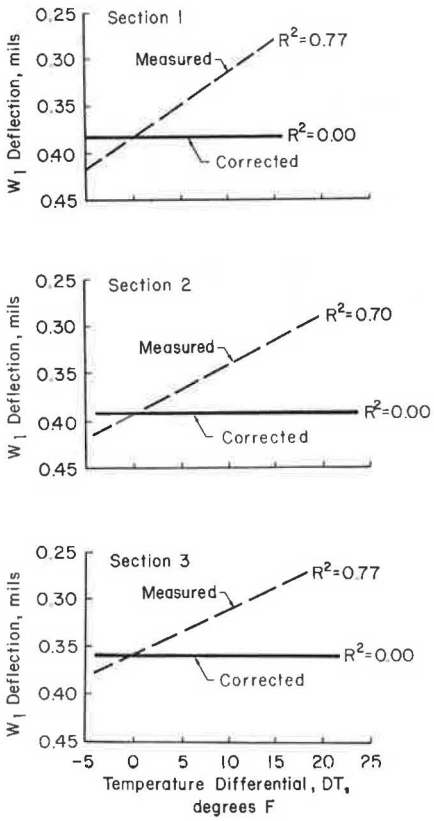

FIGURE 11 Best-fit lines for measured and corrected W_1 deflections at location 1L, Columbus bypass, SH-71, 1981 data.

TABLE 4 Summary Statistics of Measured (W_1) and Corrected (W_T) Deflections at Location 1L

Section	Summary Statistics	Dependent Variable: W_1 (measured)	Dependent Variable: W_T (corrected)
1	Mean (mils)	0.342	0.384
	SD	0.049	0.025
	CV (%)	14.0	6.6
	R^{2a}	0.72	0.00
2	Mean (mils)	0.357	0.393
	SD	0.045	0.025
	CV (%)	12.8	6.4
	R^{2a}	0.70	0.00
3	Mean (mils)	0.325	0.358
	SD	0.038	0.018
	CV (%)	11.8	5.1
	R^{2a}	0.77	0.00

[a]From simple linear-regression analysis with DT as independent variable on combined data of summer and fall 1981.

tal, with values of R^2 near zero. This means that the influence of DT has been removed from the measured W_1 deflections. The summary statistics for measured and corrected deflections are given in Table 4. Note that coefficients of variation for corrected deflections (5 to 7 percent) are practically within the expected range of inherent variability in the equipment and in the test procedure.

CONCLUSIONS

The major findings, as summarized in the following list, are based on the limited data collected on CRC pavements.

1. No significant difference in mean W_1 deflection with respect to the season is found in this study.
2. The mean W_1 deflections vary significantly for different sections.
3. W_1 deflections measured at locations that correspond to different distances from the edge are significantly different.
4. The mean W_1 deflections are influenced significantly by the position of the Dynaflect with respect to the transverse crack.
5. All these conclusions apply equally to the corresponding variance of W_1 deflections.
6. It is important to treat the W_1 deflections measured at each location (corresponding to crack position and distance from the edge) separately in order to develop a regression equation and statistical inferences.

The following recommendations relate to removal of the influence of the DT in the surface concrete layer on measured Dynaflect deflections.

1. Dynaflect deflection measurements should begin at least 2 hr after sunrise to avoid making any deflection measurements under negative DT conditions.
2. For material characterization, Dynaflect deflection data should be obtained in the midspan position (between the transverse cracks) in the wheelpath or at the centerline of the slab. In practice, the data do not need to be corrected for any positive DT within the range observed in this study.
3. For void detection purposes, Dynaflect deflections should be measured near the pavement edge, and the data should be corrected to correspond to zero DT.

ACKNOWLEDGMENTS

The research presented in this paper was conducted as part of the Cooperative Highway Research Program sponsored by the Texas State Department of Highways and Public Transportation and FHWA, U.S. Department of Transportation. Thanks are due to Gary Fitts, graduate research assistant, who designed and carried out most of the experimental work and helped in the preliminary analysis. Appreciation is extended to T.W. Sager and Mary Whiteside of the University of Texas at Austin Business School, who provided help and suggestions in the statistical analyses. Thanks are also due to B. Frank McCullough and Virgil Anderson for their constructive comments during the course of this research.

REFERENCES

1. W. Uddin, S. Nazarian, W.R. Hudson, A.H. Meyer, and K.H. Stokoe II. Investigations into Dynaflect Deflections in Relation to Location/Temperature Parameters and In Situ Material Characterization of Rigid Pavements. Research Report 256-5. Center for Transportation Research, University of Texas, Austin, Dec. 1983.
2. B.F. McCullough and H.J. Treybig. A Statewide Deflection Study of Continuously Reinforced Concrete Pavement in Texas. Tech. Report 46-5. Texas Highway Department, Austin, Aug. 1966.
3. A. Taute, B.F. McCullough, and W.R. Hudson. Improvements to the Material Characterization and Fatigue Life Prediction Methods of the Texas Rigid Pavement Overlay Design Procedure. Research Report 249-1. Center for Transportation Research, University of Texas, Austin, March 1981.
4. E.S.W. Metwali. Framework for a Pavement Evaluation System. Report FHWA/IM/JHRP-81/7. Joint Highway Research Project, Purdue University, West Lafayette, Ind., May 1981.
5. J.W. Birkhoff and B.F. McCullough. Detection of Voids Underneath Continuously Reinforced Concrete Pavements. Research Report 177-18. Center for Transportation Research, University of Texas, Austin, Aug. 1979.
6. G.O. Wesolowsky. Multiple Regression and Analysis of Variance. Wiley, New York, 1976.

Publication of this paper sponsored by Committee on Pavement Rehabilitation.

Examination of Pavement Deterioration in the Presence of Automobile Traffic

W. RONALD HUDSON and STEPHEN B. SEEDS

ABSTRACT

In recent years, and particularly in association with discussions of the federal highway cost-allocation study reported to Congress in 1982, a variety of statements and reports have surfaced alleging that automobile traffic, such as that on the Merritt Parkway in Connecticut and the Baltimore/Washington (B/W) Parkway in Maryland, causes as much overall pavement damage over the long term as does mixed truck and automobile traffic on highways of the same design in the same areas. A study was undertaken at the request of the Association of American Railroads to perform on-the-spot condition surveys of the Merritt Parkway, the B/W Parkway, and adjacent Interstate highways in both areas. In addition, intensive searches were made of records of the Connecticut Department of Transportation (which constructed and maintains the Merritt Parkway), FHWA (which built the B/W Parkway), and the U.S. Park Service (which maintains the B/W Parkway). The records of construction details and maintenance costs associated with the pavements under consideration were incomplete; nevertheless, a significant amount of information was obtained on which certain conclusions could be made. Basically, the results of the study clearly demonstrate that under the weather conditions, environment, construction materials, and pavement design and time frame involved in these cases, the damaging effect of trucks on heavy-duty highways is indeed greater than the damaging effect of automobiles. The data available and the scope of the study did not make it possible to derive quantitative relationships from these findings; however, they clearly refute the assertions that pavements deteriorate as rapidly under automobile traffic alone as they do under mixed truck and automobile traffic.

In recent years increasing pressure has been exerted by the trucking industry on Congress to have legal load limits increased and truck user fees and taxes decreased. One of the arguments that has been used is that trucks are not significantly more damaging to highway pavements than automobiles. Examples of pavement performance that have been used to support this argument are the somewhat poor pavement conditions of two parkways that are used by automobiles only: the Baltimore/Washington (B/W) Parkway (between Washington, D.C., and Baltimore, Maryland) and the Merritt Parkway in southern Connecticut. Two papers by Reith (1,2) of the American Trucking Associations, which refer to the two parkways, essentially make the same argument and conclude that "the parkways, without heavy truck traffic, lasted about the same time as other roads."

Although the idea of comparing the performance of these parkways with that of other highways is certainly valid, a thorough examination of the facts is required before any statements regarding the subject of relative pavement damage can be made. Therefore a study was conducted of the Merritt and B/W parkways and nearby truck-trafficked highways to determine, insofar as possible, the current condition of those roads and the possible reasons for their condition.

The primary objective of the study was to perform on-site examinations and surveys and subsequently make reasonable comparisons of the condition and performance of the two types of facilities. While conducting the examinations at the two locations, condition and riding quality surveys were performed, interviews with knowledgeable individuals were conducted, and records pertaining to construction, maintenance, and traffic loads were examined. The information from the field trips and subsequent research is presented in this paper.

It should be recognized that this was a relatively small study. Obviously, it would have been desirable to have collected more detailed measurements and to have conducted a more complete study. Unfortunately, these were not possible within the limited scope, and no attempt is being made to claim absolutely conclusive results about these roadways. Conclusive findings would require considerably more expensive research efforts than those that were undertaken. Nevertheless, this study (which was based on a well-founded set of engineering observations) and other recent studies (3,4) support realistic conclusions regarding the effect of vehicle load on pavement damage.

DESCRIPTION AND RECENT OBSERVATIONS OF THE CONDITION OF THE B/W PARKWAY AND NEARBY PAVEMENTS

The purpose of this section is to summarize all pertinent information collected relative to the design, construction, and performance of the B/W Parkway. Additional information was also collected from one other roadway section on I-495 to help provide a basis for comparison.

The sources of the information collected were primarily from FHWA and the U.S. Park Service; however, some pertinent data were also obtained from the Maryland Department of Transportation (DOT).

B/W Parkway

The B/W Parkway is a segment of a four-lane divided highway between Washington, D.C., and Baltimore, Maryland. The parkway is approximately 19 miles long, extending from just east of Jessup, Maryland (near the intersection with MD-175), south to the Washington, D.C., line. By definition, the B/W Parkway is restricted against truck traffic, although buses and mail trucks are allowed to use it.

The original pavement structure of the B/W Parkway was designed and built by the Bureau of Public Roads (now the FHWA) between 1951 and 1954. It con-

sists of an 8-in. jointed-concrete pavement reinforced with wire mesh. The spacing between each of the joints is 60 ft, and dowel bars were used to provide load transfer across these joints. The entire length of this portland cement concrete (PCC) pavement is supported by a minimum of 11 in. of granular subbase material. The course aggregate used in the concrete mix is what is known locally as "Prince George's aggregate," which has a high sulfate content and an apparent high coefficient of thermal expansion.

The B/W Parkway was originally designed to provide access to several federal agencies in the area (and not to provide access to Baltimore). The facility was not designed for truck traffic or for the average daily traffic (ADT) volumes now being carried.

Maintenance

The U.S. Park Service has always been responsible for carrying out maintenance on the B/W Parkway. Unfortunately, recent poor budgets have frequently resulted in a policy of deferring routine maintenance (i.e., joint and crack sealing). For example, the budget for 1983 was only $307,000, which must also be used for snow removal. (The 1982 cost for snow removal was approximately $50,000.)

Initial Performance

The personal recollections of several individuals interviewed indicated that problems with roughness and distress at many of the joints on the parkway began in the early 1960s, less than 10 years after initial construction. This observation was verified by the examination of a condition survey report prepared in 1965. This survey indicated that partial joint distress (an indication of future deterioration) was prevalent. The survey also indicated that more than 100 full 24-ft-width pavement blowups had occurred in the 36 miles of the two-lane pavement. A blowup (or joint compression failure) is primarily the result of temperature-change-related horizontal slab movements, which cause slabs to butt against each other with such force that joint crushing occurs. The likelihood of a blowup is increased by the use of an expansive-type coarse aggregate (such as the Prince George's type used in the concrete mix on the B/W Parkway). Favorable conditions for blowups will also develop when a loss of joint sealant occurs and incompressible materials (such as sand and dirt) fill the voids.

Traffic Estimates

Traffic on the B/W Parkway was about 24,000 vehicles per day in 1956 and has grown linearly to about 74,000 vehicles per day in 1980. This corresponds to an arithmetic growth rate of almost 9 percent per year.

HMAC Overlay Construction

Between 1976 and 1977 the entire length of the B/W Parkway (19 miles) was overlaid with hot-mix asphalt concrete (HMAC), which consisted of 2.5 in. of binder and 0.75 in. of an open-graded surface/wearing course. Personnel at the FHWA office that designed the overlay stated that it was placed to improve the riding quality of the road and not to provide structural rehabilitation. The thickness was selected based on economics and an effort to minimize subsequent reflection cracking.

Considerable maintenance and repair were carried out on the original pavement before placement of the overlay. According to overlay construction plans and the recollection of FHWA personnel, this maintenance was primarily joint repair in the form of full-depth hot-mix patching. However, some full-depth PCC patching and PCC slab replacement was also performed. Records on the frequency of these joint repairs were apparently not kept, but recollection indicates that it was extensive. The cause of this extensive maintenance and the reason for the overlay is primarily related to the choice of a poor aggregate coupled with the long joint spacing; it is not a direct function of traffic.

Condition and Performance of HMAC Overlay

The following observations and comments relative to the current condition and performance of the HMAC overlay constructed on the B/W Parkway in 1975-1976 are based on a recent inspection and condition survey of the facility.

1. Above every joint in the original pavement is a moderate to severe width (0.25- to 0.50-in.) reflection crack in the HMAC overlay. This is shown in Figure 1. In many cases excessive horizontal movements of the underlying slab have resulted in a

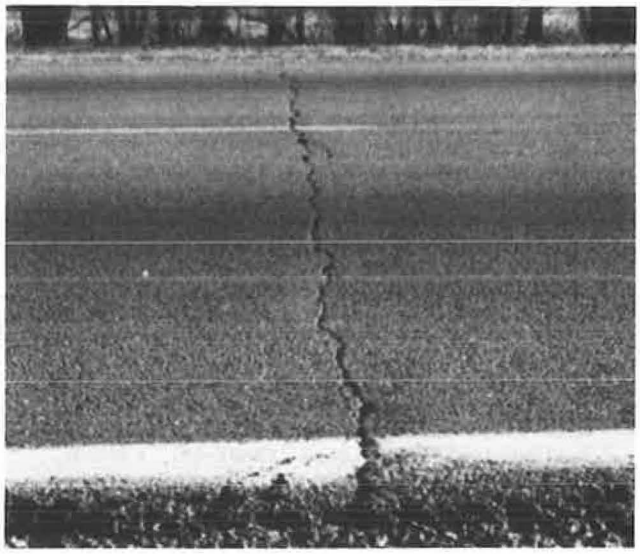

FIGURE 1 Reflection crack in HMAC overlay, B/W Parkway.

"hump" above the joint, as shown in Figure 2. The hump is probably the result of some type of joint distress in the underlying slab. It is difficult to detect this visually, but it can be easily felt when riding across it in an automobile. If not for the roughness generated by these humps, the riding quality of the pavement would be high [AASHO present serviceability index (PSI) estimated at 4.0].

2. In cases where there are likely underlying full-depth hot-mix patches in the original joint area, there are two cracks at the surface (Figure 3). Between these two cracks a heave of material will generally be found that is most likely the result of the shoving of the hot-mix patch, which occurs as the long PCC slabs expand during warm

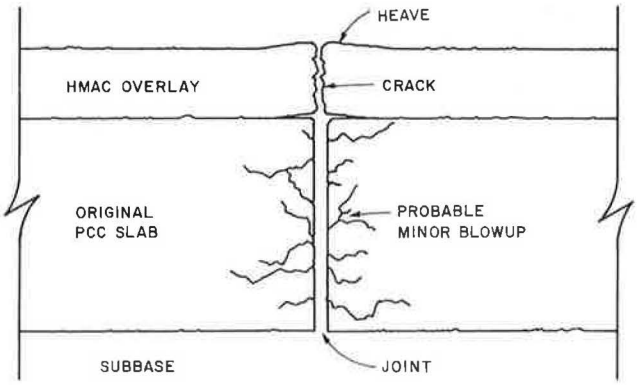

FIGURE 2 Illustration of probable joint condition beneath humps in overlay.

FIGURE 3 Heave of material above underlying hot-mix patch.

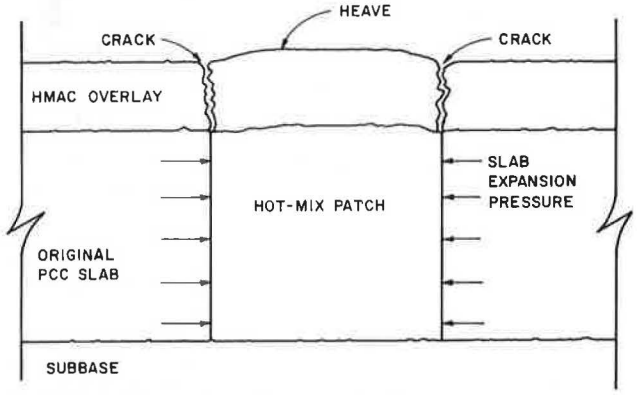

FIGURE 4 Illustration of heave mechanism.

weather (see Figure 4). Because of its width, this heave has an even greater detrimental effect on riding quality.

3. The roughness from these humps and heaves in the HMAC overlay occur throughout the length of the B/W Parkway; however, they are most severe in the sections close to the Capitol Beltway (I-495).

Capitol Beltway

To provide evidence of the relative poor quality Prince George's coarse aggregate used in the concrete mix on the B/W Parkway, the current condition of nearby portions of the Capitol Beltway (I-495) were examined, in which two different types of coarse aggregate were used--the Prince George's aggregate and a type of trap rock. Because of their difference in color, it was easy to distinguish between these two types of aggregate.

The trap rock section is located between the University Boulevard and the New Hampshire Boulevard exits. The other two segments examined are located on either side of this middle trap rock section and were constructed using the Prince George's type concrete coarse aggregate. Other then some surface deterioration, such as aggregate polishing and wheel track wear, the trap rock section exhibited almost no signs of distress in either the eastbound or westbound lanes (see Figure 5). However, the sections on either side definitely showed the effects of the poor coarse aggregate used. The western segment exhibited considerable amounts of joint failures, cracking, and cold-mix patching at the joints (see Figure 6). The eastern section, which extends to the interchange at the B/W Parkway, exhibited the more costly full-depth PCC patching in all three outside lanes in both eastbound and westbound directions (see Figure 7). It should be noted that all three of these segments consist of eight lanes in which the inner lane was constructed more recently than the original structure.

FIGURE 5 Capitol Beltway (I-495), middle section constructed with Prince George's coarse aggregate.

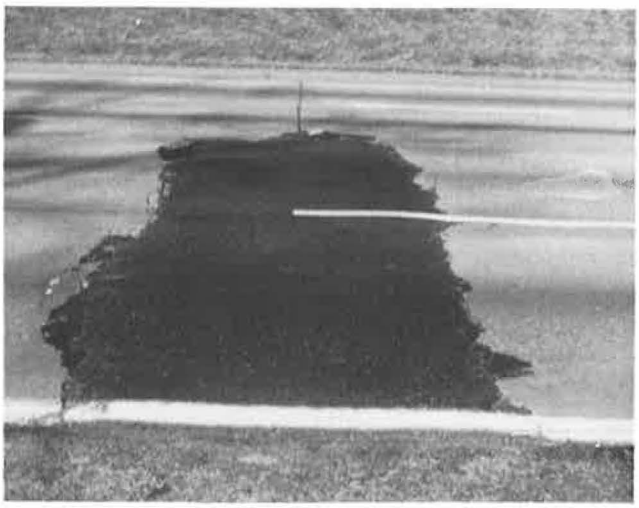

FIGURE 6 Capitol Beltway (I-495), western section constructed with Prince George's coarse aggregate.

FIGURE 7 Capitol Beltway (I-495), eastern section constructed with Prince George's coarse aggregate.

DESCRIPTION AND RECENT OBSERVATIONS OF THE CONDITION OF THE MERRITT PARKWAY AND NEARBY PAVEMENTS

The purpose of this section is to summarize all the pertinent information collected relative to the design, construction, and performance of the Merritt Parkway along Route 15 in Connecticut. To provide a basis for the evaluation and comparison of parkways (which only carry automobile traffic) and normal highways (which carry both automobile and truck traffic), pertinent information is also provided for sections of roadway adjacent or close to the Merritt Parkway. These additional highway sections include I-95 (between the New York State line and Housatonic River Bridge), I-91 (between Wallingford and Rocky Hill), and the Wilbur Cross Parkway (along Route 15, north of the Merritt Parkway). With the exception of the condition surveys performed by the authors, the primary sources of the data collected were from the Connecticut Department of Transportation (ConnDOT) and some records obtained from the American Trucking Associations.

Merritt Parkway

The Merritt Parkway is a section of four-lane highway located in Connecticut between the New York State line and the Housatonic River Bridge. Like most parkways, the Merritt Parkway has almost always had a restriction against truck traffic (although some truck traffic was allowed during World War II). The design, construction, and maintenance of the Merritt Parkway has always been the responsibility of ConnDOT. The facility is approximately 40 miles long.

The original pavement structure of the parkway consists of 8 in. of jointed reinforced-concrete pavement on top of from 12 to 24 in. of subbase (depending on whether in earth or rock cut). The original pavement was built in four different segments between 1938 and 1940.

Pavement Resurfacing

Actual historical construction records for the various resurfacing projects on the Merritt Parkway (as well as for every highway in the state) are buried in the archives of the different ConnDOT district offices. Because of the extensive effort that would have been required to piece it together, an actual overlay construction history of the Merritt Parkway could not be established as a part of this study. Suffice it to say that, with the exception of the pavement areas adjacent to toll booths, the entire parkway has been resurfaced at least once with HMAC overlays. According to available information and history obtained from the American Trucking Associations, the earliest HMAC resurfacing project was 4.5 miles long and occurred in 1956, 18 years after the original pavement had been opened to traffic. Scaling of the original PCC surface resulting from excessive use of salt (in de-icing operations) was identified as the reason for resurfacing.

According to ConnDOT personnel, however, most of the overlays on the Merritt Parkway (all of which were HMAC) were constructed in the early 1970s, some 30 years after initial construction. ConnDOT personnel pointed out that these overlays were required to alleviate the problems associated with surface deterioration and wheel track wear in the original concrete surface, and were not intended for structural rehabilitation. They further identified the use of studded snow tires (which began in the early 1960s) as the primary reason for the PCC surface deterioration problems. It was suggested that the use of studded tires, combined with the fact that the parkway does not have shoulders (which has resulted in a channeling effect on traffic), may explain why wheel track wear and distress have been such problems.

Studies and reports by ConnDOT (5,6) definitely demonstrate the deteriorating effect of studded snow tires on pavement surfaces. Field measurements in Connecticut indicated that PCC wear rates were 0.08 in. per million studded tire vehicle passes. (Data presented from Minnesota indicated that this rate was roughly twice as high for bituminous surface). Photographs (see Figure 8) taken in the toll booth areas (which have not been overlaid) illustrate the extent of this type of surface deterioration. [It is also useful to note that these and other photographs in this area (see Figure 9) indicate little other distress in the original PCC pavement, providing evidence that it is indeed still structurally sound.]

According to ConnDOT personnel, the policy for overlays on the parkway has been to place 2 in. of HMAC if the extent of surface deterioration dictated it. This is comparable to their policy of using 2.5 in. of HMAC on truck-trafficked roads if the ADT is less than 50,000 and 3.0 in. if the ADT is greater than 50,000.

Traffic Estimates

ADT estimates obtained from ConnDOT for the Merritt Parkway vary considerably, depending on the location along the facility. In 1980 the ADT at a point near

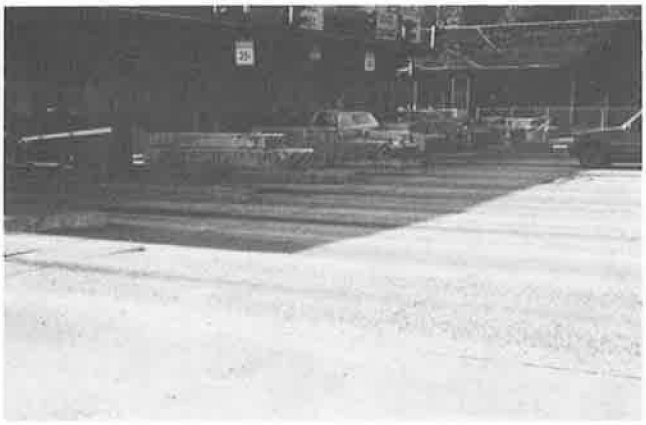

FIGURE 8 Wheel track wear and surface deterioration on Merritt Parkway, Greenwich toll station.

FIGURE 9 Structural condition of PCC pavement on Merritt Parkway at Greenwich toll station.

the New York State line was approximately 23,000 vehicles per day, whereas at a point on the opposite end (near Trumbull) it was 42,000 vehicles per day.

Most of the traffic on the Merritt Parkway has certainly been automobiles; however, the facility has not been completely free of truck traffic. According to ConnDOT personnel there has been at least one occasion (during World War II) when the truck restriction was lifted. They had no information, however, as to how long or how many trucks were carried, although they estimate that the number was probably small.

Condition and Performance Observations

Based on both a windshield survey and a study of the condition surveys of the Merritt Parkway, the following observations and comments can be made.

1. The roadway is completely overlaid (with the exception of the toll booth areas), and the older overlay sections do display significant amounts of distress and maintenance. All the longitudinal and transverse cracking observed, however, appeared to be related to the reflection of horizontal movements in the underlying joint. Some edge longitudinal cracking was also observed, which is probably related to the fact that the parkway has no shoulders.
2. In addition to environmentally induced reflection cracking, a considerable amount of distress in the HMAC overlays was observed, which is probably related to surface deterioration from studded tire use. The distress takes the form of slight to moderate rutting, raveling, pop-outs, and both large and small areas where skin patching had been accomplished to repair surface distress (see Figures 10 and 11). It was also evident that many of the overlaid bridge decks required considerable maintenance in the form of small skin patches.

FIGURE 10 Surface deterioration and raveling on HMAC overlay, Merritt Parkway.

FIGURE 11 Full lane width skin patching to repair surface deterioration along Merritt Parkway.

3. The riding quality of the parkway was basically good (AASHO PSI estimated at 3.0 to 3.5). There were some areas of recent overlay construction in which the riding quality was excellent (PSI of 4.0 to 4.2). There were also those sections that had large areas of maintenance and skin patching, in which the riding quality was poor (PSI of 2.5). The riding quality was also poor at many of the bridge decks and approaches, where considerable amounts of level-up patching and surface repair had been accomplished.
4. As a final note about the condition of the parkway, no signs of faulting were observed. All the reflection cracking observed is most likely attributable to the horizontal rather than vertical movements of the underlying PCC slabs, because there were no signs of pumping or loss of support. This

was further demonstrated by the good transition in riding quality across the joints and examination of the joints in the concrete slabs around the toll booths.

Interstate 95

The segment of I-95 examined as a part of this study is south of and roughly parallel to the Merritt Parkway (between the New York State line and the Housatonic River Bridge). The original pavement structure basically consists of 10 in. of jointed reinforced-concrete pavement with a varying depth of subbase. The pavement was constructed mostly in 1958-1959; however, one short section was built in 1954.

Based on both a windshield survey and a study of the condition surveys of I-95 between the New York State line and West Haven, the following observations and comments can be made.

1. The pavement is largely overlaid with HMAC; however, there are some sections in both the eastbound and westbound lanes that consist only of the original PCC structure.
2. In areas where the original PCC surface has not been overlaid, several different types of distress were observed, including surface defects (such as polishing, wheel track wear, scaling, raveling, and potholes), faulting, joint deficiencies (such as spalling, creeping, and loss of sealant material), and cracking (primarily single transverse, but also some D-cracking and corner breaks). Some of these distress manifestations are shown in Figures 12 and 13. Some lane separation at longitudinal joints and sizable amounts of cold-mix patching and full-depth joint repair were also observed. Faulting (both at transverse cracks and joints), however, was identified as the primary distress problem in these nonoverlaid sections. Overall, the riding quality of these original PCC sections was poor (AASHO PSI estimated at 2.5).
3. Concerning the HMAC overlaid sections, the overall riding quality was relatively good (AASHO PSI estimated at 3.5). However, condition surveys did indicate some of the same signs of surface wear exhibited on the Merritt Parkway (i.e., wheel track wear, raveling, scaling, and skin patching) that were associated with the use of studded snow tires.
4. As part of its overall road inventory program, ConnDOT conducts pavement serviceability ratings to augment its yearly pavement serviceability log. The statewide summary of the log presents objective ratings (on a 1 to 9 scale) for five different categories of pavement condition: cracking, distortion, disintegration, drainage, and riding quality. For regions (such as the toll booth areas) that still exhibit the original PCC surface, this summary log provides the basis for an objective comparison between the performance of truck-trafficked roads and roads that carry only automobile traffic. The data in Table 1 represent an excerpt from the 1981 log in which the ratings were performed at three different toll stations, one on the Merritt Parkway and two on I-95. Obviously, there is a definite difference between the ratings for automobile-only versus mixed-traffic roads. With the exception of drainage, the scores for the parkway station are excellent compared with those on I-95.

FIGURE 12 Structural condition of PCC pavement along I-95, Norwalk toll station.

FIGURE 13 Severe faulting in outside lanes of PCC pavement along I-95, Housatonic River Bridge.

Wilbur Cross Parkway and Berlin Turnpike

Another case provided by ConnDOT, which illustrates the difference in performance between truck-loaded roads and those that carry automobile traffic only, are adjacent sections of Route 15 (the Berlin Turnpike) and the Wilbur Cross Parkway.

1. Both sections have the same cross section (8 in. of jointed reinforced-concrete pavement). The Wilbur Cross Parkway was constructed in 1946-1947 and the Berlin Turnpike was constructed in 1942.
2. The Wilbur Cross Parkway has carried no truck traffic, but the Berlin Turnpike has.
3. According to ConnDOT personnel, the Berlin Turnpike has had considerable problems associated with higher edge deflections (i.e., pumping, corner breaks). In fact, one 0.8-mile section of the turnpike had to be reconstructed in 1954 because of its deteriorated condition. Since then the entire length of the turnpike has been overlaid and has also required a considerable amount of ConnDOT's "skid-box" skin patch maintenance treatment.
4. Conversely, the adjacent section of the Wilbur Cross Parkway has performed extremely well. In fact, at an age of 35 years, parts of it have yet to be rehabilitated.

Interstate 91

In examining the condition of I-91 between New Haven and Hartford, a marked difference between the condi-

TABLE 1 ConnDOT Ratings for Original PCC Pavement Structures

	Cracking		Distortion		Disintigration		Drainage		Riding Quality	
	EB	WB	EB	WB	EB	WB	EB	WB	EB	WB
Merritt Parkway, Greenwich toll station	8	8	8	8	8	8	8	8	8	8
I-95										
Greenwich toll station	4	4	4	4	4	4	6	7	5	5
Norwalk toll station	4	5	5	4	4	4	7	7	5	6

Note: EB = eastbound and WB = westbound.

tion and performance of the northbound and southbound lanes was observed in areas that had not been overlaid. The northbound lanes exhibited a considerable amount of concrete patching, faulting, and roughness (especially in the outside lane), whereas the southbound lanes exhibited almost none. Furthermore, a much greater percentage of the northbound lanes had been overlaid. Not surprisingly, W-4 loadometer tables from ConnDOT indicate that in 1979 the split between 18-kip equivalent single-axle loads was 61 to 39 percent (northbound over southbound). Figures from 1981 indicated a 65 to 35 percent split (northbound over southbound).

DISCUSSION AND COMPARISON OF RESULTS

In the previous sections detailed observations on the parkways and nearby Interstate highways in the Baltimore/Washington area and in Connecticut were presented. It should be noted that these were not designed experiments, and detailed follow-up investigations have not been carried out. However, significant comparative information does emerge that sheds light on the question of damage caused by truck loading versus damage caused by automobile loading.

Connecticut Highways

1. The primary difference observed between the condition of the Merritt Parkway and the parallel section of I-95 is that the I-95 section exhibited considerable amounts of faulting, particularly in the outside lane, whereas none could be detected on the Merritt Parkway. Faulting is a severe form of pavement damage characterized by rough rides and accelerated pavement deterioration. The difference in this condition between the two facilities was particularly apparent in comparisons between unoverlaid sections (primarily around toll booth areas where faulting, cracking, and patching were more prominent on I-95).

2. The primary reason for overlays on the Merritt Parkway was identified by ConnDOT personnel as the presence of excessive wheel track wear and surface deterioration. The use of studded tires combined with channelized parkway traffic because of a lack of shoulders was identified as the primary cause of this deterioration. These same personnel also noted that the reason for overlays on I-95 was primarily to provide structural rehabilitation and increased load-carrying capacity for a worn-out pavement exhibiting both moderate and severe distress manifestations.

3. A comparison of adjacent sections of the Wilbur Cross Parkway (no trucks) and the Berlin Turnpike (normal truck traffic) provides more information relative to the effects of truck traffic. Portions of the Berlin Turnpike (constructed in 1942) had to be reconstructed in 1954 because of serious deterioration. Furthermore, the turnpike has since been completely overlaid. Conversely, adjacent sections of the Wilbur Cross Parkway [which have the same cross section and were constructed only 4 to 5 years later (1946 and 1947)] have performed extremely well, with portions still consisting of only the original structure.

4. The ConnDOT policy for parkway overlays is 2 in. of HMAC, which has historically only been required to remedy surface deterioration. This compares with a typical 2.5- to 3-in. HMAC overlay policy that has been used to provide structural rehabilitation on roads carrying truck traffic. This indicates that practical engineering experience dictates more significant repairs for roads subjected to truck traffic.

5. Examination of loadometer data for I-91 (northbound versus southbound) indicate that the percentage of truck traffic split was 61 to 39 (in terms of equivalent axle loads) in 1979 and 65 to 35 in 1981. Correspondingly, observation of the pavement condition at this time clearly indicates that significantly more rehabilitation, full-depth patching, pavement distress, damage, and deterioration exists in the northbound lanes than in the southbound lanes. This is further accentuated by the fact that this distress and the maintenance observed was confined to the outside lane, where most trucks travel.

To summarize the observations in Connecticut, rehabilitation has been accomplished on all highways, regardless of traffic, but it appears that, both in terms of practical and engineering judgments, far more damage has been sustained by those highways carrying truck traffic than by the parkways. Furthermore, it appears apparent that the damage to the parkways has been significantly associated with studded tires, which are now banned and are no longer affecting the roads. Thus this type of damage has now decreased, and continued observation of the highway system might well reveal that damage in future years would be even more greatly associated with truck than with automobile traffic.

Baltimore/Washington Highways

An earlier section of this paper presented the description and recent condition survey observations of the B/W Parkway and the nearby Capitol Beltway. The findings may be summarized as follows.

1. The primary cause of damage on the B/W Parkway appears to be caused by the unfortunate combination of a 60-ft joint spacing and the use of an expansive concrete aggregate known locally as Prince George's aggregate. The effects of this combination are excess horizontal movements at slab ends that ultimately resulted in compression failures, blowups, full-depth patching at the joints during the life of the original structure, and severe reflec-

tion cracking and hot-mix patch heaving since overlay construction.

2. Because of the use of different types of concrete aggregate on adjacent sections of the nearby Capitol Beltway (I-495), a comparison of their performance was possible. The section between University Boulevard and New Hampshire Boulevard was constructed with a trap rock concrete aggregate, whereas the sections both east and west of this middle section were constructed with the same Prince George's type aggregate used on the B/W Parkway. The section with the trap rock aggregate exhibited little or no signs of distress, whereas the sections on either side exhibited significant effects of the poor aggregate in terms of pavement condition. Specifically, the western section exhibited considerable amounts of joint failures, cracking, and patching. The eastern section exhibited even more costly full-depth PCC patching. In both cases the poor condition of the joints appeared across all lanes, except for locations where there was a recently constructed inside lane.

In summary, although not as easy to sort out and as conclusive as the observations in Connecticut, the observations in the Baltimore/Washington area still indicate that pavement damage is greater when associated with mixed truck and automobile traffic than with automobile traffic alone. The relative effects of traffic on the pavements studied are certainly masked to some degree, however, by the poor materials involved in construction and a poor selection of joint spacing.

FINDINGS

As pointed out in the beginning of this paper, it was not possible within the budget for the study to make detailed engineering measurements of the pavements investigated. Furthermore, conclusive observations would require many years of measurement. Nevertheless, this study clearly provides substantive evidence against assertions that damage on parkways carrying automobile traffic alone is at least as great as that on nearby highways carrying normal traffic, including trucks. In the present study condition surveys were made of the Merritt Parkway, the B/W Parkway, and nearby parkways and Interstate highways in both areas to provide a basis for comparison.

Clearly, from an engineering and economic point of view, the damage observable on Interstate highways carrying mixed truck and automobile traffic is more severe and has required more rehabilitation and maintenance than that on comparable sections of the parkways carrying automobile traffic alone. Although quantitative statements of relative damage and relative costs are not possible within the limits of this study, the results are more than adequate to refute recent claims by industry representatives concerning the effects of truck traffic on the nation's highways.

ACKNOWLEDGMENTS

The results of a small engineering study that examined damage to pavements that have nominally been subjected to passenger car traffic only over their past service lives have been presented. This study was commissioned by the Association of American Railroads. The support of many people, too numerous to mention, in FHWA, the U.S. Park Service, and ConnDOT is gratefully acknowledged. Douglas L. Johnson, the sponsor's technical representative on the project, was helpful in providing information, locating sources, and making appointments with persons involved in this study.

REFERENCES

1. J.L. Reith. Highway Cost Allocations: The Incremental Cost Solution. Proc., 66th Annual Meeting, AASHTO, Las Vegas, Nov. 17-19, 1980.
2. J.L. Reith. Highway Cost Allocation--Are Trucks Paying Their Fair Share for Highway Maintenance. Presented at the Highway Maintenance and Finance Seminar of the National Conference of State Legislatures, St. Louis, Mo., Aug. 26, 1980.
3. W.R. Hudson and V.L. Anderson. An Assessment of Load and Environmental Effects on Pavement Deterioration. Report RR-1/3. Austin Research Engineers, Inc., Austin, Tex., Dec. 1981.
4. W.R. Hudson. An Examination of Use and Non-Use Related Causes of Pavement Deterioration. Report RR-1/2. Austin Research Engineers, Inc., Austin, Tex., June 1981.
5. R. Christman. Report to the Legislature on the Performance and Effects of Studded Tires. Office of Engineering Services, Research and Development Section, Connecticut Department of Transportation, Wethersfield, Dec. 1972.
6. R. Christman. Report to the Legislature on the Performance and Effects of Studded Tires. Report 2. Office of Engineering Services, Research and Development Section, Connecticut Department of Transportation, Wethersfield, Jan. 1974.

Publication of this paper sponsored by Committee on Pavement Rehabilitation.

Overlay Thickness Design for Flexible Pavement

MICHAEL S. MAMLOUK and BOUTROS E. SEBAALY

ABSTRACT

An overlay design method for flexible pavement is presented in which both functional and structural types of performance are considered. The method relates the overlay thickness to various types of failure of the overlaid pavement, such as fatigue and low-temperature cracking, rutting, and roughness. The viscoelastic, plastic, and fatigue properties of the pavement materials are considered. The computer program OVERLAY is developed by modifying the FHWA program VESYS-3-A in order to determine the optimum overlay thickness. The method provides a probabilistic solution and allows for the use of different material properties for different seasons. The use of the method is verified by determining the required overlay thicknesses for two typical pavement conditions under typical traffic volumes, material properties, and environmental conditions. The use of the method is justified in view of the rising cost of pavement rehabilitation.

An important part of the U.S. infrastructure is the highway system. The unfortunate fact is that the system is deteriorating in many areas of the country at an alarming rate. New rationally based methods should be developed to upgrade the performance of the existing highway system.

The performance of the overlaid flexible pavement is a function of various distress types such as fatigue cracking, rutting, and roughness. Fatigue cracking is usually controlled by the magnitude of the repeated tensile strain at the bottom of the asphalt-bound layer (1,2). On the other hand, rutting is assumed to be controlled by the subgrade strain (3,4), stresses in the other layers (5), or the strain in the asphalt-bound layer (3). Most methods of overlay design, however, limit the performance of the overlaid pavement to a single design factor such as fatigue cracking, rutting, or roughness. Therefore, each method makes the assumption that, if the specific design factor being considered is adequately controlled, other forms of distress or performance will also be controlled (1). Other methods of overlay thickness design are based on observations and correlations developed for specific pavements that do not necessarily represent pavements under other conditions. These methods are usually restricted to material types, traffic characteristics, and environmental conditions considered in the original investigations.

The performance of highway pavement can be separated into two main parts: functional and structural. Functional performance describes how well the pavement serves the user, whereas structural performance is related to the ability of the pavement to sustain the load. Although the two types of performance are related, there is currently no well-defined relationship between structural distress and functional performance (1). It is important to develop an overlay design method that considers both functional and structural types of performance and relates the overlay thickness to various types of pavement failure during the useful life of the overlay. It is also important to consider the realistic behavior of pavement materials, such as the viscoelastic and plastic properties of various layers and the variation of these properties, and not simply assume linear elastic behavior with one set of deterministic conditions.

OVERLAY THICKNESS

The overlay thickness design method suggested herein evaluates the required overlay thickness, assuming that a decision has been previously taken to provide an overlay. The method considers the functional as well as the structural types of pavement performance. In other words, the trends of the common failure types--cracking, rutting, and roughness--are evaluated throughout the expected useful life of the overlay. The method is based on obtaining an overlay thickness that provides a serviceability index (SI) at the end of the design life of the overlay equal to or higher than a predetermined limiting SI value. The AASHO SI limits (6) or other arbitrary values can be used for this purpose.

In this study the pavement serviceability under various conditions is determined by using the VESYS-3-A computer program developed by FHWA in cooperation with other agencies (7). The current version of this program considers the viscoelastic material properties as well as the plastic and fatigue properties. The program can handle up to seven pavement layers, which can further be increased within the available computer storage memory. In this program strain and deflection responses are computed and used in conjunction with other criteria to predict pavement distress in terms of fatigue as well as low-temperature cracking, rutting, and roughness.

Fatigue cracking is predicted by using a probabilistic Minor's hypothesis. The criterion for fatigue cracking is based on fatigue resulting from the tensile strain at the bottom of the asphalt-bound layer. It is given as

$$C_q(t) = n_q/N_q \quad (1)$$

where

$C_q(t)$ = increment to the crack index resulting from a repetition of loads in the qth incremental analysis period,
n_q = number of axle loads applied to the pavement in the qth incremental analysis period, and
N_q = number of loads to failure under temperature and strain conditions of the qth time interval; that is,

$$N_q = K_{1_q}(1/R_7)^{K_{2_q}} \quad (2)$$

where R_7 is the radial strain response, and K_{1_q} and K_{2_q} are material fatigue properties.

The crack index at any time is obtained by the summation of the incremental crack indices for pre-

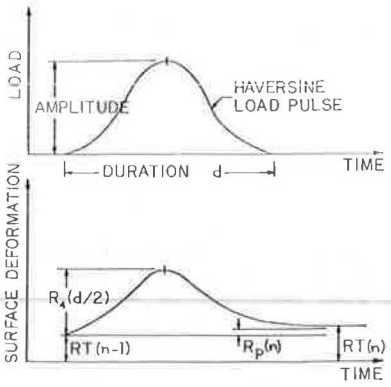

FIGURE 1 Load pulse and pavement deflection response at the nth repetition (7).

vious incremental analysis periods. A crack is initiated at the bottom of the asphalt-bound layer when the expected value of the crack index equals one. The expected area cracked in square feet per 1,000 square feet is further calculated (7).

Rut depth is determined by using viscoelastic-plastic layer theory and repeated load laboratory testing. The wheel load is represented by a haversine pulse, whereas the flexible pavement deflection response curve caused by the nth load repetition takes the form shown in Figure 1 (7). The permanent deformation is represented for each incremental analysis period as

$$R_p(n) = R_4(d/2) \cdot f(n) \quad (3)$$

where

$R_p(n)$ = permanent deformation at load repetition n,
$R_4(d/2)$ = deflection response of pavement surface as a function of load duration and temperature, and
$f(n)$ = monotonically decreasing function of the number of previously applied loads.

The integration of Equation 3 for various layers over the expected number of load repetitions yields the accumulated rut depth. Therefore, the rut depth is the summation of the permanent deformations of all layers.

On the other hand, slope variance occurs because of the accumulated deformation along the longitudinal profile of the roadway wheelpath, which is assumed to differ because of the randomness of loads, materials, and construction practices. Cracking, rutting, and slope variance are used to define the pavement performance in terms of the life history of the present serviceability index (PSI). The AASHO definition of PSI is used as follows:

$$PSI = PSI_I - 1.91 \log (1 + SV) - 0.01 \sqrt{C} - 1.38(RT)^2 \quad (4)$$

where

PSI_I = initial serviceability index,
SV = slope variance (10^6 radians),
C = area cracked (ft^2/1,000 ft^2), and
RT = rut depth (in.).

A new computer program (OVERLAY) is developed in this study to select the optimum overlay thickness

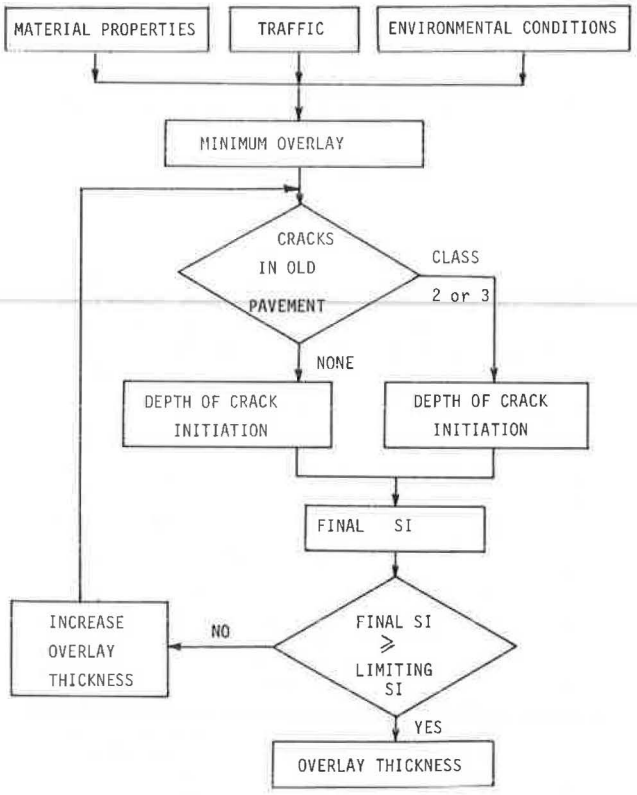

FIGURE 2 Flow diagram for the OVERLAY computer program.

on deteriorated flexible pavements. The VESYS-3-A package, which consists of a main program and a number of subroutines, was included as a part of the OVERLAY program. In this case the original VESYS-3-A main program was converted to a subroutine after minor modifications. During operation the OVERLAY program calls the VESYS subroutine, which in turn interactively calls other subroutines. The program requires the input of the existing layer thicknesses, material properties of the existing layers and the overlay, traffic data, pavement conditions, and environmental conditions, which are summarized as follows:

1. Number of existing layers and layer thicknesses;
2. Properties of materials for each layer, including the overlay, under various environmental

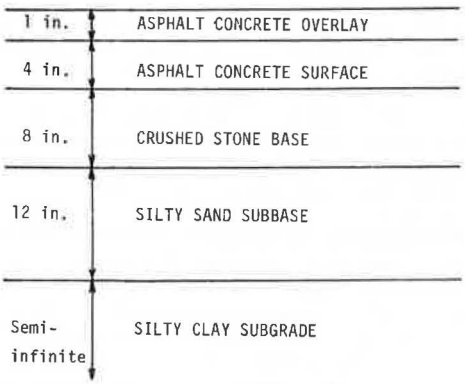

FIGURE 3 Pavement materials and layer thicknesses.

TABLE 1 Material Properties of Asphalt-Bound Layers at Various Seasons When the Existing Surface Layer is Uncracked

Material Properties	Season			
	Winter (40°F)[a]	Spring (60°F)[a]	Summer (85°F)[a]	Fall (70°F)[a]
Modulus (psi)	1,100,000	400,000	100,000	250,000
Poisson's ratio	0.35	0.35	0.35	0.35
Fatigue properties				
K_1	0.158×10^{-4}	0.155×10^{-3}	0.284×10^{-1}	0.932×10^{-3}
K_2	2.94	2.89	2.81	2.86
Permanent deformation properties				
μ	0.04	0.07	0.10	0.08
α	0.75	0.75	0.75	0.75

Note: For the detailed testing procedure, refer to Kenis (7).

[a]Temperature values are the mean temperatures during various seasons.

TABLE 2 Material Properties of Base, Subbase, and Subgrade

Material Properties	Base	Subbase	Subgrade
Modulus (psi)	30,000	15,000	4,000
Poisson's ratio	0.40	0.40	0.45
Permanent deformation properties			
μ	0.04	0.05	0.06
α	0.75	0.75	0.65

Note: For the detailed testing procedure, refer to Kenis (7).

conditions; the material properties are summarized as follows: (a) moduli and Poisson's ratio for all layers, (b) fatigue properties of the asphalt-bound layer, (c) permanent deformation properties for all layers, and (d) coefficients of variation of the material properties for all layers;

3. Pavement condition before overlay, including the cracking class (8);
4. Traffic data in the different seasons, which include (a) expected daily 18-kip equivalent axle loads (EALs) in the design lane throughout the design life of the overlay and (b) tire pressure and radius of tire imprint;
5. Environmental conditions such as the mean temperatures for various seasons;
6. Initial SI after overlaying and limiting SI at the end of the overlay design life; and
7. Desired design life of the overlay.

The OVERLAY computer program evaluates the trend in the individual types of pavement failure after overlaying and combines them by using the serviceability equation. During the evaluation of fatigue cracking, the condition of pavement before overlaying is considered. If no cracks exist in the old pavement, the depth at which the cracks may start after overlaying is assumed to be at the bottom of the old asphalt-bound layer. On the other hand, if the old surface is extensively cracked [AASHO classes 2 or 3(8)], the potential cracks after overlaying are assumed to start at the bottom of the overlay.

An initial minimum overlay thickness of 0.5 in. is assumed, and the SI is calculated and compared with the predetermined limiting SI value. If the SI value at the end of the design life is equal to or larger than the limiting SI value, the overlay thickness is taken as the assumed value. If the SI condition is not satisfied, the overlay thickness is increased by an increment of 0.5 in. and the SI is computed. This process is repeated until the SI condition is satisfied. A flow diagram of the OVERLAY computer program is shown in Figure 2.

EVALUATION OF MATERIAL PROPERTIES

The use of the overlay thickness design method described herein requires the knowledge of various material properties for all layers such as moduli, Poisson's ratios, permanent deformation properties, and fatigue properties of the asphalt-bound layer. Because there is no adequate evidence that nondestructive testing of pavement can provide the necessary material properties, these properties have to be determined in the laboratory. Detailed laboratory procedures for the evaluation of the required material properties are discussed elsewhere (7).

It should be noted that the practical values of overlay thickness vary in increments of 0.5 in. Therefore, the overlay thickness is not sensitive to minor changes in some material properties. Consequently, the method can be simplified by assuming some typical material properties based on the types of materials instead of on extensive laboratory testing. The user can also neglect some failure modes if previous experience indicates that they are not significant for the specific pavement in question. Attention should be also exercised in evaluating the modulus and permanent deformation properties of the existing asphalt-bound layer if cracks are present. Obviously, when the severity of the cracks increases, the material properties change. Therefore, the material properties of the cracked asphalt-bound layer vary between the properties of uncracked asphalt-bound layers and the properties of the base material, depending on the severity of the cracks.

TYPICAL EXAMPLES

A multilane primary road was constructed with four layers and with material types and thicknesses as shown in Figure 3. The material properties of the different layers under different climatic conditions are given in Tables 1 and 2. The old pavement is rutted, and there are no cracks at the surface. The initial 18-kip EAL is 1,000 with an expected traffic growth rate of 3 percent. It is required to determine the overlay thickness so that it will last for 5 years.

The computer program OVERLAY was used to determine the required overlay thickness. In this example the pavement system after overlaying consists of five layers, where the overlay thickness is incrementally increased until the expected SI value at the end of 5 years satisfies the SI limit (2.5 for primary roads). Because the old surface layer is uncracked, the potential cracks after overlaying are

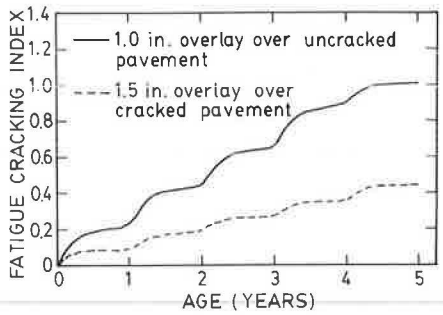

FIGURE 4 Fatigue cracking index versus age for the two pavement conditions.

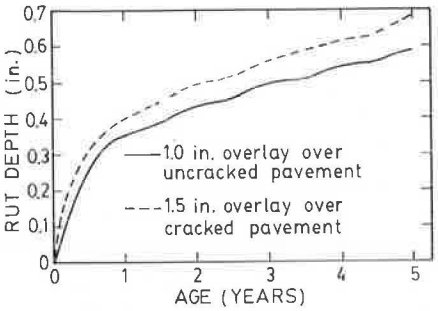

FIGURE 5 Rut depth versus age for the two pavement conditions.

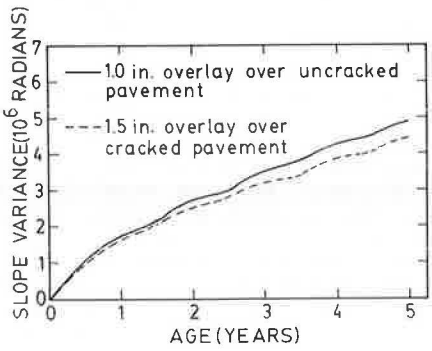

FIGURE 6 Slope variance versus age for the two pavement conditions.

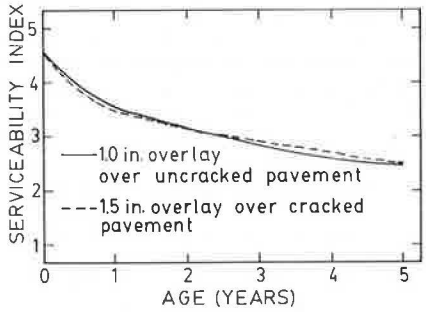

FIGURE 7 SI versus age for the two pavement conditions.

assumed to start at the bottom of the old surface layer. The results indicated that an overlay thickness of 1 in. is required to last for 5 years.

Another example was done with the same conditions as before, except that the existing pavement surface is severely cracked (type 3 cracking) with a modulus value of 38,000 psi. In this case the potential cracks after overlaying are assumed to start at the bottom of the overlay. An overlay thickness of 1.5 in. is needed in this case for a lifetime of 5 years.

The trends of the failure components--fatigue cracking index, rut depth, and slope variance in the two examples--are shown in Figures 4-6. Also, the change in SIs with age is shown in Figure 7. It should be noted that these trends are not uniform because of the change in material properties in various seasons.

CONCLUSIONS

The overlay design method presented herein can consider both functional and structural types of pavement performance and can relate the overlay thickness to various types of pavement failure such as cracking, rutting, and roughness during the design life of the overlay. The method can consider the realistic behavior of pavement materials such as viscoelastic, plastic, and fatigue properties. In this study the computer program OVERLAY has been developed by modifying the FHWA computer program VESYS-3-A in order to determine the optimum overlay thickness. The method described herein allows for the use of different material properties for different seasons, such as a brittle and stiff asphalt-bound layer in the winter, a soft and plastic asphalt-bound layer in the summer, a weak subgrade material during the spring-thaw season, and so forth. Also, because the materials are not always homogeneous, the method considers the random variation in the material properties. In addition, special considerations are available for the variation in traffic loads and volumes such as the use of seasonal load limits during the spring-thaw period.

The use of the method is verified by determining the required overlay thicknesses for two typical pavement conditions under typical traffic volumes, material properties, and environmental conditions. Although the proposed method is sophisticated, its use is justified in view of the escalating cost of highway rehabilitation programs.

ACKNOWLEDGMENTS

The authors wish to acknowledge the State University of New York at Buffalo for the financial assistance of this study. Thanks are extended to W.J. Kenis and J.A. Sherwood of FHWA for providing the computer program VESYS and for their assistance in its use.

REFERENCES

1. C.L. Monismith. Pavement Evaluation and Overlay Design: Summary of Methods. In Transportation Research Record 700, TRB, National Research Council, Washington, D.C., 1979, pp. 78-81.
2. B.D.L. Taille, P. Schneck, and F. Boudeweel. ESSO Overlay Design System. Proc., 5th International Conference on the Structural Design of Asphalt Pavements, Delft University of Technology, Netherlands, 1982, Volume 1, pp. 682-694.
3. R.C. Koole. Overlay Design Based on Falling Weight Deflectometer Measurements. In Transportation Research Record 700, TRB, National Re-

search Council, Washington, D.C., 1979, pp. 59-72.
4. R.A. Weiss. Pavement Evaluation and Overlay Design: A Method that Combines Layered-Elastic Theory and Vibratory Nondestructive Testing. In Transportation Research Record 700, TRB, National Research Council, Washington, D.C., 1979, pp. 20-34.
5. H.J. Treybig. Mechanistic Method of Pavement Overlay Design. In Transportation Research Record 700, TRB, National Research Council, Washington, D.C., 1979, pp. 72-77.
6. AASHO Committee on Design. Interim Guide for the Design of Flexible Pavement Structures. AASHO, Washington, D.C., Oct. 12, 1961.
7. W.J. Kenis. Predictive Design Procedures, VESYS User Manual--An Interim Design Method for Flexible Pavements Using VESYS Structural Subsystem. Final Report. FHWA, U.S. Department of Transportation, Jan. 1978, 128 pp.
8. The AASHO Road Test: Report 5--Pavement Research. Special Report 61E, HRB, National Research Council, Washington, D.C., 1962, 352 pp.

Publication of this paper sponsored by Committee on Pavement Rehabilitation.

Nondestructive Testing of Pavements Using Surface Waves

SOHEIL NAZARIAN and KENNETH H. STOKOE II

ABSTRACT

A nondestructive method of determining the moduli and thicknesses of pavement systems--the spectral-analysis-of-surface-waves (SASW) method--was introduced in 1982. With this method surface waves containing a wide range in frequencies are generated in the pavement system by impacting the surface. Propagation of the waves through the system is monitored with two receivers located on the pavement surface. By analysis of the phase information for each frequency determined between receivers, Rayleigh wave velocities and wavelengths over the frequency range of interest are determined. Velocity versus wavelength information represents a dispersion curve that on inversion gives Young's modulus profiles along with the thicknesses of the layers. Advancements in the theoretical aspects of the inversion method are presented in this paper. A new, rigorous inversion technique has been developed that is theoretically based and eliminates many of the earlier simplifying assumptions. The versatility and accuracy of the new inversion technique is illustrated by two series of tests that were performed on two rigid pavement sections of an airport runway with different cross-sectional profiles. In addition to being nondestructive, fast, and economical, the SASW method is shown to be capable of detecting thin layers in pavement systems with an accuracy of less than 0.5 in. and finding moduli within about 20 percent, based on comparisons with soil borings and crosshole seismic tests at the same sites. In this regard, no other nondestructive technique has the power and versatility of this method.

Many major highways and airport runways are approaching the end of their serviceable lives. A fast, economical, and precise method for evaluating the properties of these pavements is necessary if meaningful maintenance inspections are to be performed regularly or if overlays are to be designed effectively. The most common nondestructive tests (NDTs) being performed for these purposes are the Dynaflect and the falling weight deflectometer. Although these tests are carried out quite rapidly in situ, in-house data processing can be tedious, and the final solutions are not unique. Another potential deficiency with these methods is that, although a dynamic load is applied to the surface in the field, static elastic theory is employed to reduce the data. Under certain conditions, stress and strain distributions in these dynamic tests can be different from those assumed in the static analyses.

The latest developments in the spectral-analysis-of-surface-waves (SASW) method are discussed herein. The SASW method, which has been under development for some time (1-4), is a nondestructive testing technique that is based on the theory of elastic waves in a layered system. In addition to elastic moduli, layer thicknesses can be determined precisely from the modulus profile. A brief overview of the SASW testing technique is presented herein, followed by recent developments in data analysis that are needed for achieving high-quality Young's modulus profiles and precise layer thicknesses. The results of a case study on two rigid pavement sections using the rigorous data reduction technique are presented to illustrate the value of the SASW method. In conjunction with SASW tests, crosshole seismic tests were performed at each site. Crosshole tests are known as a precise way of determining the stiffnesses of different layers at a site. Young's modulus profiles obtained from these two tests are in excellent agreement, as are the layer thicknesses obtained from the SASW tests and borings.

BACKGROUND

SASW Method

The SASW method is a new method of seismic testing that is being developed for determining shear wave velocity and shear modulus profiles at soil sites and Young's modulus profiles at pavement sites (3,4). Evaluation of Young's modulus profiles at pavement sites can be used in overlay design or material characterization (5) or the profiles can be used indirectly as a tool to control compaction during construction (6). All testing is performed at the ground surface, and hence the procedure is nondestructive. The key point in SASW testing is generation and measurement of surface waves (Rayleigh waves).

The source is simply a transient vertical impact on the pavement surface. The impact generates a group of Rayleigh waves (R-waves) of various frequencies. Two vertical receivers, located on the surface, are used to monitor the propagation of Rayleigh wave energy past them. The output from the receivers is simultaneously captured and recorded on a Fourier spectral analyzer. With the Fourier analyzer, the complicated transient waveforms are divided into a group of simple harmonic waveforms that are analyzed to determine wave velocity and moduli.

The general configuration of the source, receivers, and recording device is shown in Figure 1a. The common receivers midpoint (CRMP) geometry (4) is used for testing. With this geometry, the two receivers are moved away from an imaginary centerline midway between the receivers at an equal pace, and the source is moved such that the distance between the source and the near receiver is equal to the distance between the two receivers. In addition, the location of the source is reversed for each receiver spacing so that forward and reverse profiles are run. By averaging the forward and reverse profiles, the effect of any internal phase between receivers is eliminated. This testing sequence is shown in Figure 1b. As the method is still in research stages, testing time at each site is approximately 30 min. However, after the testing procedure is automated, the testing period will be only minutes, and thus comparable with other NDT methods.

By analysis of phase information for each frequency determined between the two receivers, Rayleigh wave velocity, shear wave velocity, and eventually Young's modulus are determined. Rayleigh wave velocity (V_R) is constant in a homogeneous halfspace and is independent of frequency. Each frequency (f) has a corresponding wavelength (L_R) according to

$$V_R = f \cdot L_R \quad (1)$$

Rayleigh wave and shear wave velocities are related by Poisson's ratio. The ratio of R-wave to S-wave velocity varies slightly with Poisson's ratio but can be assumed equal to 0.90 with an error of less than 5 percent.

If the stiffness of a site varies with depth, then the velocity of the Rayleigh wave will vary with frequency. The variation of R-wave velocity

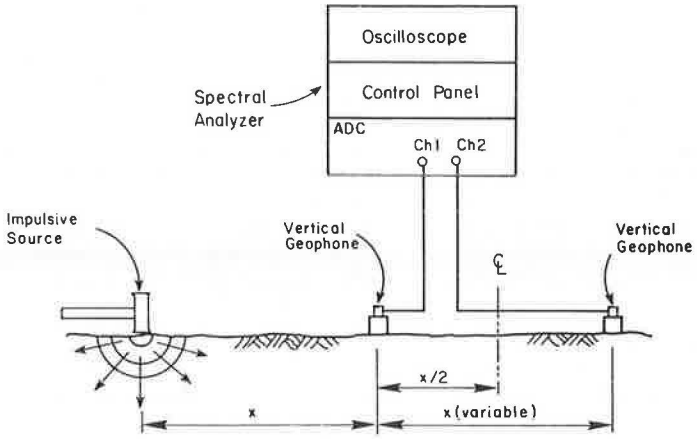

(a) General Configuration of SASW Tests

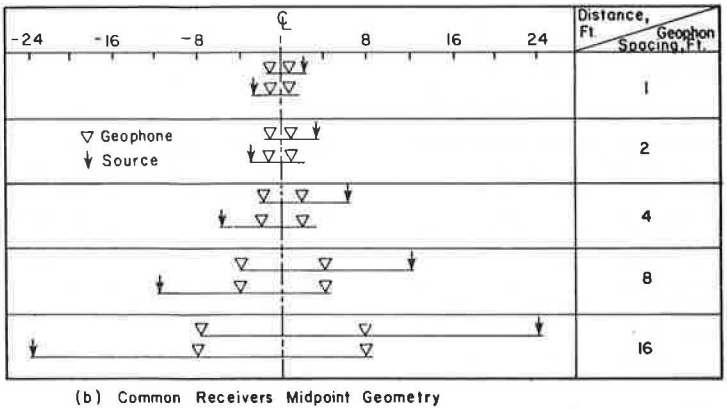

(b) Common Receivers Midpoint Geometry

FIGURE 1 Schematic of experimental arrangement for SASW tests.

with frequency (wavelength) is known as dispersion, and a plot of velocity versus wavelength is called a dispersion curve. The dispersion curve is constructed based on data collected in the field.

Inversion of the R-wave dispersion curve is the procedure of determining the actual propagation velocities at different depths from the dispersion curve. Inversion consists of determination of the depth and shear wave velocity of each layer from the R-wave velocity versus wavelength data. Inversion is the most important stage in determining a meaningful profile by the SASW method, and inversion is discussed in detail herein.

Crosshole Seismic Test

A second seismic test--the crosshole test--was used in the field to develop independently modulus profiles to compare with the SASW results. The basic concept of the crosshole test involves measurement of body waves (compression and shear) propagating along horizontal travel paths at different depths in the medium. Propagation velocities at these depths are calculated once travel times and distances have been measured. By means of elastic theory, moduli of each layer are then evaluated. The thicknesses of the layers are determined from the borings used in the crosshole test.

A schematic of the crosshole testing procedure used at the pavement sites is shown in Figure 2. The borehole array at each site consisted of three boreholes arranged in a linear array with approximately 3.5-ft spacing between adjacent boreholes. Each borehole was advanced to the appropriate measurement depth by using solid-stem augers. At each testing depth the drilling operation was stopped and the source was placed in the bottom of one hole. The receivers were located at the same depth in the other holes. A vertical impulse, which simultaneously activated the recording device, was then applied to the source. The impulse was detected by receivers in the other holes as the body waves passed. The source consisted of a sampling tube attached to a 1-in.-diameter rod. A vertical velocity transducer secured to the rod just above the sampling tube served as the trigger for the recording device. The receivers consisted of three-dimensional velocity transducers.

A typical record detected with the vertical geophone at a distance of 3.5 ft from the source is shown in Figure 3a. The upper portion of the figure is the impulse monitored by the source geophone. A time delay was used at the beginning of the record so that the triggering point could be easily distinguished (marked as I on the record). The lower part of the figure shows the record of body waves monitored by the vertical geophone. The direct P- and S-wave arrivals are marked by P and S, respectively. Shear and compressional travel times are simply the time differences between point I and points S or P, respectively. Although P-wave velocity can be identified on this record, it is preferred that this velocity be determined from a record obtained by using a transducer that is oriented in the direction of propagation (i.e., a radial, horizontal geophone). A typical travel time record monitored with a radial, horizontal geophone is shown in Figure 3b. The triggering time and direct arrival of the P-wave are marked as I and P, respectively. The amplitude on the travel time record of the P-wave is larger and easier to identify in Figure 3b than in Figure 3a because of the proper orientation of the receiver.

Propagation velocity is determined simply by dividing the distance between the source and receiver by the travel time over this distance. Moduli and Poisson's ratio are then determined according to elastic theory as

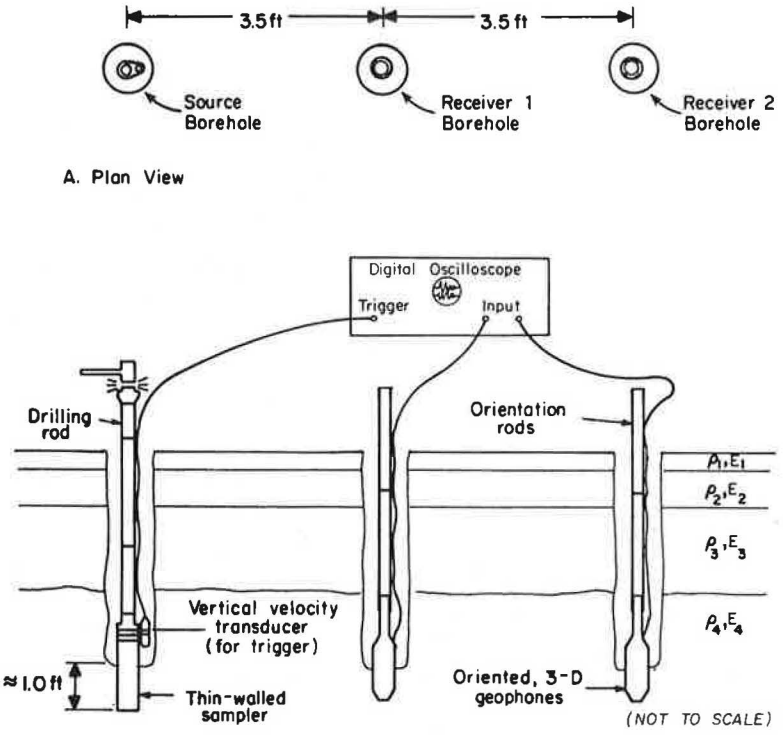

FIGURE 2 Crosshole testing technique used at runway sites.

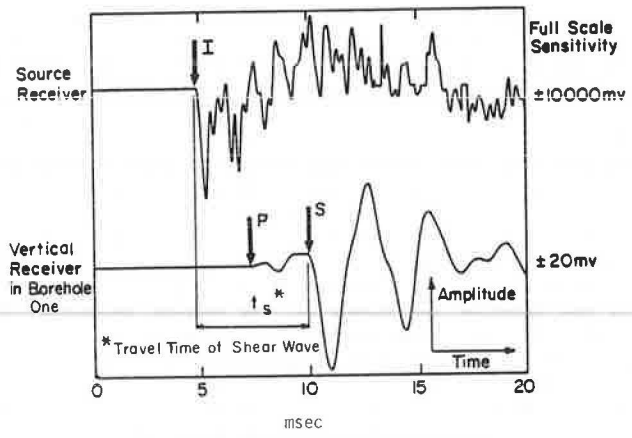

a) Travel Time Record of Shear Wave

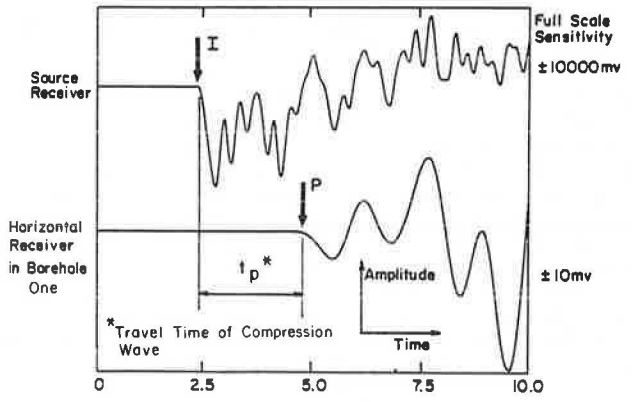

b) Travel Time Record of Compression Wave

FIGURE 3 Typical travel time records generated with vertical impulses in crosshole seismic test.

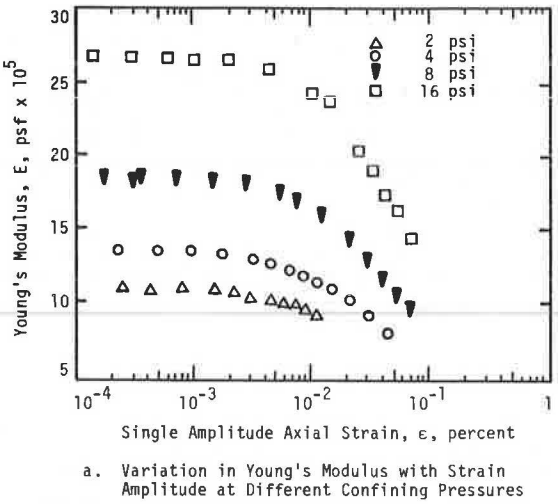

a. Variation in Young's Modulus with Strain Amplitude at Different Confining Pressures

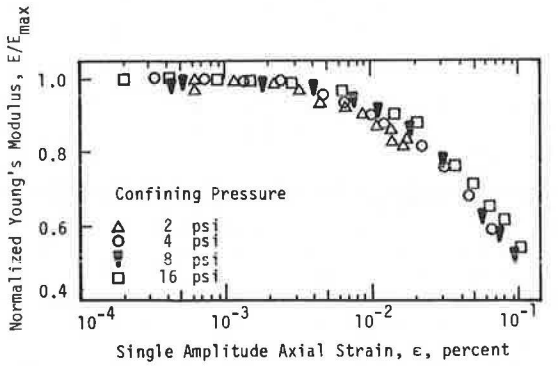

b. Variation in Normalized Young's Modulus with Strain Amplitude

FIGURE 4 Effect of axial strain amplitude on Young's modulus of an unsaturated clay subgrade.

$$G = (\gamma/g)V_S^2 \quad (2)$$

$$E = (2\gamma/g)V_S^2 (1 + \nu) = (\gamma/g)V_P^2 \times \{[(1 + \nu)(1 - 2\nu)]/(1 - \nu)\} \quad (3)$$

$$M = (\gamma/g)V_P^2 \quad (4)$$

$$\nu = [0.5(V_P/V_S)^2 - 1]/[(V_P/V_S)^2 - 1] \quad (5)$$

where

V_P = compression wave velocity,
V_S = shear wave velocity,
G = shear modulus,
E = Young's modulus or modulus of elasticity,
M = constrained modulus,
γ = total unit weight of the material,
g = gravitational acceleration, and
ν = Poisson's ratio.

Values of these parameters determined from seismic measurements represent the material behavior at small shearing strains, that is, strains less than 0.001 percent (7). In this strain range material behavior, particularly subgrade material, is typically independent of strain amplitude.

A typical example of the variation in E with normal strain (ε) for subgrade is shown in Figure 4. An undisturbed sample of unsaturated clay from San Antonio, Texas, was tested by using the resonant column method (8). The variation in E with log ε at several confining pressures is shown in Figure 4a. It is evident that, below strains of about 0.001 percent, E is constant and independent of strain at each pressure.

The effect of strain on modulus is easily seen by plotting the variation of normalized modulus (E/E_{max}) with log ε, as shown in Figure 4b. In Figure 4b, E_{max} is taken as the maximum value of Young's modulus at each confining pressure and is often termed the low-amplitude modulus or elastic modulus. Note that Young's modulus is constant below a strain of about 0.001 percent and is equal to E_{max}. As such, any seismic measurement in which modulus is measured at strains below about 0.001 percent results in measurement of a strain-independent modulus (E_{max}). This is a beneficial characteristic of seismic measurements in that different techniques, if properly performed, result in essentially the same value of modulus, E_{max}. In addition, if a normalized modulus versus strain curve such as that shown in Figure 4b is available for the material, then the reduced modulus in the nonlinear range can be determined once E_{max} has been measured seismically.

EXPERIMENTS ON RIGID AIRPORT PAVEMENTS

The SASW method was used at two sites in the apron area of Tyndall Air Force Base (AFB) near Panama City, Florida, in June 1983. The method was used to

determine the variation of in situ shear wave velocity and Young's modulus with depth for two pavement systems. In conjunction with SASW testing, crosshole tests were also performed as previously described. The crosshole tests were conducted so that Young's modulus profiles could be compared with those determined by SASW tests at each site.

Location

Two sites were tested in the apron area at Tyndall AFB. An overview of the sites and the test locations is shown in Figure 5. The apron consists of two different pavement sections constructed at different times. Slabs A and B in Figure 5 correspond to old and new pavements, respectively.

The old pavement, which was constructed during the World War II era, consists of approximately 6 in. of unreinforced concrete underlain by sand. The dimensions of individual slabs in this area are 10 ft by 15.5 ft. The new pavement, which was constructed recently, consists of approximately 10 in. of unreinforced concrete underlain by approximately 4 in. of cement-treated base and then natural sand. This area is divided by sawed joints into slabs about 14.5 ft wide and 25.5 ft long. No significant cracking was evident within the slabs tested at either location.

Procedure

The testing procedure (shown in Figure 1) was carried out at each site. Vertical geophones with a natural frequency of 4.5 Hz were used. Also, a series of back-up data was collected at each site by using geophones with a natural frequency of 2 Hz. In the case of the old pavement, geophone spacings of 1, 2, 4, 8, 14, and 24 ft were used. The closer spacings were used to sample near-surface material, and the larger spacings were used to sample deeper materials. As shallower depths correspond to higher frequencies, a frequency range of 0 to 12,800 Hz was selected for the geophone spacing of 1 ft. The upper limit of this frequency range was then decreased as the spacing increased to a final limit of 400 Hz at the 24-ft spacing.

Geophone spacings used on the new pavement were 1, 2, 4, 8, 16, and 32 ft, and the frequency limits were similar to those used at the old pavement. Different sources were also used with different geophone spacings. At close spacings (1 and 2 ft), a small chisel and hammer were used. A claw hammer was used for a spacing of 4 ft, and a 15-lb sledge hammer was used for spacings equal to or greater than 8 ft.

At each site the last receiver spacing was greater than the length of the slab, and the geophones were located across joints. These joints had a minor effect on the measurements because of the low frequencies (long wavelengths) measured with this spacing. As such, the wavelengths were significantly longer than the depth of the joints, causing negligible disturbance in the wavepath.

Construction of Dispersion Curves

A spectral analyzer was used to record and analyze outputs from the two receivers. After each travel time record from the receivers was captured in the time domain, the signals were transformed into the frequency domain and spectral analyses were performed. The portions of the spectral analyses of interest in SASW testing are the phase information of cross-power spectrum and the coherence function. The coherence function is an indicator of the amount of random background noise at each frequency that is interfering with the actual impact. The coherence is a real-valued function analogous to a signal-to-noise ratio and ranges between zero and one. A coherence of unity at a given frequency can generally be translated into complete elimination of undesirable background noise and total correlation between the signals detected by the two receivers if it is based on the average of several impacts. The phase information of the cross-power spectrum is indica-

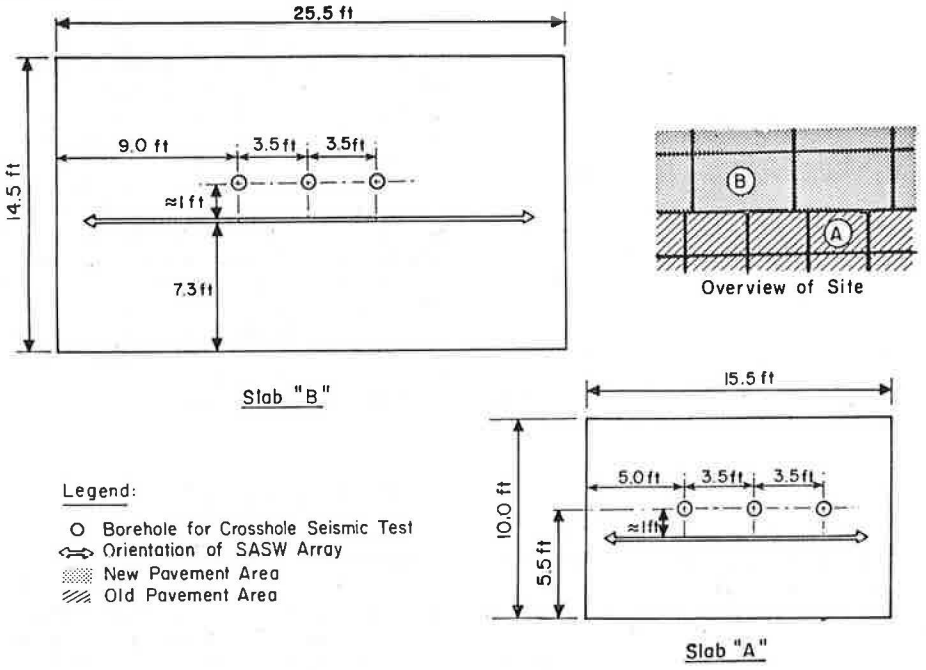

FIGURE 5 Plan view of testing locations.

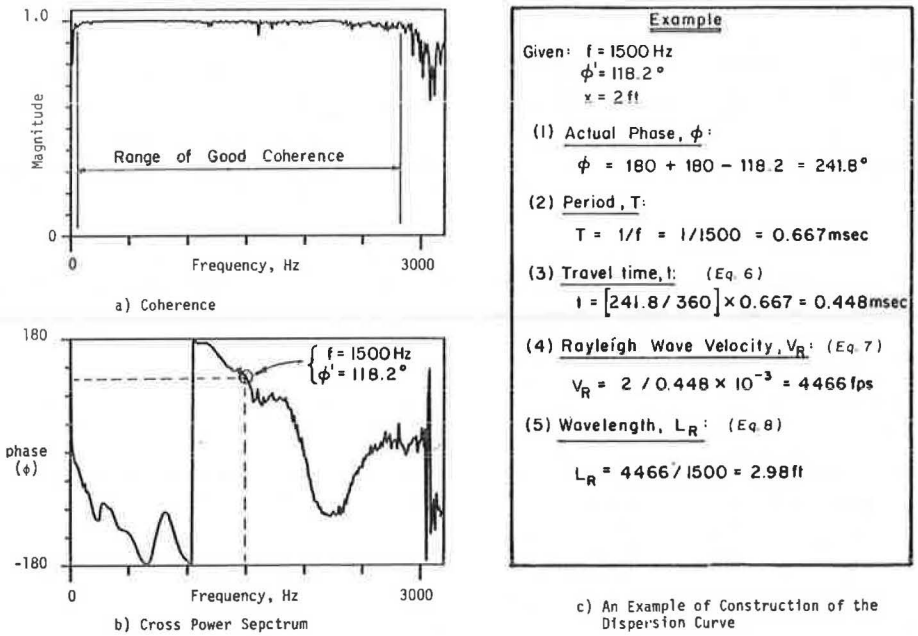

FIGURE 6 Typical coherence and cross-power spectrum used in construction of dispersion curve.

tive of the relative phase difference between signals at each frequency in the range of the measured frequencies.

A typical coherence function and phase information from the cross-power spectrum are shown in Figure 6. From the coherence function, the range of frequencies that should be initially considered in data reduction is chosen. For each frequency in this range the phase shift associated with that frequency is determined by using the phase of cross-power spectrum (Figure 6b). A phase shift equal to 360 degrees corresponds to a travel time equal to one period. As such, the travel time of the Rayleigh wave within the distance between the two receivers for a given frequency (f) can be calculated from

$$t = (\phi/360) \cdot T \quad (6)$$

where

t = travel time of the Rayleigh wave,
ϕ = phase shift, and
T = 1/f = period corresponding to the given frequency (f).

As the distance (X) between the geophones is known, the Rayleigh wave velocity (V_R) for the known frequency (f) is equal to

$$V_R = X/t \quad (7)$$

The wavelength (L_R) associated with frequency (f) is

$$L_R = V_R/f \quad (8)$$

By repeating this procedure for other frequencies on each record, a number of data points (representing R-wave velocity versus wavelength) are obtained, from which the dispersion curve is constructed. A numerical example that uses Equations 6-8 to find the R-wave velocity at one wavelength (frequency) is shown in Figure 6c.

On the basis of studies at several soil sites, Heisey et al. (3) suggested that the distance between receivers (X) should be less than two wavelengths and more than one-third of a wavelength. Based on these criteria, any point with a wavelength less than half of the geophone spacing or more than three times the distance between the geophones is eliminated from construction of the dispersion curve. Fortunately, portions of the dispersion curve from different receiver spacings partially overlap, and the final dispersion curve is continuous.

Dispersion curves from the old and new pavement sections are shown in Figures 7a and 7b, respectively. Scatter in the first few feet of wavelengths is basically because of scaling of the figure. In other words, the scale of the wavelength axis is so large that the data points appear to form horizontal lines. To demonstrate the actual distribution of points, two portions of the dispersion curve for the old pavement (Figure 7a) are shown in Figure 8. Different branches of the dispersion curve can be easily distinguished. These branches represent different modes of Rayleigh waves (9). These modes could not be detected clearly in the earlier work (3) because only a few data points from each cross-power spectrum were picked manually. In the past year construction of dispersion curves has been fully automated. As such, all data points on the digitized records of the cross-power spectrums (which are within the filter criteria) are used. This results in a comprehensive dispersion curve that consists of thousands of data points, as opposed to a few hundred points in the past.

Inversion of Dispersion Curve

Inversion of the dispersion curve (or simply inversion) is the process of determining the layer thicknesses and shear wave velocity profile from the dispersion curve. The most crude type of inversion that has been used for many years is to assume that the sampling depth is equal to one-half to one-third of the wavelength and the shear wave velocity is equal

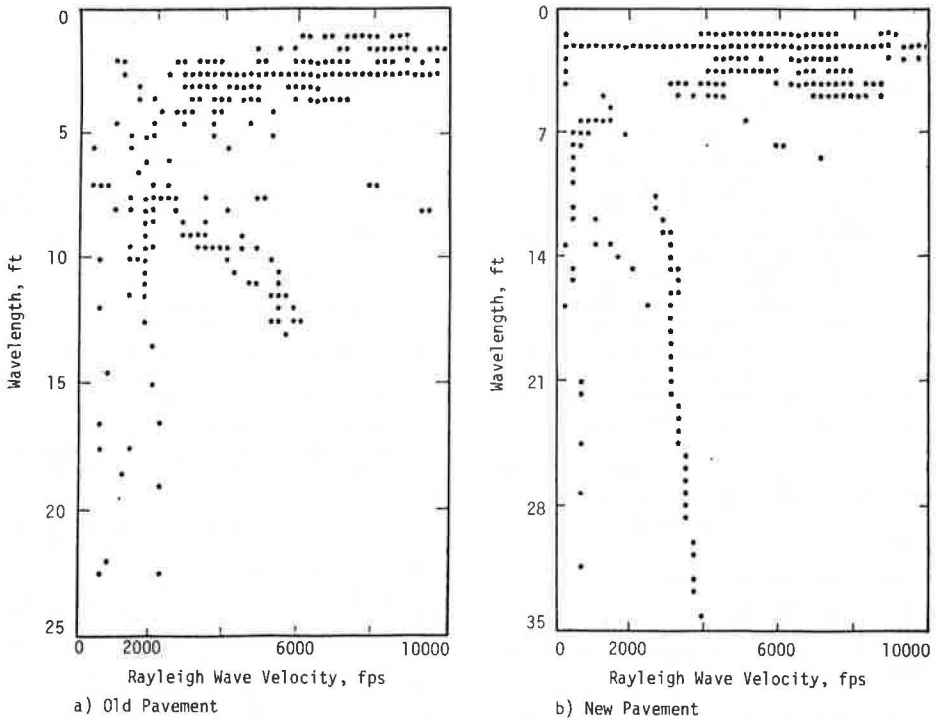

FIGURE 7 Dispersion curves from pavement sections.

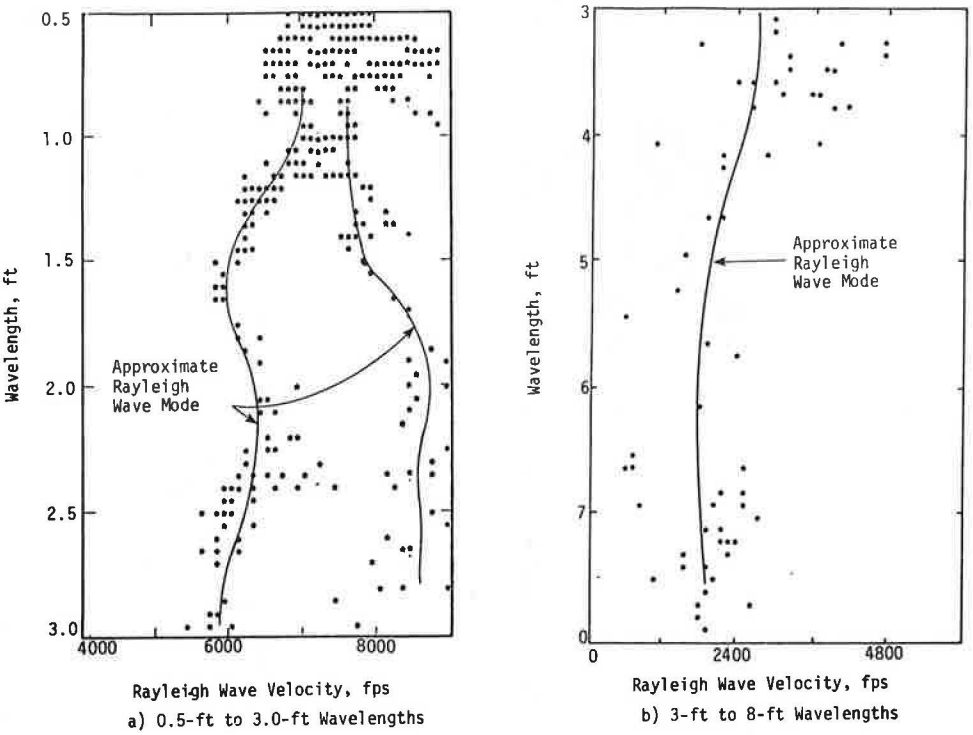

FIGURE 8 Portions of dispersion curve from old pavement section.

to 1.1 times the Rayleigh wave velocity (3,8). In other words, simply multiply the scale of the wavelength axis by one-half or one-third and the scale of Rayleigh wave velocity axis by approximately 1.1 to obtain the S-wave velocity profile. Existence of a layer that has a significantly higher or lower velocity at the surface of the medium affects measurement of the velocities of the underlying layers. As such, R-wave velocities determined by this method are not actual velocities of the layers but are apparent R-wave velocities. Naturally, the shear wave velocity profile determined by this method is in error. However, in a layered medium in which no significant contrast in velocities exists, the apparent and actual R-wave velocities are approximately equal.

Nazarian et al. (4) presented an approximate inversion process. In this process the depths of the layers were assumed to be equal to one-third of the wavelength. Based on Haskell's (10) matrix for elastic surface waves in a layered media and assuming that the apparent and actual R-wave velocities of the top layer are equal, the S-wave velocity profile was constructed from the top to the bottom sequentially.

The new inversion process is rigorous, and all simplifying assumptions made in other techniques (such as sampling depth) are eliminated. The only assumptions are that

1. The layers are horizontal, and thus if any dipping layers exist in the profile the average property of those layers are determined, and
2. The layers are laterally homogeneous over the geophone spacing and are linearly elastic.

The inversion process is based on a modified version of Haskell's (10) and Thompson's (11) matrix for elastic surface waves in a multilayered solid media. In this process shear wave velocities of different layers are assumed and a theoretical dispersion curve, based on this profile, is generated. Poisson's ratios and mass densities are assumed. However, Grant and West (9) and Ewing et al. (12) indicate that the effect of these two parameters on the process of inversion is not significant (especially in the case of pavement materials and soil layers in which these two parameters have reasonably narrow ranges). This theoretical curve is then compared with the experimental dispersion curve constructed from field data. If the two curves agree reasonably well, the shear wave velocity profile is obtained. If the two curves do not match, velocities of the layers are changed, and a new theoretical curve is generated and compared. This iterative process is continued until the two curves (theoretical and experimental dispersion curves) match. It should be mentioned that, as an initial trial, use of the first crude inversion process is advised (especially for soil sites).

To illustrate the matching process, the dispersion curves from the first 8 ft of the old pavement section (Figure 8) are compared in Figure 9 with the theoretical dispersion curves generated with the inversion algorithm. Symbols U and L represent the upper and lower boundaries, respectively, of possible locations of a theoretical data point in the figures. Upper and lower boundaries are displayed (as opposed to a mean value) so that the resolution of the theoretical solution can be interpreted. The symbol O is used to show a perfect match, and the symbol X is used to represent a point where the upper and lower boundaries overlap. As can be seen in Figure 9, the trends in the experimental data follow the theoretical dispersion curves quite closely. At this site the scatter in experimental data was unusually high for unknown reasons. However, the trends are still predicted closely. It is estimated that the accuracy with which R-wave velocities were measured and the use of the inversion process together cause less than a ±10 percent error in shear wave velocities reported herein.

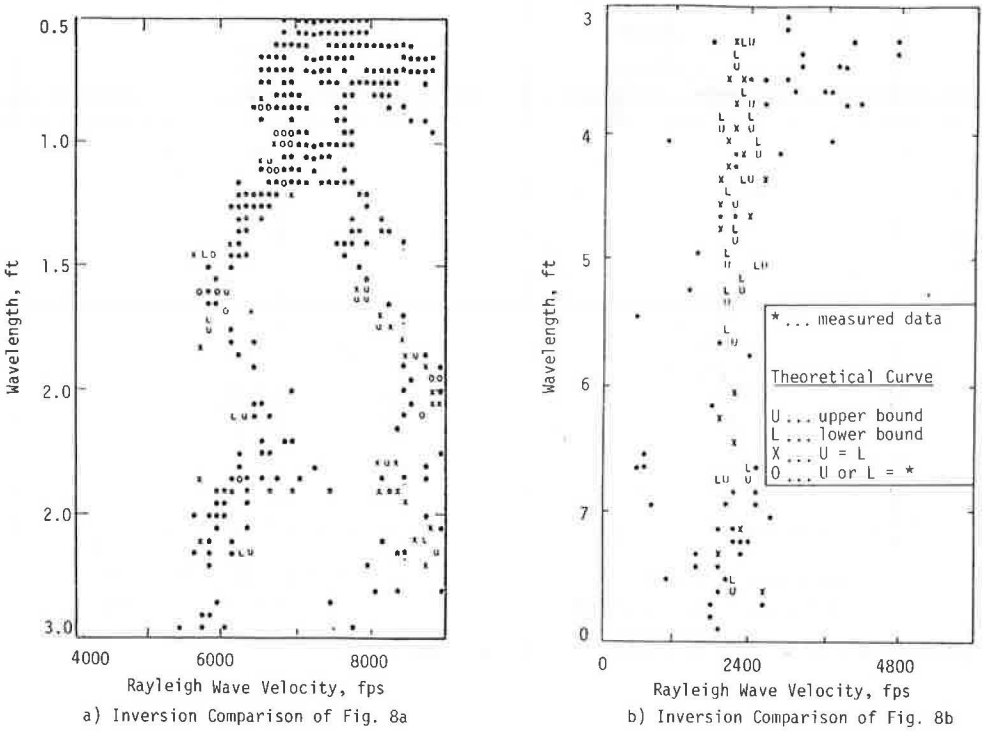

FIGURE 9 Comparison of theoretical and measured portions of dispersion curves from old pavement section.

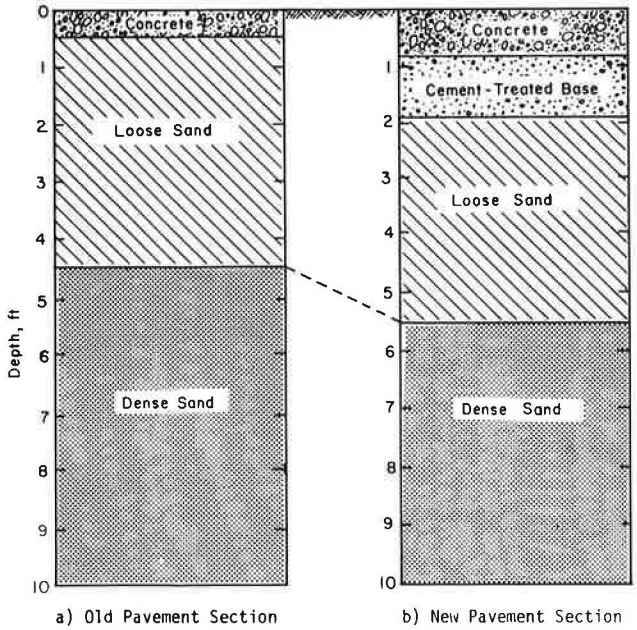

FIGURE 10 Material profile at each test section.

Presentation of Results

As mentioned, two types of seismic tests were performed at the runway sites. With the SASW test, shear wave velocity profiles were first determined. Shear wave velocity and compression wave velocity profiles were obtained with the crosshole test. By knowing shear and compression wave velocities from the crosshole test, values of Poisson's ratio were calculated by using Equation 5.

Soil profiles under the old and new pavements are shown in Figures 10a and 10b, respectively. From the borings for the crosshole tests, the old section was determined to consist of 6 in. of concrete underlain by approximately 4.5 ft of loose gray sand and then dense sand. The material profile at the new pavement section was made up of 10 in. of concrete underlain by approximately 14 in. of cement-stabilized base, which was followed by loose sand underlain by dense sand.

The shear wave velocity profiles of the two sections are shown in Figures 11 and 12. A total of 16 layers was selected in the first 9 ft of the profile to analyze (in the inversion process) the old pavement (Figure 11a). The layer thicknesses became progressively thicker with depth, as the properties of the near-surface materials were most important in this study. The number of layers selected to analyze the new pavement was 18 layers, as shown in Figure 12a. No other NDT method has the ability to enable the user to choose such a fine layering or to have such accuracy.

Also shown in Figures 11 and 12 are the shear wave velocities determined by the crosshole method. In stiff material such as concrete, the crosshole test can have the drawback of not generating measurable shear waves, as was the case in this study. However, the compression wave velocity was obtained very accurately. As such, shear wave velocities determined by the crosshole test in the concrete and the near-surface base material were back-calculated from P-wave velocities assuming Poisson's ratios of 0.15 and 0.25, respectively.

The shear wave velocity profiles shown in Figures 11 and 12 are in excellent agreement. Shear wave velocities from the two methods for the old and new pavement sections are given in Tables 1 and 2, respectively. The average difference between velocities determined by the crosshole and SASW methods is 10 percent at the old pavement and 12 percent at the new pavement.

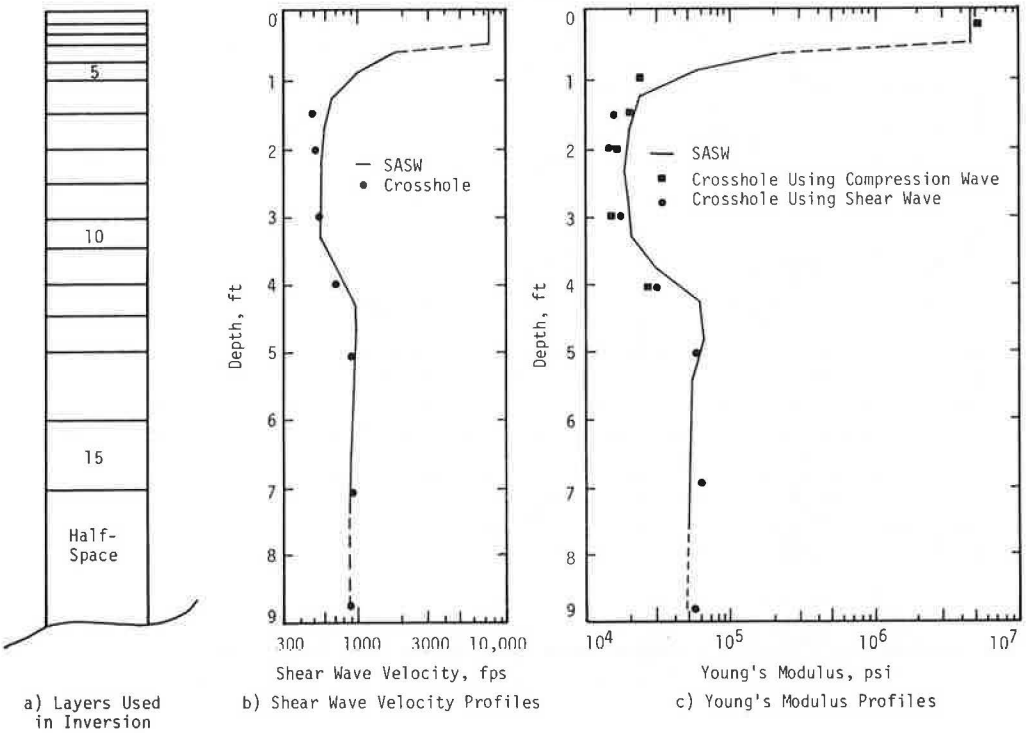

FIGURE 11 Comparison of shear wave velocities and Young's moduli from crosshole and SASW methods at old pavement section.

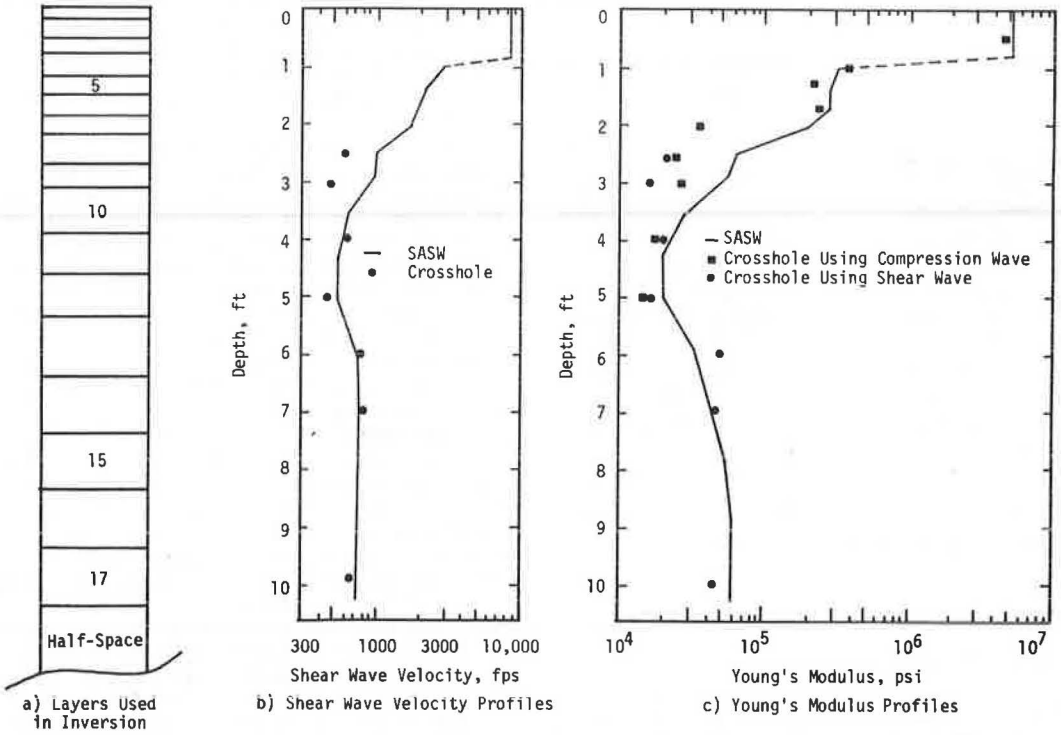

FIGURE 12 Comparison of shear wave velocities and Young's moduli from crosshole and SASW methods at new pavement section.

TABLE 1 Comparison of Wave Velocities from Crosshole Seismic and SASW Tests on Old Pavement Section

Depth (ft)	Shear Wave Velocity		Range of Compression† Wave Velocity from Crosshole Tests (fpc)	Poisson's Ratio		Assumed Unit Weight (pcf)
	Range from Crosshole† Tests	SASW Tests		from† Crosshole Tests	Assumed$^{\Psi}$	
(1)	(2)	(3)	(4)	(5)	(6)	(7)
0.3	-*	7950	11460-13740 [12800]	-*	.15	145
1.0	-*	640	1100-1330 [1210]	-*	.33	110
1.5	436-523 [484]	580	1000-1325 [1145]	.38 - .41 [.39]	.33	110
2.0	476-538 [507]	580	1000-1025 [1012]	.30 - .36 [.33]	.33	110
3.0	538-561 [548]	570	875-1022 [949]	.20 - .28 [.24]	.33	110
4.0	695	700	1311	.30	.33	110
5.0	928	990	5571#	.47	.49	110
7.0	896-1009 [952]	890	5581-5708# [5620]	.49	.49	110
9.0	870-954 [912]	890	5282-5531# [5406]	.49	.49	110

* Inconclusive data
† Numbers in brackets are the average values
# As the soil is saturated, reported compression wave velocities basically represent wave velocities in water, not the soil skeleton
Ψ SASW analysis performed before crosshole data analyzed, therefore Column 5 differs from Column 6

TABLE 2 Comparison of Wave Velocities from Crosshole Seismic and SASW Tests on New Pavement Section

Depth (ft)	Shear Wave Velocity		Range of Compression† Wave Velocity from Crosshole Tests (fpc)	Poisson's Ratio		Assumed Unit Weight (pcf)
	Range from Crosshole† Tests	SASW Tests		from† Crosshole Tests	Assumed$^{\Psi}$	
(1)	(2)	(3)	(4)	(5)	(6)	(7)
0.5	-*	8750	12160-13770 [12736]	-*	.15	145
1.0	-*	2290	3720	-*	.15	145
1.3	-*	2110	3248	-*	.25	125
1.5	-*	2080	3225	-*	.25	125
2.0	-*	1010	1046-1545 [1221]	-*	.25	125
2.5	595	1010	1182	.33	.33	110
3.0	496	950	1271	.24	.33	110
4.0	608-609 [608]	560	954-1121 [1038]	.12 - .29 [.20]	.33	110
5.0	470-511 [496]	560	870-958	.27 - .30	.33	110
6.0	833-933	780	833-933# [883]	.49	.49	110
7.0	783-854 [818]	780	4897-5029# [4963]	.49	.49	110
10.0	783-816 [799]	837	5262-5123#	.49	.49	110

* Inconclusive data
† Numbers in brackets are the average values
# As the soil is saturated, reported compression wave velocities basically represent wave velocities in water, not the soil skeleton
Ψ SASW analysis performed before crosshole data analyzed, therefore Column 5 different from Column 6

Determination of Elastic Moduli

Once the propagation velocities of each layer have been determined, Young's moduli and shear moduli can be easily calculated. In the case of the SASW method, the shear wave velocities are determined from which shear moduli (G) are calculated by using Equation 2. Young's modulus and shear modulus are related through Poisson's ratio by

$$E = 2(1 + \nu)G \qquad (9)$$

In crosshole tests both shear and compression wave velocities are determined. Therefore, Young's modulus can be calculated from either Equation 3 or 5.

Young's modulus profiles from the old and new pavements are shown in Figures 11 and 12, respectively. The profiles obtained from the crosshole and SASW tests are in good agreement, except in the range of 2 to 3 ft, over which some scatter exists. The assumed mass densities and Poisson's ratios and calculated Young's moduli are presented in Tables 3 and 4. The excellent agreement between the profiles from these two independent testing techniques illustrates the value and versatility of the SASW method.

SUMMARY AND CONCLUSIONS

Nondestructive testing of rigid pavement with the SASW method is discussed. This method has been under continuous development during the past few years. Construction of dispersion curves from data collected in situ is fully automated, resulting in a comprehensive dispersion curve consisting of thousands of data points. As a result, different modes of the Rayleigh wave can now be detected, serving as a multiple check on the accuracy of the data reduction.

A new, rigorous inversion process has been developed that eliminates all significant simplifying assumptions used in the past. This new inversion process was applied to data collected at two airport runway sites. Young's modulus profiles obtained by the SASW method illustrate the power of this method in determining fine layering in the pavement section with excellent accuracy. Also, Young's modulus profiles agreed closely with those determined by the well-established crosshole seismic method.

In the aspect of automation, the SASW technique is still in research and development stages. Once the system is automated, it would be just as fast to perform a test in situ with this method as any other NDT method carried out today. In addition, the method has the advantage of developing a unique profile and determining layer thicknesses with great accuracy.

ACKNOWLEDGMENTS

This work was supported by the Texas State Department of Highways and Public Transportation (TSDHPT) under research 3-8-79-256 and by the U.S. Air Force. The authors wish to thank the personnel of these two organizations, especially Lt. Colonel B. Tolson and Captain J.D. Wilson of Tyndall AFB and G. Peck and R.B. Rogers of TSDHPT. The technical assistance and funding provided by the U.S. Air Force and TSDHPT are sincerely appreciated. Thanks are also extended to Tony Ni, research assistant at the University of Texas, for performing the resonant column tests.

TABLE 3 Comparison of Young's Moduli from Crosshole Seismic and SASW Tests on Old Pavement Section

Depth (ft)	Young's Modulus (psi)			Difference (percent)	
	SASW	Crosshole		$\frac{(2)-(3)}{(2)}$ † (range)	$\frac{(2)-(4)}{(2)}$ † (range)
		Using Compression† Wave Velocity (range)	Using Shear† Wave Velocity (range)		
(1)	(2)	(3)	(4)	(5)	(6)
0.3	4.55×10^6	$(4.11\text{-}5.90) \times 10^6$ [5.14×10^6]	-*	9.7 - 29.7 [13.1]	-*
1.0	2.6×10^4	$(1.95\text{-}2.84) \times 10^4$ [2.35×10^4]	-*	7.0 - 25.0 [9.6]	-*
1.5	2.13×10^4	$(1.60\text{-}2.81) \times 10^4$ [2.13×10^4]	$(1.26\text{-}1.83) \times 10^4$ [1.56×10^4]	9.0 - 24.9 [0.0]	14.1 - 40.8 [26.9]
2.0	2.13×10^4	$(1.60\text{-}1.68) \times 10^4$ [1.64×10^4]	$(1.46\text{-}1.79) \times 10^4$ [1.63×10^4]	21.1 - 24.9 [23.0]	16.0 - 31.5 [23.5]
3.0	2.06×10^4	$(1.23\text{-}1.67) \times 10^4$ [1.45×10^4]	$(1.63\text{-}1.91) \times 10^4$ [1.77×10^4]	18.9 - 40.3 [29.6]	7.3 - 20.9 [14.1]
4.0	3.13×10^4	2.75×10^4	2.98×10^4	12.1	4.8
5.0	6.91×10^4	-#	6.01×10^4	- #	13.0
7.0	5.62×10^4	-#	$(5.68\text{-}7.09) \times 10^4$ [6.39×10^4]	- #	1.1 - 26.2 [13.7]
9.0	5.62×10^4	-#	$(5.35\text{-}6.39) \times 10^4$ [5.87×10^4]	- #	4.8 - 13.7 [4.4]

* Inconclusive data
† Numbers in brackets are the average values
# As the soil is saturated, reported compression wave velocities basically represent wave velocities in water, not the soil skeleton

TABLE 4 Comparison of Young's Moduli from Crosshole Seismic and SASW Tests on New Pavement Section

Depth (ft)	Young's Modulus (psi)			Difference (percent)	
	SASW	Crosshole		$\frac{(2)-(3)}{(2)}$ † (range)	$\frac{(2)-(4)}{(2)}$ † (range)
		Using Compression† Wave Velocity (range)	Using Shear† Wave Velocity (range)		
(1)	(2)	(3)	(4)	(5)	
0.5	5.51×10^6	$(4.62\text{-}5.93) \times 10^6$ [5.09×10^6]	-*	7.6 - 16.2 [7.7]	-*
1.0	3.55×10^5	3.73×10^5	-*	5.1	-*
1.3	3.00×10^5	2.37×10^5	-*	21.4	-*
1.5	2.93×10^5	2.8×10^5	-*	4.4	-*
2.0	6.42×10^4	$(2.46\text{-}5.36) \times 10^4$ [3.47×10^4]	-*	61.7 - 16.5 [45.9]	-*
2.5	6.42×10^4	2.24×10^4	2.23×10^4	65.1	65.3
3.0	2.83×10^4	2.59×10^4	1.58×10^4	8.5	44.2
4.0	1.99×10^4	$(1.46\text{-}2.01) \times 10^4$ [1.74×10^4]	$(1.96\text{-}2.27) \times 10^4$ [2.12×10^4]	26.1 - 1.0 [17.8]	1.51 - 14.1 [6.3]
5.0	1.99×10^4	$(1.21\text{-}1.47) \times 10^4$ [1.34×10^4]	$(1.39\text{-}1.61) \times 10^4$ [1.50×10^4]	26.1 - 39.2 [32.7]	19.1 - 30.2 [24.6]
6.0	4.30×10^4	-#	$(4.91\text{-}6.15) \times 10^4$ [5.53×10^4]	-#	13.4 - 42.0 [27.7]
7.0	4.30×10^4	-#	$(4.33\text{-}5.12) \times 10^4$ [4.73×10^4]	-#	0.7 - 19.1 [9.9]
10.0	5.11×10	-#	$(4.33\text{-}4.70) \times 10^4$ [4.52×10^4]	-#	15.3 - 7.8 [11.6]

* Inconclusive data
† Numbers in brackets are the average values
# As the soil is satruated, reported compression wave velocities basically represent wave velocities in water, not the soil skeleton

REFERENCES

1. J.P. Nielsen and G.T. Baird. Air Force System for Nondestructive Testing of Pavements. Presented at Symposium on Nondestructive Test and Evaluation of Airport Pavements, Vicksburg, Miss., Nov. 18-20, 1975.
2. J.P. Nielsen and G.T. Baird. Evaluation of an Impulse Testing Technique for Nondestructive Testing of Pavements and Recommended Follow-On Research. Report CEEDO-TR-77-46. U.S. Air Force Civil and Environmental Engineering Office, Tyndall Air Force Base, Fla., Sept. 1977.
3. J.S. Heisey, K.H. Stokoe II, and A.H. Meyer. Moduli of Pavement Systems from Spectral Analysis of Surface Waves. In Transportation Research Record 852, TRB, National Research Council, Washington, D.C., 1982, pp. 22-31.
4. S. Nazarian, K.H. Stokoe II, and W.R. Hudson. Use of Spectral Analysis of Surface Waves Method for Determination of Moduli and Thicknesses of Pavement Systems. In Transportation Research Record 930, TRB, National Research Council, Washington, D.C., 1983, pp. 38-45.
5. S. Nazarian and K.H. Stokoe II. Evaluation of Moduli and Thicknesses of Pavement Systems by SASW Method. Report 256-4. Texas State Department of Highways and Public Transportation, Austin, 1982.
6. K.H. Stokoe II and S. Nazarian. Effectiveness of Ground Improvement from Spectral Analysis of Surface Waves. Proc., 8th European Conference on Soil Mechanics and Foundation Engineering, Helsinki, Finland, May 1983.
7. K.H. Stokoe II and R.J. Hoar. Variables Affecting In Situ Seismic Measurements. Proc., ASCE Conference on Earthquake Engineering and Soil Mechanics, Pasadena, Calif., 1978, Volume II, pp. 919-939.
8. F.E. Richart, Jr., J.R. Hall, Jr., and R.D. Woods. Vibration of Soils and Foundations. Prentice-Hall, Englewood Cliffs, N.J., 1970.
9. F.S. Grant and G.F. West. Interpretation Theory in Applied Geophysics. McGraw-Hill, New York, 1965.
10. N.A. Haskell. The Dispersion of Surface Waves in Multilayered Media. Bull., Seismological Society of America, Vol. 43, No. 1, 1953, pp. 17-34.
11. W.T. Thompson. Transmission of Elastic Waves Through a Stratified Solid Medium. Journal of Applied Physics, Vol. 21, Feb. 1950, pp. 89-93.
12. W.M. Ewing, W.S. Jordetsky, and F. Press. Elastic Waves in Layered Media. McGraw-Hill, New York, 1957.

Publication of this paper sponsored by Committee on Pavement Rehabilitation.